

THESIS

DESIGN AND CONSTRUCTION OF ELECTRIC MOTOR DYNAMOMETER AND GRID  
ATTACHED STORAGE LABORATORY

Submitted by

Markus Lutz

Department of Mechanical Engineering

In partial fulfillment of the requirements

For the Degree of Master of Science

Colorado State University

Fort Collins, Colorado

Fall 2011

Master's Committee:

Advisor: Thomas Bradley

Daniel Zimmerle  
Peter Young

Copyright by Markus Lutz 2011

All Rights Reserved

## ABSTRACT

### DESIGN AND CONSTRUCTION OF ELECTRIC MOTOR DYNAMOMETER AND GRID ATTACHED STORAGE LABORATORY

The purpose of this thesis is to describe the design and development of a laboratory facility to both educate students on electric vehicle components as well as allow researchers to gain experimental results of grid-attached-storage testing. With the anticipated roll out of millions of electric vehicles, manufacturers of such vehicles need educated hires with field experience. Through instruction with this lab, Colorado State University plans to be a major resource in equipping the future electric vehicle work force with necessary training and hands-on experience using real world, full-scale, automotive grade electric vehicle components. The lab also supports research into grid-attached-storage. This thesis explains the design objectives, challenges, selections, construction and initial testing of the lab, and also provides context for the types of education and research which can be performed utilizing the laboratory.

## ACKNOWLEDGEMENTS

This material is based on work supported by the Department of Energy under Award Number DE-EE0002627. This report was prepared as an account of work sponsored by an agency of the United States Government. Neither the United States Government nor any agency thereof, nor any of their employees, makes any warranty, express or implied, or assumes any legal liability or responsibility for the accuracy, completeness or usefulness of any information, apparatus, product, or process disclosed, or represents that its use would not infringe on privately owned rights. Reference herein to any specific commercial product, process, or service by trade name, trademark, manufacturer, or otherwise does not necessarily constitute or imply its endorsement, recommendation, or favoring by the United States Government or any agency thereof. The views and opinions of authors expressed herein do not necessarily state or reflect those of the United States Government or any agency thereof.

## THANKS

I would like to take this opportunity to thank everyone who made this research possible. Dr. Thomas Bradley and Daniel Zimmerle provided countless hours of guidance and support. They both have been critical in my graduate research and my development as an engineer. I sincerely thank them for all of the time and support they have given me.

This research would not have been possible without the contributions of the American Recovery and Reinvestment Act, Clean Energy Super Cluster, Engineering Student Technology Fee Committee, Colorado State University, and the Engines and Energy Conversion Laboratory (EECL). Phil Bacon, Jacob Renquist, Andrew Geck, Brian Huff and Justin Wagner, supplied a significant amount of technical expertise and assistance in the construction of the lab and for them I am very thankful.

I would also like to thank God, my family and my friends who continually provided for me and showed support and encouragement to overcome the many obstacles I faced as well as for helping me pursue my dreams as an engineer.

## TABLE OF CONTENTS

ABSTRACT.....	ii
ACKNOWLEDGEMENTS.....	iii
THANKS .....	iv
TABLE OF CONTENTS.....	v
LIST OF FIGURES.....	viii
LIST OF TABLES.....	xii
LIST OF ABBREVIATIONS .....	xiv
1. Introduction to the Electric Drivetrain Teaching Center .....	1
1.1 Motivation for Education .....	1
1.2 Motivation for Grid-Attached-Storage Research .....	3
1.3 Modes of Education for Dynamometer Laboratory.....	5
1.4 Modes of Research for Grid-Attached-Storage.....	6
1.5 Objectives of the eDTC.....	7
2. Grid-Attached-Storage.....	10
2.1 Grid-Attached-Storage Background .....	10
2.1.1 Ancillary Services.....	10
2.1.2 Energy Arbitrage .....	12
2.1.3 Renewable Energy Firming.....	14
2.1.4 Second Use Batteries .....	15
2.1.5 Islanded Power Grids, Expeditionary Military, or Emergency Uses.....	16
2.2 System Overview.....	17
2.3 Challenges to Overcome .....	19
2.3.1 Comply with Standards .....	19
2.3.2 Unusual Cooling Requirements for Industrial Labs.....	22
2.3.3 Voltage Mismatch .....	23

2.3.4	Time Delay Impact on Voltage/Frequency Measuring Device.....	24
2.4	Design.....	28
2.4.1	Inverter/Variable Frequency Drive .....	28
2.4.2	Active Front End and Line Sync Card.....	30
2.4.3	Battery Pack .....	30
2.4.4	Transformer .....	33
2.4.5	LC Filter.....	34
2.4.6	Cooling Circuit .....	36
2.4.7	Voltage and Frequency Sensor.....	37
2.4.8	Unique Safety Requirements .....	39
2.4.8.1	Insulation Monitoring Device .....	41
2.4.8.2	Insulated Connectors.....	42
2.5	Check Out and Verification .....	43
2.5.1	Finalized System Construction .....	43
2.5.2	System Operation.....	46
2.5.3	Testing Results .....	48
3.	Electric Vehicle Component Education through a Dynamometer.....	51
3.1	Dynamometer Introduction .....	51
3.1.1	Various Methods of Motor Testing To Date .....	52
3.1.2	Uniqueness of this Set-Up.....	53
3.2	High-level System Overview of the Dynamometer Lab .....	53
3.3	Design Challenges .....	55
3.3.1	Cogging and Other Vibration Effects.....	55
3.3.2	Sizing of DC Power Supply.....	56
3.4	Design of this Equipment .....	59
3.4.1	Electric Motors .....	60
3.4.2	Variable Frequency Drive .....	63
3.4.3	DC Power Supply .....	63
3.4.4	Current Sensor .....	65
3.4.5	Torque Sensor and Coupler Selection.....	68
3.4.5.1	Objectives .....	68
3.4.5.2	Method .....	68

3.4.5.3	Results .....	72
3.4.5.4	Torque Sensor Selection .....	73
3.4.6	Mounting Box for Torque Sensor and Two Electric Motors.....	75
3.4.7	Powertrain Control Module .....	81
3.4.8	Control Computer .....	81
3.4.9	Data Acquisition System.....	81
3.4.10	Emergency Stop Circuit.....	83
3.5	Check Out and Verification .....	84
3.5.1	Implementation and Construction.....	85
3.5.2	Motor Spin-Up and Coast Down Operation.....	88
3.6	Course Work Examples .....	89
3.6.1	Lab #1: Map Torque versus Speed Curve.....	90
3.6.2	Lab #2: Map Motor Efficiency Lab.....	94
3.6.3	Lab #3: Investigate Temperature Effects on Electric Motors.....	99
3.6.4	Lab #4: Intro to Grid-Attached-Storage Lab.....	101
4.	Summary and Conclusions .....	105
4.1	Future of the eDTC .....	105
	WORKS CITED.....	107
	Appendix A – Wiring Schematics .....	113
	Appendix B – Artisan Vehicle Systems Pin-Out Listings.....	128
	Appendix C – GD&T Print for Motor Mounting Box .....	133
	Appendix D –Natural Frequency MatLab Procedure .....	134
	Appendix E – Instructions for Changing the Absorber Inverter from Line Sync Control to Resolver Control (GAS to Dyno Set-Up).....	151



## LIST OF FIGURES

Figure 2-1: Simplified Layout of Grid-Attached-Storage Equipment.....	18
Figure 2-2: Liquid Cooling System Layout.....	22
Figure 2-3: Control Loop for GAS Systems.....	25
Figure 2-4: Impact of Measurement Delay on Microgrid Performance .....	26
Figure 2-5: Detailed Highlights of Battery Pack Components .....	32
Figure 2-6: Cell Monitors for Each Cell of the Battery Pack.....	33
Figure 2-7: LC Filter Cabinet with Pre-Charge Circuit Schematic.....	36
Figure 2-8: Cooling Pumps with Priming Valves, Flow Meters, and Foot Valves .....	37
Figure 2-9: Cooling Circuit Fans, Radiators, and Reservoir.....	37
Figure 2-10: Caddock Electronics Voltage Divider .....	39
Figure 2-11: Bender IR155 Ground Fault Circuit Interrupter.....	41
Figure 2-12: Cam Connectors by Marinco. Clockwise: Female Cam Connector, Male Cam Connector, and Demonstration of Installation, Panel Mounts .....	42
Figure 2-13: Overview of Components and Their Locations in 3D CAD Model.....	44
Figure 2-14: Actual Layout of GAS Components.....	45
Figure 2-15: Actual Layout LC Filter Cabinet.....	46
Figure 2-16: Desk Control Box with Switch Callouts.....	47
Figure 2-17: Display Parameters in DSE Lite with Arbitrary Values for Display Purposes Only .....	48
Figure 2-18: Screenshot of DSE Lite in Background with PCM GUI BMS Monitor in Foreground .....	49

Figure 2-19: PCM GUI BMS Plot of Pack Current and Voltage vs. Time Plot (left) and Max and Min Cell Voltage vs. Time Plot (right) .....	49
Figure 2-20: Voltage and VAR vs. Time Plot for DC Voltage Command and Real as well as Reactive Power during the Discharge Event.....	50
Figure 3-1: Simplified Diagram of Dyno Set-Up .....	54
Figure 3-2: Schematic for Efficiency Calculations .....	57
Figure 3-3: Schematic for eDTC Dynamometer Set-Up .....	59
Figure 3-4: Output Torque of GP150WC Motor from Artisan Vehicle Systems .....	61
Figure 3-5: Output Power of GP150WC Motor from Artisan Vehicle Systems .....	62
Figure 3-6: Efficiency Curve of GP150WC Motor from Artisan Vehicle Systems .....	62
Figure 3-7: DC Disconnect Internals Showing Diode Installation .....	64
Figure 3-8: DC Bus Cabinet with Current Sensors Shown on Right .....	67
Figure 3-9: Model Definitions Used to Determine System Natural Frequency with Mass Numbers Labeled above Different Components .....	71
Figure 3-10: Amplitude at each Different Mass Number for the Three Different Modes	72
Figure 3-11: Visual Representation of Sensor and Coupling Cost vs. Natural Frequency Comparison with a Dashed Red Line Representing the Motor Natural Frequency .....	73
Figure 3-12: R+W America BK2 Bellows Coupling with Clamping Hub.....	74
Figure 3-13: Sensor Technologies RWT320 Torque Sensor .....	74
Figure 3-14: Mounting Design Concept A. Motors Mounted on Reinforced Stands with Cantilevered L-Bracket Supports .....	76
Figure 3-15: Mounting Design Concept B. Square Box Mounted within Square Plate with Motor Mounting Holes .....	77
Figure 3-16: Mounting Design Concept C. Square Box Rotated 45 Degrees to Allow for Most Interior Volume for Sensor and Couplers, Yet Still within Motor Mounting Holes	77
Figure 3-17: Fundamental Finite Element Analysis of Design C with Concentrated Forces at the Motor Mounting Bolt Holes .....	78

Figure 3-18: CAD Model Showing Dimensions between Motor Mounting Bolt Hole and the Next Surface .....	79
Figure 3-19: 3D CAD Model of Design C with Mounting Feet Brackets and Bushings .....	80
Figure 3-20: Simplistic Schematic of E-stop Logic.....	84
Figure 3-21: 3D CAD Model Detailed Layout with Component Call-Outs .....	85
Figure 3-22: Inverter Rack with DC Bus Bar Cabinet.....	86
Figure 3-24: Dyno Rig with Key Components Called Out .....	87
Figure 3-25: Control Cabinet Layout.....	87
Figure 3-26: Physical Layout of Constructed Components.....	88
Figure 3-27: Torque Curve at Continuous and Peak Torque .....	91
Figure 3-28: PV Simulator Screenshot of Manual_Voltage.vi.....	93
Figure 3-29: Screenshot and Explanations of Motor_Map.vi .....	93
Figure 3-30: Flow Schematic with Efficiencies at Each Component .....	95
Figure 3-31: Example Motor Efficiency Map .....	96
Figure 5-1: Control Cabinet Wiring .....	114
Figure 5-2: DAQ Wiring .....	115
Figure 5-3: Linear Power Supply Wiring .....	116
Figure 5-4: Powertrain Control Module Wiring.....	117
Figure 5-5: E-Stop, Breakers, and Light Tower Wiring.....	118
Figure 5-6: GFCI and Battery Pack Wiring.....	119
Figure 5-7: Control Desk and Computer Wiring .....	120
Figure 5-8: GAS Set-Up Wiring.....	121
Figure 5-9: Dyno Set-Up Wiring .....	122
Figure 5-10: Eagle 500W CPU Power Supply Wiring.....	123

Figure 5-11: Electric Fans Wiring .....	124
Figure 5-12: Terminal Block Layout in Control Cabinet .....	125
Figure 5-13: Terminal Block Layout in Control Cabinet (continued) .....	126
Figure 5-14: Wiring Bundle Distribution in Control Cabinet.....	127
Figure 5-15: Natural Frequency Amplitude Response Plot .....	135
Figure 5-16: Spring-mass diagram for the Sensor Tech and R+W couplings set-up.....	135
Figure 5-17: Caveat #1 Mode Amplitudes for Each Mass in the Spring-Mass System ...	141
Figure 5-18: Caveat #2 Mode Amplitudes of Each Mass .....	141
Figure 5-19: Mass-Spring Diagram of Interface Torque Sensor with Caveat #1 Shown (Coupler and Torque Sensor Shaft Springs Paired Together) .....	142
Figure 5-20: Detailed View of Caveat #1 with Only the First Three Modes Shown .....	145
Figure 5-21: Mode Amplitude Plot of Caveat #2 for Interface Sensor .....	145
Figure 5-22: Mode-Amplitude Plot of Caveat #1 with the Interface Sensor and the Supplied Interface Coupling.....	146
Figure 5-23: Mode-Amplitude Plot for Caveat #1 with Interface Sensor and BKM Couplings.....	147
Figure 5-24: Binsfeld Torque Sensors .....	148
Figure 5-25: Spring-mass diagram of Binsfeld torque sensor set-up .....	148

## LIST OF TABLES

Table 2-1: Summary of Different Ancillary Services .....	11
Table 2-2: Current Distortion Limits for General Distribution Systems ( $I_{SC}$ and $I_L$ are defined as system short circuit and load size respectively) .....	21
Table 2-3: Voltage Distortion Limits .....	21
Table 2-4: VFD Selection Comparison Chart .....	29
Table 2-5: GBS 40Ah Battery Cell Specifications.....	31
Table 2-6: Jefferson Electric 150kVA Transformer Specifications .....	34
Table 2-7: Voltage/Frequency Sensor Comparison .....	38
Table 3-1: Required Make-Up Power by the Power Supply Calculations.....	58
Table 3-2: Compilation of Torque Sensors Considered for Selection.....	69
Table 3-3: Coupling Selection Values.....	70
Table 3-4: Design Comparison for Different Mounting Box Designs.....	76
Table 5-1: PCM 35 Pin Assignments .....	129
Table 5-2: PCM 25 Pin Assignments .....	130
Table 5-3: Absorber Inverter Feedback Cable Assignments for Dyno and GAS Set-Ups	130
Table 5-4: UUT Feedback Cable Pin Assignments.....	131
Table 5-5: Deutsche Pin Battery Connector Assignments .....	132
Table 5-6: Colored Bundle Assignments and CAN Labeling.....	132
Table 5-7: Sensor Tech with R+W Couplers Caveat Comparison Results .....	140
Table 5-8: Interface Sensor with R+W Couplers Caveat Comparison.....	144

Table 5-10: Interface coupling comparison results (all using caveat#1) .....	146
Table 5-12: Binsfeld natural frequency results .....	149
Table 5-14: Summary of Natural Frequency of Different Torque Sensors and Couplings (lowest reported natural frequency shown for each case) .....	150

## LIST OF ABBREVIATIONS

AVS	-	Artisan Vehicle Systems
AE	-	Advanced Energy
AFE	-	Active Front End
BMS	-	Battery Management System
CAN	-	Controller Area Network
cRIO	-	Compact RIO Data Acquisition Chassis
CSU	-	Colorado State University
DAQ	-	Data Acquisition
Dyno	-	Dynamometer
eDTC	-	Electric Drivetrain Teaching Center
EMF	-	Electromotive Force
EVs	-	Electric Vehicles
FPGA	-	Field-Programmable Gate Array
GAS	-	Grid-Attached-Storage
GFCI	-	Ground Fault Circuit Interrupter
GUI	-	Graphical User Interface
ICE	-	Internal Combustion Engine
PCC	-	Point of Common Coupling
PCM	-	Powertrain Control Module
POI	-	Point of Interference

SAW	-	Surface Acoustic Waves
SOC	-	State of Charge
UUT	-	Unit Under Test
V2G	-	Vehicle to Grid
VFD	-	Variable Frequency Drive



## **1. Introduction to the Electric Drivetrain Teaching Center**

The purpose of this section of the paper is to describe the motivation behind the Electric Drivetrain Teaching Center (eDTC) for both the educational and the research components of the lab, the research possible in the lab, and finally the objectives for both the drive-train teaching configuration and grid-attached-storage (GAS) configuration of the lab.

### **1.1 Motivation for Education**

In the U.S. there are over 137 million passenger vehicles on the road using the finite source of fossil fuel available on Earth. The United States of America has plans to reduce this heavy dependence on fossil fuels, particularly on liquid fossil fuels <sup>(Bureau of Transportation: Statistics, 2010)</sup>. President Obama proposes to have 1 million hybrid vehicles on the road by 2015 in order to reduce these emissions and the country's dependence on foreign oil <sup>(Mitlitski, 2011)</sup>. Additionally, the American Recovery and Reinvestment Act supported increased growth in the electric vehicle sector. Due to these initiatives, the need for educated and trained students by automotive manufactures and clean technology companies is increasing. Ford plans to hire 7,000 new employees to manufacture hybrid and electric vehicles and BMW seeks to hire 2,600 new employees for hybrid and electric system designs <sup>(Naughton, 2011) (Reiter, 2010)</sup>. With these anticipated job openings, the demand for students educated in hybrid vehicle technologies is increasing

substantially. However, educational research has shown that a key component to successful engineering students is hands-on experience<sup>(Warrington, Kirkpatrick, & Danielson, 2010)</sup>. Therefore, there is a need for a facility to provide real world training for students with electric vehicle technology. Research has also shown that “...students have indicated that using testing stations aids significantly in their understanding”<sup>(Slocombe, Wagner, Heber, & Harner, 1990)</sup>.

Currently, most vehicle drivetrain test systems are designed to test conventional, that is internal combustion engines, drivetrains, and do not readily accommodate electric drivetrain architectures. Electric drivetrain test systems must include special considerations to account for the use of regenerative braking and electrical system components not found in conventional drivetrains, including the harmonics generated by the inverters and support for power electronics<sup>(Gavine, 2011)</sup>. Development of drivetrain test benches for conventional vehicles is a well-understood science, based upon many years of experience. However, since the electric drive train and battery components differ greatly from conventional vehicle drivetrains, experience gained from these applications is only partially transferable to electric vehicle, battery, and grid testing<sup>(Uhlenbrock, 2010)</sup>.

There are independent test stands for traction drives and batteries but none that integrate the two with grid regeneration. For battery-grid interaction, most test labs emulate the battery using a suitable power supply, or utilize a scaled battery. Few test stands utilize full-scale automotive battery pack, including the associated protection and thermal management systems.

## 1.2 Motivation for Grid-Attached-Storage Research

Grid-attached-storage (GAS) research studies the use of energy storage that is connected to the grid and can be used to either discharge or store energy when desired. GAS research exists at two scales, based upon the size of the battery system – distributed, vehicle level, storage, such as Vehicle-to-Grid (V2G) - and scale-model testing of utility-scale storage.

As more electric vehicles (EVs) enter the garages of U.S. homes and businesses, utilities are faced with an increasing problem of meeting increased electrical energy demand. Utilities are also under pressure to reduce use of fossil fueled generation <sup>(Hadley & Tsvetkova, 2008)</sup>. Consumer preferences for when to charge their EVs could challenge utilities and charging service providers by increasing grid congestion if charging occurs simultaneously with peak electricity demand. Specifically, utilities are concerned that cars that will return from the evening work commute and begin charging immediately, at a time when the demand is typically at peak levels. Solutions have been proposed to mitigate this problem include: controlled charging and using V2G to assist utilities in the provision of ancillary services, such as peak shaving (e.g. demand response), frequency regulation and renewables firming.

Several studies have estimated the impact of significant penetration of plug-in electric vehicles – whether hybrid or purely electric – on the national grid <sup>(Duvall, 2008)</sup>, <sup>(Short & Denholm, 2006)</sup>, <sup>(Denholm & Short, 2006)</sup>. Pacific Northwest National Laboratory stated: “... for the United States as a whole, 84% of U.S. cars, pickup trucks and sport utility vehicles (SUVs) could be supported by the existing infrastructure, although the local percentages vary

by region. This has a gasoline displacement potential of 6.5 million barrels of oil equivalent per day, or 52% of the nation's oil imports," (Kintner-Meyer, Schneider, & Pratt, 2006). Mike Duvall of the Electric Powertrain Research Institute, adds, "a few decades from now, there will be a 60 percent market share for plug-in hybrids which would add 6 to 7 percent to electrical demand. The U.S. can handle most of this with existing capacity if utilities and consumers have smart charging dialed in correctly," (Brockman, 2008). These reports highlight that significant penetrations of electric and plug-in hybrid electric vehicles can be accommodated with existing infrastructure if charging locations and timing can be controlled.

Many researchers have studied the process of utilizing electric vehicles to provide energy storage or ancillary services, known as vehicle to grid. Studies have shown that the adoption of V2G has many variations and implications<sup>(Parks, Denholm, & Markel, 2007), (Vazquez & Lukic, 2010), (Kempton, Udo, & Huber, A Test of Vehicle-To-Grid (V2G) for Energy Storage and Frequency Regulation in the PJM System, 2008), (Kempton, Tomić, Letendre, Brooks, & Lipman, 2001), (Kempton & Tomić, 2005), (Moura, 2006), (Turton & Moura, 2008), (Tomić & Kempton, 2007)</sup>. More recent studies have identified challenges with the V2G model including reliability and aggregation challenges<sup>(Quinn, Zimmerle, & Bradley, 2009)</sup>.

In addition to the global and techno-economic impacts listed above, integration of vehicles into power systems may cause local power quality and control issues that would benefit from laboratory testing of grid integration. Miller reports that, "voltage depressions and power interruptions are rapidly becoming two of the hottest topics in the field of power quality. Of particular interest is the need to supply a dependable,

efficient and controllable source of real and reactive power, which is available instantly to support a large (greater than 0.5 MVA) load, even if the utility connection is lost”

(Miller, Zrebiec, Delmerico, & Hunt, 1996). Other studies have also indicated that distributed batteries may be advantageous for ancillary services and energy buffering to minimize distribution congestion<sup>(UC Davis, 2010)</sup>. Distributed, vehicle-scale battery storage provides an attractive platform for providing such services.

Utilization of renewable resources such as wind, water, and solar has become a key method to reduce fossil fuel consumption for electricity generation. However, most renewable energy resources produce intermittent power, increasing the risk of voltage and frequency instability, and requiring additional power generation assets to “fill in” when renewable resources are not producing. In the case of instabilities, energy storage systems, particularly short-term buffering or “power smoothing” resources, will become increasingly essential to grid operations.

Current research focuses on modeling and simulation to understand GAS but little testing has been completed, particularly for islanded power systems or high-speed applications of grid-connected systems. Real results can help automotive companies, utilities, municipalities, and other intermediaries to make educated decisions on component packaging, testing, safety, and charging related to GAS.

### **1.3 Modes of Education for Dynamometer Laboratory**

As stated above in the motivation section, there exists a need for students to obtain real world, hands-on experience to supplement traditional coursework. For vehicle studies, a lab should provide a safe environment to experience dynamometer

concepts, electric motors, inverters, controllers, data acquisition, high voltage safety, and experimental methods. Students can learn about torque curves, efficiency maps, and controller strategies in traditional classroom instruction, but only real world interaction with a motor test stand can translate classroom instruction into a rounded learning experience. The laboratory presented here is primarily targeted at supplementing classroom instruction, with secondary objectives as a research platform.

#### **1.4 Modes of Research for Grid-Attached-Storage**

Several different modes of GAS research are currently being studied at national labs, universities, and in industry, at a variety of size scales. One useful method to classify GAS research is to classify based upon the operational timescale of the GAS control algorithms: Slow – operating at a time scale of minutes to hours – or fast – operating at time scales of milliseconds to minutes. “Slow” timescale applications focus on energy-related topics, such as arbitrage and peak shifting, which:

- Require large amounts of energy storage relative to charge/discharge rates, i.e. “low-C” rated storage systems,
- Use relatively slow control algorithms, typically in the range of 1-4 second control loops,
- Are primarily driven by economic criteria such as variable electricity pricing.

“Fast” timescale applications focus on power-balance topics, such as frequency regulation, which:

- Require relatively small amounts of energy storage relative to charge/discharge rates – i.e. “high-C” rated storage systems,
- Use fast closed-loop control algorithms, typically in the range of milliseconds,
- Are primarily driven by technical criteria, such as frequency or voltage stability.

The classification of GAS into “fast” and “slow” categories is not clear-cut; some applications (e.g. wind firming) could fall into either category, depending upon the objectives being optimized.

Vehicle battery systems are better tuned for “fast” applications, and that is the primary target for the GAS research capability of this laboratory. It is also important to note that GAS mode of the laboratory was designed with research, not teaching, in mind.

## **1.5 Objectives of the eDTC**

The eDTC at Colorado State University will have two focuses: research and education. Corresponding to these are grid-attached-storage and electric vehicle dynamometer education respectively. These two focuses each have their own objectives that contribute to the key areas of study mentioned above in the motivation sections.

The GAS lab is primarily focused on research, and its objectives are:

- To provide a research facility that utilizes industry-standard components, at production scale.

- To provide a flexible development platform for research into GAS systems.

Typical questions that could be researched in the lab include:

- Integration of GAS systems into grid systems
- Dynamic response of automotive-type components in GAS applications
- Battery degradation and life-time impacts of GAS operation modes
- Development of control algorithms for GAS applications

The dynamometer component of the eDTC lab is primarily focused on education, and its objectives are:

- To educate students about electric vehicle components such as motors and inverters.
- To support development of laboratory hardware and coursework for vehicle power plant testing and experiments.
- To provide an environment for learning experimental methods.

Typically, educational topics include:

- Dynamometer fundamentals
- Motor torque curves
- Motor-Inverter efficiencies
- Temperature effects

While each mode of operation has different objectives, the two operational modes must utilize the same components (i.e. inverters, wiring, emergency stop circuits, cooling circuits, etc.) whenever possible to reduce cost and space.



The next two chapters describe the GAS research mode Chapter 2 and the dynamometer mode in Chapter 3. Each chapter contains a description of the challenges, design, and results for each system. Finally, Chapter 4 presents summary results and conclusions.

## **2. Grid-Attached-Storage**

This chapter discusses the current GAS research (Section 2.1), the design challenges (Section 2.3), design implementation (Section 2.4), and testing checkout results (Section 2.5) of the GAS portion of the eDTC lab.

### **2.1 Grid-Attached-Storage Background**

In order to understand the design of the GAS portion of the eDTC, this section introduces the range of GAS research topics envisioned for the laboratory. These topics include: an introduction of ancillary services (Section 2.1.1), energy arbitrage (Section 2.1.2), renewables firming (Section 2.1.3), battery second use (Section 2.1.4), and islanded power grids (Section 2.1.5). While this is not a comprehensive coverage of GAS research topics, it identifies the topics for which the lab was designed.

#### **2.1.1 Ancillary Services**

Utilities must balance load and generation on a second by second basis. To maintain this balance, utilities engage in forward planning, ranging from hours to years in advance of the current period. They also maintain reserve capacity at all times, to compensate for unforeseen events such as loss of a generation unit, and to balance between load forecasts and actual load. Reserves are typically provisioned using “ancillary services” – i.e. generation services beyond simple energy production. Table

2-1<sup>(Kirby, 2004)</sup> shows a typically set of ancillary services and their response speeds, durations, and cycle times.

**Table 2-1: Summary of Different Ancillary Services**

Service	Service Description		
	<i>Response Speed</i>	<i>Duration</i>	<i>Cycle Time</i>
Regulation	Power sources online, on automatic generation control, that can respond rapidly to system-operator requests for up and down movements; used to track the minute-to-minute fluctuations in system load and to correct for unintended fluctuations in generator output to comply with Control Performance Standards (CPSs) 1 and 2 of the North American Reliability Council (NERC 2002)		
	<i>~1 min</i>	<i>Minutes</i>	<i>Minutes</i>
Spinning reserve	Power sources online, synchronized to the grid, that can increase output immediately in response to a major generator or transmission outage and can reach full output within 10 min to comply with NERC's Disturbance Control Standard (DCS)		
	<i>Seconds to &lt;10 min</i>	<i>10 to 120 min</i>	<i>Days</i>
Supplemental reserve	Same as spinning reserve, but need not respond immediately; units can be offline but still must be capable of reaching full output within the required 10 min		
	<i>&lt;10 min</i>	<i>10 to 120 min</i>	<i>Days</i>
Replacement reserve	Same as supplemental reserve, but with a 30-min response time; used to restore spinning and supplemental reserves to their pre-contingency status		
	<i>&lt;30 min</i>	<i>2 hours</i>	<i>Days</i>
Voltage control	The injection or absorption of reactive power to maintain transmission-system voltages within required ranges		
	<i>Seconds</i>	<i>Seconds</i>	<i>Continuous</i>

As seen above from Table 2-1, there are many different services that utilities must use to maintain proper power supply each with different characteristics. Eyer shows there are many potentials for GAS based on the operational scenarios desired<sup>(Eyer & Corey, 2010)</sup>. One way to choose between the different services is based on comparing time scales. At a time scale of hours or longer, GAS units can be utilized for energy arbitrage – i.e. charging the battery when electricity is less expensive and then discharging when energy prices are higher. In shorter time frames, milliseconds to

minutes, GAS units can be used for voltage and frequency regulation. Voltage and frequency control require the fastest response speeds of the types of ancillary services shown in Table 2-1. These applications are of high importance to many researchers because they require rapid changes between charge and discharge operations that are difficult to manage and create uncertain impacts on battery life. Additionally, current research has found that the greatest near-term economic return for grid storage is quick-response, high-value electric services <sup>(Brooks, 2002)</sup>.

In regulation and voltage control applications, batteries have several crucial strengths relative to other generation systems. Batteries have a fast dynamic response, allowing them to vary discharging (and charging) rates quickly, unlike large thermal generation units. Batteries can also transition rapidly from an off-line status full operation, often within seconds. However, batteries are expensive, due to high up-front capital costs and short operational lives, relative to other generation assets.

The next sections discuss several applications of battery-based GAS, both ancillary services and other applications.

### **2.1.2 Energy Arbitrage**

Infrequent but high electricity demands – commonly known as peak demands – place significant strains on grid operations. One method of reducing peak demand is to shift demand to non-peak periods, a process commonly known as “peak shifting.” In electrical markets with time-of-use or real-time pricing, peak shifting applications can be economically driven by energy arbitrage: Capturing electricity at times of low pricing, and selling it back to the utility at times with higher pricing <sup>(Sioshansi, Denholm, Jenkin, & Weiss,</sup>

<sup>2009</sup>). For example, for Pacific Gas and Electric, high prices occur during peak pricing periods, which are noon to 6:30pm and low prices occur during nighttime hours of 9:30pm to 8:30am<sup>(Pacific Gas and Electric, 2011)</sup>. Energy arbitrage using existing price structures provides a method to evaluate the economics of a particular GAS technology<sup>(Eyer & Corey, 2010)</sup>.

As mentioned above, V2G is one method that has been proposed to implement energy on a large scale. The practical impacts of V2G, however, have not been fully tested. Test results could illuminate energy arbitrage performance, grid impacts, and the impact of repeated deep cycling on vehicle batteries. Vehicle owners are worried that if they participate in energy arbitrage, their car will not be charged and ready for use when needed. Since most electric vehicles for sale on the market today have an empty-to-full charge time of 8-10 hours, the charging period could play a substantial role on customer acceptance<sup>(EPRI, 2011)</sup>. In addition, researchers are currently modeling penetration rates, time of charge, and state of charge of battery to determine usefulness of energy arbitrage<sup>(Quinn, 2011)</sup>. However, little research has utilized physical system testing to show validity of chosen control algorithms, to quantify the impact on vehicle batteries, or to help utilities and consumers make educated decisions.

Utilities can also use GAS to create additional demand when system load is lower than the lowest practical operation output of its conventional generators. “Since it can take many hours to ramp up fossil fuel-fired generation, the utility cannot simply curtail the primary generation during periods of low demand. Consequently the utility curtails renewable production instead (wind at night, solar during the day) and supplements

with fossil fueled backup”<sup>(Demand Energy, 2011)</sup>. Alternatively, utilities could utilize GAS to save power during these periods for use during periods of high demand.

### **2.1.3 Renewable Energy Firming**

Many renewable electricity generation systems (e.g. solar or wind) typically produce power intermittently, when the resource is available. The “challenge of load balancing when the grid has a substantial portion of variable generation, and the costs associated with providing dispatchable power to back up that variable generation, raises the bar even higher [on grid control]”<sup>(Jost, 2011)</sup>. One possible approach is to utilize GAS systems to convert intermittent resources into “firm” generation sources – i.e. generators that produce power output that can be predicted hours to days in advance. This application is commonly known as “firming,” and is most often applied to wind farms as “wind firming.”

In this case, GAS allows a renewable power producer to establish a firm power production contract with a utility. To account for unpredictability in power production, the power producer utilizes a GAS system to ensure a consistent power output over the contract period<sup>(Walawalkar & Apt, 2008)</sup>.

Where large amounts of renewables are connected to weak or small grid systems, variable renewable power output can also create local frequency or voltage instabilities. Several studies have been conducted to determine the technical and economic feasibility of GAS as a method for smoothing unpredictable frequency spikes (millisecond time scale)<sup>(Bredenberg, 2011), (Sandia National Laboratories, 2010), (Goggin, 2008), (Levitan, 2010),</sup>

<sup>(McGuinness & Fields, 2011)</sup>.

#### **2.1.4 Second Use Batteries**

Utilizing batteries after their useful life in electric vehicles, an application frequently termed “second life,” has also been a topic of recent research for GAS. The defining point for end-of-life for electric vehicle batteries is defined as the point when a battery has lost 20% of its original energy storage capacity or 25% of its peak power capacity<sup>(Wolkin, 2011)</sup>. While this definition is somewhat arbitrary and still in flux, it recognizes that an electric vehicle depends upon its battery to provide sufficient energy to meet range expectations and peak power to meet acceleration requirements. A battery that no longer meets automotive requirements still has significant storage and power capacity ... but either or both has fallen below levels acceptable to the vehicle owner.

Used automotive batteries can be utilized in several applications before they are deemed unusable and need to be recycled. Applications include: back-up power supplies, utility stationary power supplies, emergency power supplies, and renewable energy storage. In all these cases, both the initial and secondary customer can have cost savings. However, numerous barriers have been identified<sup>(Cready, Lippert, & Phil, 2003)</sup>.

According to Neubauer, second use of batteries is limited due to: “sensitivity to uncertain degradation rates in second use, high cost of battery refurbishment and integration, lack of market mechanisms and regulations, and the perception of used batteries”<sup>(Neubauer & Pesaran, 2010)</sup>.

Initial research has indicated that several alternatives exist for second use before the battery is dismantled for recycling, including grid applications such as: frequency

regulation, energy buffering, and energy arbitrage. Battery re-use for grid purposes is also seen as an opportunity to reduce vehicle price through reduced recycling costs (Neubauer & Pesaran, 2010). Other battery cost reduction options that may drive vehicle cost down include leasing and increased standardization (Williams, 2010).

Research at EPRI (Electric Power Research Institute), University of California at Davis, Sandia, and NREL (National Renewable Energy Laboratory) has made suggestions for “second life” applications, but little of this research includes realistic physical testing. Since there are many factors that determine the viability for second life batteries, more specific case studies are required to prove economic, performance, and lifetime viability of battery second use. Even tests on new batteries, such as testing performed by Xcel Energy using batteries for frequency regulation, recommended that additional testing is necessary to determine the rate of long-term damage caused by rapid, frequent charging and discharging of the battery (Himelick & Novacheck, 2010). Southern California Edison and DTE Energy also conducted real world testing of GAS applications. They used a large system constructed using battery packs built by A123Systems to charge and discharge energy at large wind power and solar power sites (Gupta, 2009).

These field tests used new batteries since large-scale packs of used batteries are currently unavailable. As a result, the performance characteristics of used automotive packs are unknown.

#### **2.1.5 Islanded Power Grids, Expeditionary Military, or Emergency Uses**

The stabilization of electric microgrids utilized in emergency or expeditionary military environments represents a technically distinct application of GAS systems.



These microgrids are small “island” power systems, unattached to any continental-scale grid. They are characterized by multiple, small, local generation sources servicing local loads. Expeditionary military bases face some of the highest fuel costs for electricity generation <sup>(Coomb, 2011), (Sheets, 2011)</sup>. Therefore, these system operators have a strong incentive to implement renewables to displace fuel consumption. However, implementation of high-penetration renewables on islanded grids may cause significant voltage and frequency transients due to instantaneous power imbalance between load and generation. In these applications, GAS could be implemented at a scale similar to automotive battery applications – typically 5-100KW – to dynamically eliminate power imbalance, and thus the associated transients. This makes the use of automotive-grade equipment an attractive source of robust, inexpensive components for small GAS systems. While this application has been modeled in simulation studies, physical testing has been rare. In addition, physical testing is required to better understand component requirements and integration into microgrid systems.

## **2.2 System Overview**

The purpose of this section is to introduce the key components of the GAS laboratory as a basis for subsequent discussion.

The key components necessary for grid-attached-storage are: a battery pack, an inverter, an LC filter, and a transformer. Figure 2-1 shows a simplified block diagram of the major components of the GAS system and their configuration.

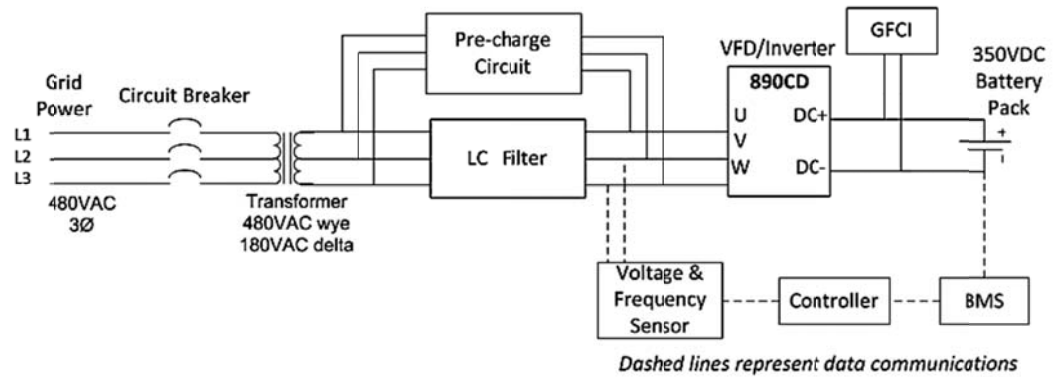


**Figure 2-1: Simplified Layout of Grid-Attached-Storage Equipment**

Beginning at the right hand side of Figure 2-1 and working left, the components are:

- 1) The electric vehicle battery pack, which stores electricity.
- 2) The inverter, which inverts the DC voltage into grid-frequency AC when discharging, and rectifies AC grid power into DC power when charging.
- 3) The LC filter with a pre-charge circuit, which filters out the switching harmonics created in the inverter.
- 4) The transformer steps up the inverter voltage to the grid voltage, which is 480V<sub>AC</sub> in this laboratory.
- 5) Between the inverter and the LC filter is a voltage measurement device, the output of which is used to determine voltage and frequency output of the inverter.
- 6) The voltage and frequency measurements are fed to a controller, which adjusts set points for the inverter and battery management system (BMS) to meet system performance goals.

The key component to the system is the variable-frequency drive (VFD), also referred to as an inverter, which is equipped with a line synchronization card to allow the drive to synchronize with the grid as a line-synchronized inverter. The system also contains protection elements, such as ground-fault circuit interruption (GFCI) to monitor battery isolation, a battery management system (BMS), and circuit disconnects. The following section will discuss the challenges associated with these components.

## **2.3 Challenges to Overcome**

This section of the grid-attached-storage lab describes the challenges with designing and constructing a lab with automotive grade, full scale components. Key design issues include the compliance with standards (Section 2.3.1), differences in cooling requirements between industrial and automotive equipment (Section 2.3.2), voltage mismatch between the automotive battery pack and the grid connection (Section 2.3.3), and time delay impacts on designing a voltage/frequency measurement device (Section 2.3.4).

### **2.3.1 Comply with Standards**

While the utilization of automotive components provides unique research capabilities, these components create special concerns with grid-attached operation. Inverter output must meet appropriate grid interconnection standards, including IEEE-519, thus requiring an LC filter and active front end (AFE) control. During normal operation the variable frequency drive (VFD) produces significant current harmonics, which can cause substantial impacts to other local loads or violate grid interconnection

standards. Current harmonics can distort the supply voltage, overload electrical distribution equipment (such as transformers) and resonate with power factor correction <sup>(Hoevenaars, 2003)</sup>. The standard IEEE-519 sets requirements for harmonic control in electrical power systems. IEEE-519 was first introduced in 1981 to provide direction on dealing with harmonics introduced by static power converters and other nonlinear loads. Section 10.1 of IEEE-519 says: "The recommendation described in this document attempts to reduce the harmonic effects at any point in the entire system by establishing limits on certain harmonic indices (currents and voltages) at the point of common coupling (PCC), a point of metering, or any point as long as both the utility and the consumer can either access the point for direct measurement of the harmonic indices meaningful to both or can estimate the harmonic indices at point of interference (POI) through mutually agreeable methods." <sup>(Blooming & Carnovale, 2007)</sup>. Table 2-2 and Table 2-3 highlight the limits recommended by IEEE-519.

**Table 2-2: Current Distortion Limits for General Distribution Systems ( $I_{sc}$  and  $I_L$  are defined as system short circuit and load size respectively)**

Current Distortion Limits for General Dist. Systems (120 V – 69 000 V)						
Maximum Harmonic Current Distortion in Percent of $I_L$						
Individual Harmonic Order (Odd Harmonics)						
$I_{sc}/I_L$	$<11$	$11 \leq h < 17$	$17 \leq h < 23$	$23 \leq h < 25$	$35 \leq h$	TDD
$<20^*$	4.0	2.0	1.5	0.6	0.3	5.0
$20 < 50$	7.0	3.5	2.5	1.0	0.5	8.0
$50 < 100$	10.0	4.5	4.0	1.5	0.7	12.0
$100 < 1000$	12.0	5.5	5.0	2.0	1.0	15.0
$>1000$	15.0	7.0	6.0	2.5	1.4	20
Even harmonics are limited to 25% of the odd harmonic limits above.						
Current distortions that result in a dc offset, e.g., half-wave converters, are not allowed						
* All power generation equipment is limited to these values current distortion, regardless of actual $I_{sc}/I_L$						

Notice that there are stricter limits for larger load and weaker systems as well as for higher order current harmonics.

**Table 2-3: Voltage Distortion Limits**

Bus Voltage at PCC	Individual Voltage Distortion (%)	Total Voltage Distortion THD (%)
69 kV and below	3.0	5.0
69.001 kV through 161 kV	1.5	2.5
161.001 kV and above	1.0	1.5
NOTE: High-voltage systems can have up to 2.0% THD where the cause is an HVDC terminal that will attenuate by the time it is tapped for a user.		

As the use of variable frequency drives and other non-linear loads has grown more common, IEEE-519 is being adopted by more utilities as a standard. In the particular case of the eDTC laboratory, Fort Collins Utilities requires IEEE-519 compliance for all grid-attached devices which generate electricity, either as a primary function (e.g. photovoltaic system) or as a side effect of usage (e.g. regenerative VFD).

### 2.3.2 Unusual Cooling Requirements for Industrial Labs

Most industrial inverters or VFDs are air-cooled while automotive units require liquid cooling loops. Typically, industrial inverters have sufficient space and are therefore mounted in large cabinets using forced-air cooling. In contrast, automotive inverters are designed to be mounted in confined spaces within vehicles where there is insufficient space or access to outside air to utilize air-cooling. Therefore, automotive inverters and motors typically utilize liquid cooling circuits. This circuit presents design issues with the construction of the lab. These additional requirements include layout, temperature control, and proper pumping performance. Therefore, an automotive-grade water-cooling circuit must be implemented, utilizing a radiator and electric fan combination, similar to the set-up in a vehicle.

Given the required cooling specifications from the inverter and motor suppliers, a liquid cooling circuit was constructed. Figure 2-2 illustrates the major system components.

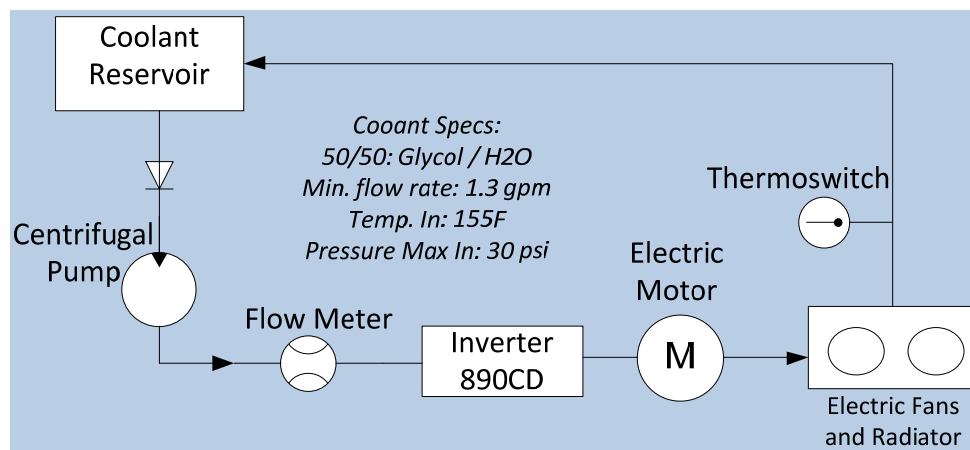


Figure 2-2: Liquid Cooling System Layout

The cooling system is divided into two identical circuits, one for each inverter-motor pair, to ensure proper cooling when the units are asymmetrically loaded. Each circuit utilizes a continuous 10gpm centrifugal pump running through a flow meter, an automotive radiator with an electric fan, and an automotive closed loop thermocouple relay switch to activate the fans.

The cooling circuit uses electric fans and radiators from a 1992-1998 Honda Del Sol. These were chosen based on small size, 12V<sub>DC</sub> operation, and low cost. A decision was made to isolate thermal management from the control system to simplify control modifications for research projects. This adds a degree of separation between the control system of the lab and the cooling circuit, increasing overall system safety should the computer for the controller crash. Automotive thermocouples and relays are used to monitor the cooling circuit and activate cooling fans, without requiring any interface from the control system.

### **2.3.3 Voltage Mismatch**

The laboratory is connected to the grid at the standard industrial service voltage of 480V<sub>AC</sub> 3-Phase. In contrast, the battery voltage typical of automotive applications is typically between 350 and 250V<sub>DC</sub>. As the state of charge (SOC) of the battery declines, the voltage of the pack decreases. The automotive VFDs utilized for the laboratory do not contain a “boost” section, typical of photovoltaic inverters. Therefore the maximum AC output voltage is constrained by the DC voltage applied to the inverter by the battery. The VFD utilized in the eDTC outputs 208V<sub>AC</sub> 3-Phase at mid-to-high battery voltages. At lower battery voltages the inverter output voltage drops as low as 184 V<sub>AC</sub>.

This lower voltage is not a common voltage for transformers, which are designed for 208-480V<sub>AC</sub>. Ideally, a custom-designed transformer would be procured with the optimum turns ratio of 184:408. However, custom transformers were beyond the budget available for this laboratory. Instead, the lab utilizes standard 208:480 transformer equipped with a -10% connection tap on the 208 V side. Use of the -10% tap provides an effective turns ratio of 187:480, sufficiently close to the 184 V for operation of most of the usable range of the battery.

In field applications, two methods exist to eliminate this voltage mismatch, should companies wish to reduce the size, cost, and complexity of similar systems. The first method is to specify a higher voltage battery, allowing the inverter to operate at the grid voltage over the entire voltage range of the battery. This option would require a 600 to 750V<sub>DC</sub> battery pack for direct interconnection to 480V<sub>AC</sub>. The tradeoffs to this design include costs related to the higher DC voltage and a significantly larger battery system. Alternatively, the inverter could be equipped with a boost converter to match the DC battery voltage to the desired AC voltage. Since the boost section is unneeded during normal vehicle operation, a bypass circuit or bypass mode would be required.

#### **2.3.4 Time Delay Impact on Voltage/Frequency Measuring Device**

In all operation modes, accurate measurement of voltage and frequency is required in order to properly control the output of the GAS system. In addition, for stability applications, such as the small-islanded systems described earlier, the latency of voltage and frequency measurements is particularly critical. Measurements must be completed quickly enough to support high-speed control algorithms. The active control



loop can be represented by five delay components: voltage measurement, frequency calculation, controller latency, inverter response, and LC filter response. This loop represents the time required to extract information from the voltage signal, exercise the feedback control algorithm, and then execute the control signal in the inverter. Figure 2-3 highlights these steps.

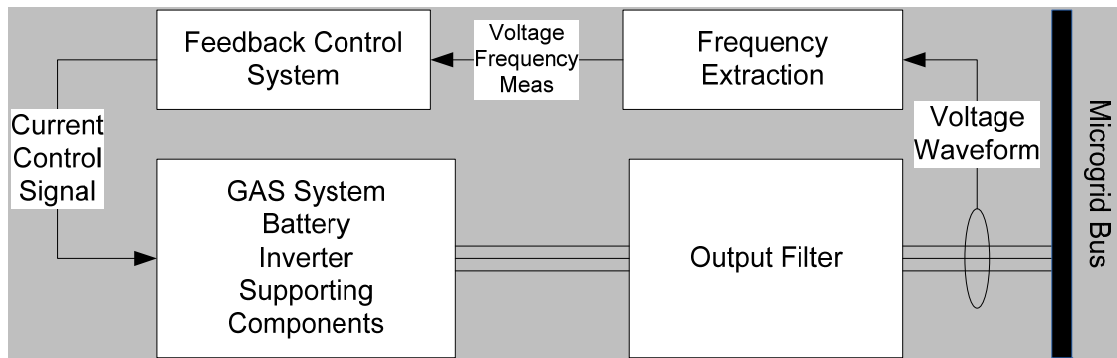


**Figure 2-3: Control Loop for GAS Systems**

Since control algorithms will frequently change during the life of the system, all potential algorithms will rely upon the fundamental measurement capabilities designed into the system. These measurements need to be carefully designed to allow the widest range of algorithms to be tested. And according to Zimmerle, simulation and test results indicate that a key contributor to GAS system performance is the measurement delay in frequency measurements <sup>(Lutz, Zimmerle, Huff, & Bradley, 2011)</sup>.

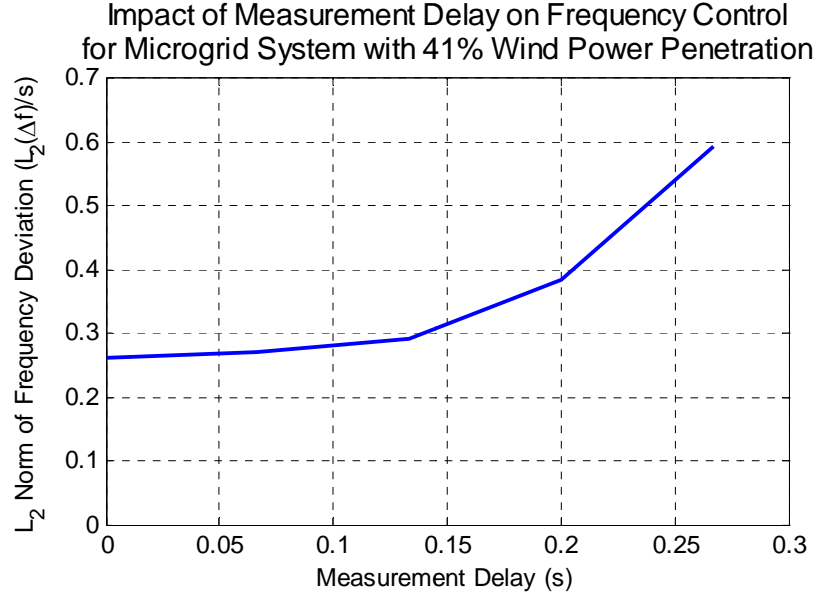


**Figure 2-4: Impact of Measurement Delay on Microgrid Performance**

Figure 2-4 illustrates typical results from a simulation of a small microgrid with constant load and a wind power penetration of approximately 41%. In this test, the GAS system is responsible for primary frequency control – i.e. the control system reads system frequency and adjusts battery output to maintain a constant frequency set point, as illustrated in Figure 2-3. For this experiment, all control system functions are held constant, except for a variable delay in the frequency measurement function. Performance of the system is shown as an  $L_2$  norm of frequency error, normalized to per-second values. Equation 1, shown below, highlights this.

$$\epsilon = \frac{L_2\{f - f_{nom}\}}{T} \quad (1)$$

From Figure 2-4, measurement delays in the range of 0-8 cycles (0-130 ms) have minimal impact on control system performance. Above 8 cycles, performance degrades quickly. The sensing delay can be considered as the sum of delays from each of the principal components described earlier, as shown Eqn. 2:

$$\tau = \tau_{volt} + \tau_{fmeas} + \tau_{control} + \tau_{drive} + \tau_{filter} \quad (2)$$

Where  $\tau_{volt}$  is the time required to collect the voltage waveform,  $\tau_{fmeas}$  is the time required to convert the voltage waveform to a frequency measurement,  $\tau_{control}$  is the controller cycle time,  $\tau_{drive}$  is the control response time of the VFD/inverter, and  $\tau_{filter}$  is the first-order time constant of the output stages of the inverter, which is dominated by the first-order time constant of the LC filter.

The chosen automotive inverters exhibit fast control response times, with  $\tau_{drive} \leq 10 \mu s$ . The output LC filter exhibits a first-order time constant where  $\tau_{filter} \leq 1.5 ms$ . Utilizing a high-speed controller with anticipated control algorithms, it is believed that the control latency should not exceed 20 ms. However, most low-cost frequency transducers exhibit measurement response times of 100-200 ms while higher-cost transducers, often costing \$800-2000 as an integrated component of a power meter, are inappropriate for small grid systems. To meet cost and performance objectives, a decision was made to compute frequency directly from voltage waveforms. This was achieved using a zero-crossing algorithm capable of producing a frequency measurement every  $\frac{1}{2}$  cycle, from samples collected during the previous half cycle. The resulting delay is approximately data collection time plus computational time, or  $\tau_{volt} \cong 17 ms$  for a 60 Hz system. Due to measurement noise, the computed frequency must be filtered. While the signal filter may be modified during control algorithm development, initial estimates indicate filter characteristics will produce an effective delay of  $20 ms < \tau_{fmeas} < 60 ms$ . Summing estimated response times, the system design will exhibit a total control response time of  $60 ms < \tau < 99 ms$ , which is within

the control requirements of 0-130ms as described above. Simulation results indicate that this response time is adequate for controlling hybrid diesel-wind grid systems operating as small as 100 KW, although control of smaller grids may also be possible.

## **2.4 Design**

Details on the choices for key components are described in this section. Specifics of the inverter selection (Section 2.4.1) as well as its software (Section 2.4.2), the battery pack (Section 2.4.3), transformer (Section 2.4.4), LC filter (Section 2.4.5), cooling circuit (Section 2.4.6), and voltage/frequency measurement device (Section 2.4.7) are included in the following subsections. Lastly, a discussion on the designed safety (Section 2.4.8) is included. The core portion of the system was sourced from Artisan Vehicle Systems (AVS) and was delivered as an integrated system.

### **2.4.1 Inverter/Variable Frequency Drive**

Several suppliers were considered for the selection of the inverters or variable frequency drives. Selections were narrowed based on automotive component use, dual-purpose (GAS and dynamometer) capabilities, cost, and design complexity. Table 2-4 describes three different package options: an Artisan Vehicle Systems (previously called Calmotors) assembly, a combination between an existing Advanced Energy (AE) power supply and AVS, and third, an entire Eaton supplied package.

Table 2-4: VFD Selection Comparison Chart

Package	Three AVS VFDs plus LS Card	AE DC Power Supply plus two AVS VFDs	Three Eaton VFDs
Specifications	(3) 890CD Frame F, Line Sync Card, AFE, Pre-Charge, LC Filter, Connection Kit	(1) AE Summit 57000007D, (2) 890CD Frame F, Line Sync Card, AFE, Pre-Charge, LC Filter, Connection Kit	(1) RGX10014AAP1 Regenerative Drive, (2) SPI140A1-4A3N1 Inverter Drive, AFE, Pre-Charge, DC Chopper, Sine wave Filter
Allows for Grid Connectivity for both dyno and GAS?	Yes	Partially. Dyno: use a simulated battery (power supply), GAS: use a simulated load (P Q demand)	No. Only GAS
Cost	\$31,200	\$22,800	\$35,000
Design Complexity	Simplest	Requires heavy modifications when changing between dyno and GAS modes	Missing parts (motors, PCM, and battery pack) would be from AVS so there would need to be a lot of cooperation between AVS and Eaton when designing the lab

Based on the results from Table 2-4, it was determined that selection number two, the combination design between AVS and AE, would best fit all the requirements of the lab except for regeneration to the grid during dyno mode. The requirement for vehicle simulation favored this implementation of the AVS solution, as the Eaton solution did not have automotive drives. The weakness to this solution is that an additional component (AE DC Power Supply) is needed. Fortunately, the eDTC lab is

housed within the *InteGrid* laboratory of the Engines and Energy Conversion Laboratory, which has volunteered an AE DC Power Supply for utilization when it's not in use.

#### **2.4.2 Active Front End and Line Sync Card**

The active front end (AFE) and line sync card (LS) were sourced from AVS because of the compatibility between the GAS and dynamometer (dyno) mode set-up using the same automotive grade inverter. The LS allows the AFE to monitor the three-phase supply voltage waveform and synchronize the inverter to the grid. Once synchronized, the AFE acts as a four-quadrant, sinusoidal, bi-directional power supply. Since the AFE and LS card are options for the inverter, one inverter can serve two purposes. However changeovers between software, hardware, and cable connections need to be made when switching between GAS and dyno set-up with the inverter.

#### **2.4.3 Battery Pack**

The battery pack was sourced from AVS because it has the same scale and performance as full-size automotive electric vehicle packs. This pack came assembled with a battery management system (BMS), as well as positive, negative, and pre-charge contactors, all packaged within an air-cooled case. The manufacturer of the cells is GBS. Specifications are listed below in Table 2-5.

**Table 2-5: GBS 40Ah Battery Cell Specifications**

<b>Nominal Capacity</b>	40Ah	<b>Working Voltage</b>	Single cell charging : 3.8V
			Battery pack charging : 3.65V
			Single cell discharging : 2.5V
			Battery pack discharging : 2.8V
<b>Max. Charging Current</b>	$\leq 3C$	<b>Max. Discharging Current</b>	Consistent Current : $\leq 3C$
			Impulse Current : $\leq 10C$
<b>Standard Charging Current</b>	0.3~0.8C	<b>Best Charging Current</b>	0.5C
<b>Internal Resistance</b>	$\leq 2.5m\Omega$	<b>Cycle Life</b>	Single cell $\geq 1500$ times (80%DOD)
			Battery pack $\geq 1200$ times (80%DOD)
<b>Temp. resistance of Shell</b>	$\leq 135^{\circ}C$	<b>Working Temperature</b>	Charging : $> 0^{\circ}C$
			Discharging : $-20^{\circ}C \sim 65^{\circ}C$
<b>Self Discharge rate ( month)</b>	$\leq 3\%$	<b>Cell Weight</b>	1.4kg $\pm$ 100g
<b>Energy Density</b>	85-100wh/kg	<b>Power Density</b>	$> 800w/kg$
<b>Dimension</b>	126mm*46mm*180mm		

Several components of Table 2-5 require further definition including: capacity, charging current, discharging current and power density. The capacity of each cell is 40Ah, which is the amount of electric charge, which it can store. This performance is fairly typical of batteries currently utilized in electric vehicles. The charging and discharging current rating is given in units of C, which is a measurement of the continuous current draw that the cell will support. For example, this 40Ah cell with a 10C impulse discharge rating can discharge at 400A during an impulse. Power density is the ratio of power over weight, by cell, and indicates how heavy the cells are compared to other cells producing the same power.

The AVS battery pack features 110 cells in series laid out in a custom designed enclosure to house all the cells, fuses, contactors, wiring, ground fault circuit interrupter

(GFCI), and proper ventilation. Since the pack is designed for lab use, the spacing of the modules within the pack was increased for ease of access and air circulation using only one fan. There are built-in air passages under the pack to flow cool air under and then over the batteries. In a pure automotive application, the cells would be packed more tightly and multiple fans would be used with different air passages. However, since the pack will be used for lab work, it was deemed necessary to have easy access to components should anything fail, need more specific testing, or modifications. Figure 2-5 shows the pack and it's key components.

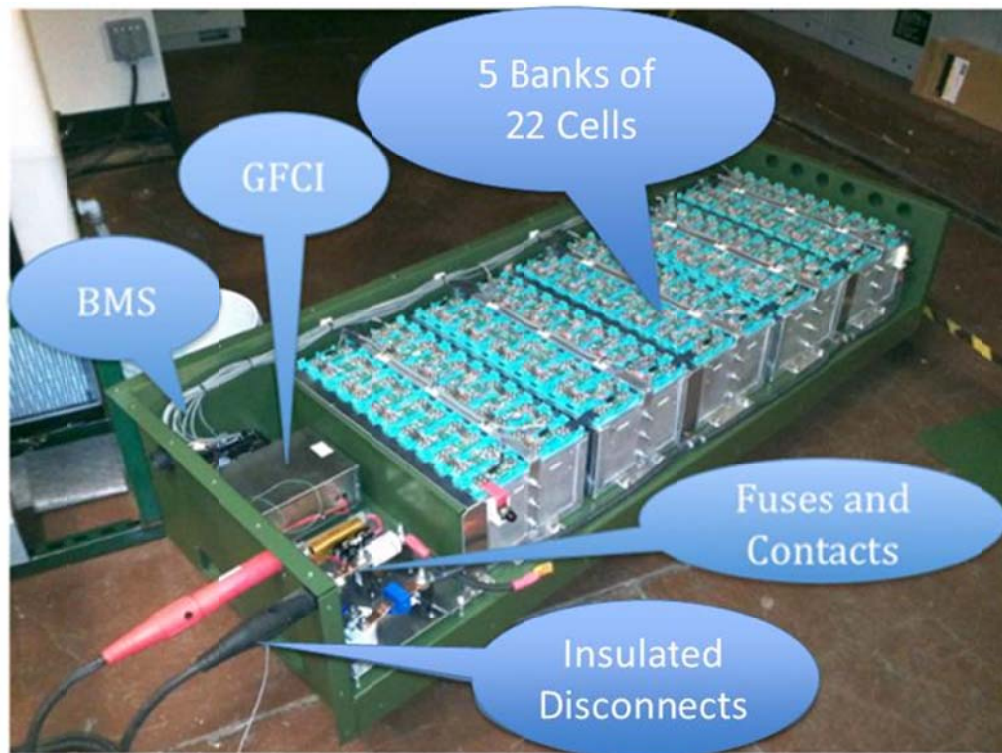


**Figure 2-5: Detailed Highlights of Battery Pack Components**



A closer view of each cell, Figure 2-6, reveals the BMS cell voltage sensors. The BMS monitors each cell voltage, current, and temperature but only reports the max value of the highest cell to the user.

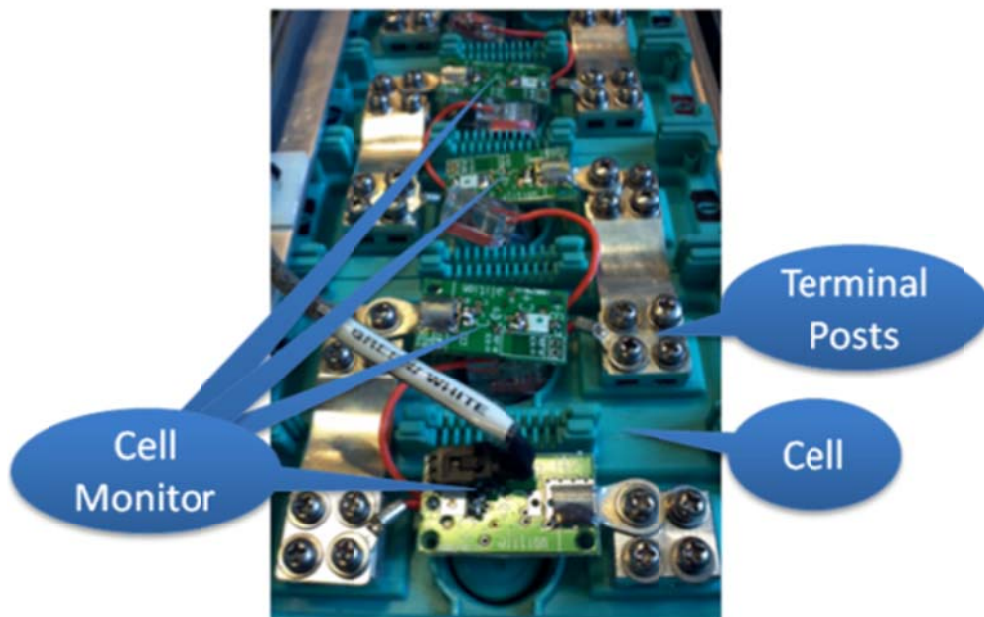


Figure 2-6: Cell Monitors for Each Cell of the Battery Pack

#### 2.4.4 Transformer

The transformer was sized based on the output from the VFD and battery due to voltage mismatch as discussed in the challenges section. Quotes were sent out to different suppliers to provide a transformer that was designed for three-phase, 150kVA, 208V primary, and 480Y/277V secondary. The lowest cost bid was chosen from Jefferson Electric. Specifications are shown in Table 2-6.

Table 2-6: Jefferson Electric 150kVA Transformer Specifications

Transformer Ratings			
Phase	3	Voltages are nominal Losses at rated temperature %IZ at 60 Hz	
Winding Material	AL		
kVA	150		
Temperature Rise C	150		
Primary Voltage	208		
Secondary Voltage	480Y/277		
Frequency:	60 Hz		
Typical Performance Data			
Load Loss (Watts)	4356	Resistances (Ohms) @ 20C	
No Load Loss (Watts)	501	HV Coil	.00871
Total Loss (Watts)	4857	LV Coil	.01014
% IX	4.8%		
% IR	2.9%	Efficiency @ 100%	96.86%

The Jefferson Electric 150kVA transformer is a dry-type aluminum-wound NEMA TP1 style transformer, rated for a 150 °C temperature rise and 220 °C insulation. It is housed in a ventilated, floor-mount NEMA 1 enclosure. The part number for future reference is: 423-7261-000. The taps are listed as: 1 at 5% FCAN and 2 at 5% FCBN, which means that the secondary can be tapped as low as 187.2V<sub>AC</sub> for a nominal 480 V<sub>AC</sub> primary voltage.

#### 2.4.5 LC Filter

An LC filter and pre-charge circuit were designed and sourced by AVS with the help of Parker to meet the IEEE-519 standards. The filter was designed to stabilize

within a few seconds at power up. The cutoff frequency was designed for less than half the inverter switching frequency (2.5 kHz). The filter operates as an LCL filter, with the transformer providing the secondary inductance. Parker was chosen to design the LC filter to maintain capability with the inverter.

The final components were modeled in SimPower Systems to determine the response time of a pre-charge filter. However, since Jefferson did not provide sufficiently detailed design information, it was only possible to create a basic model. The model indicated that the pre-charge resistors needed to be greater than  $0.25\ \Omega$  in order to limit the in-rush current to less than three times the nominal current. Due to concerns with the model, it was decided to utilize prior experience by AVS to size the charging resistors. As a result, AVS sized the resistors at  $45\ \Omega$ . Figure 2-7 presents the circuit schematic of the LC filter cabinet packaging, including the pre-charge circuit.

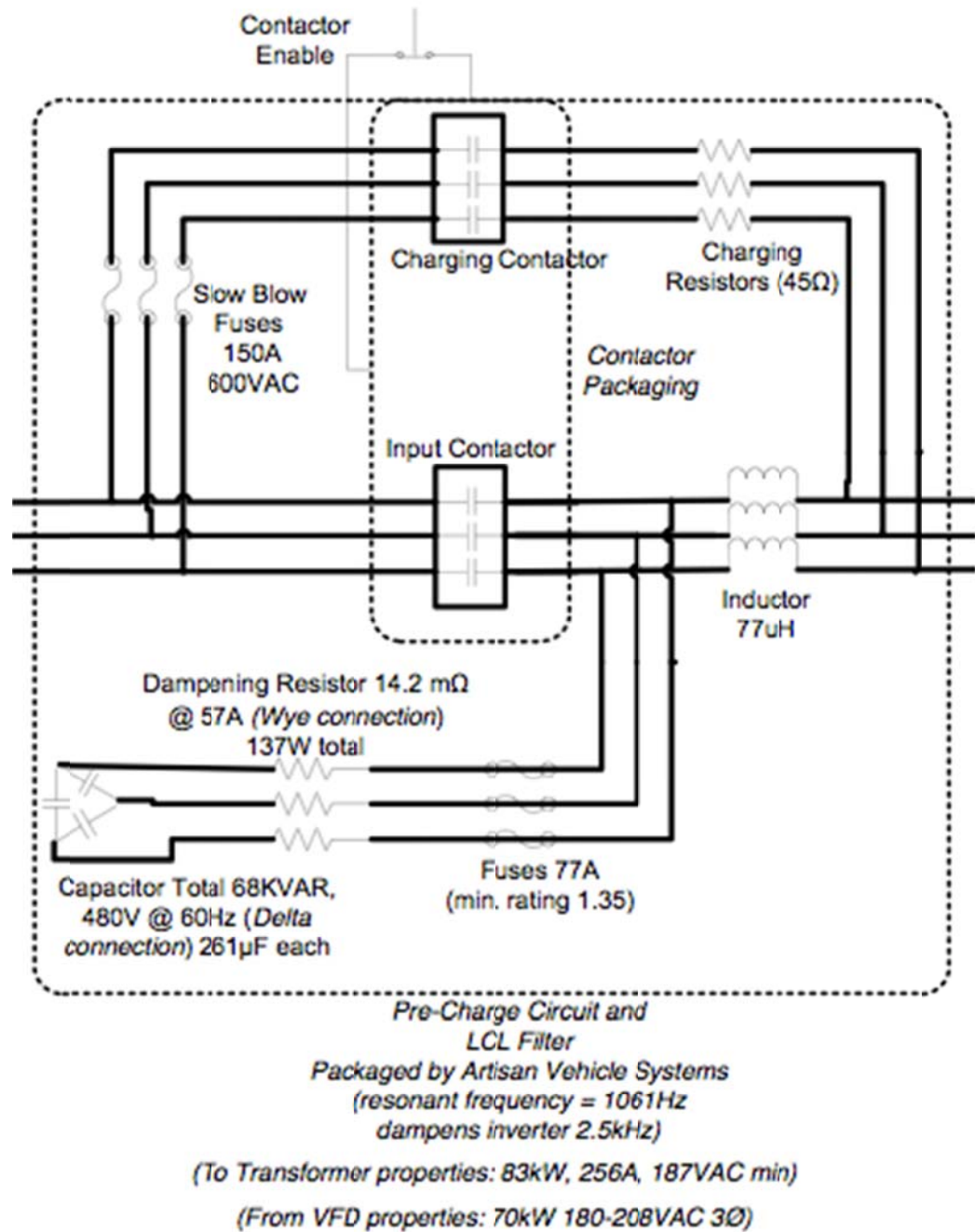


Figure 2-7: LC Filter Cabinet with Pre-Charge Circuit Schematic

#### 2.4.6 Cooling Circuit

The liquid cooling circuit was implemented based on the cooling requirements provided from Artisan Vehicle Systems and addresses the challenges presented in

Section 2.3.2. Photos in Figure 2-8 and Figure 2-9 illustrate key components of the cooling circuit.

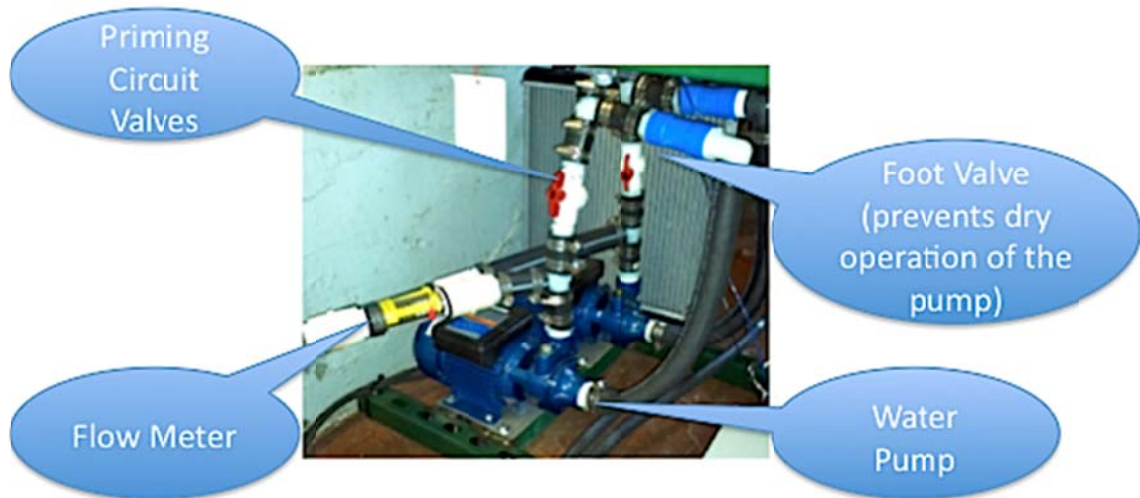


Figure 2-8: Cooling Pumps with Priming Valves, Flow Meters, and Foot Valves



Figure 2-9: Cooling Circuit Fans, Radiators, and Reservoir

#### 2.4.7 Voltage and Frequency Sensor

As described previously, GAS control algorithms require fast measurement of voltage and frequency. The sensor must support 480V<sub>AC</sub> operation, fit within the

budget, and produce fast measurement time (less than 0.13s; see section 2.3.4). Table 2-7 highlights the results of the various sensors considered for selection.

**Table 2-7: Voltage/Frequency Sensor Comparison**

<b>Sensor</b>	<b>AC Voltage Range</b>	<b>Response Time</b>	<b>Price</b>	<b>Output</b>
Ohio Semitronics Inc. DMT-1024	100-636V	<100ms	\$1,405	±20mA, RS-485
Ohio Semitronics DSP-008	600V	<100ms	\$1,025	4-20mA, RS-422
Elkor WattsOn-1200-MSCT1	480V	500ms	\$376	RS-485
Power True Systems Corp. 2V-33-AD-6-A5-D2 and 2F-33-AD-6-A5-D2	0-500V	<400ms A/D conversion not included	Not Available	0-10V or 4-20mA
Custom Built Voltage Divider and National Instruments cRio Data Acquisition	0-750V	As fast as LabView program is designed	\$480	±4.8V

As seen above, the best sensors with the lowest response time (Ohio Semitronics) are also the most expensive solutions. Therefore a custom-built voltage divider with NI DAQ solution was chosen. The sensor was built using a precision decade resistor. The 1776-C54 voltage divider by Caddock Electronics is shown in Figure 2-10.

The divider provides  $1\text{M}\Omega$  of resistance across the divider with taps at 1K, 9K, 90K, and 900K  $\Omega$ .

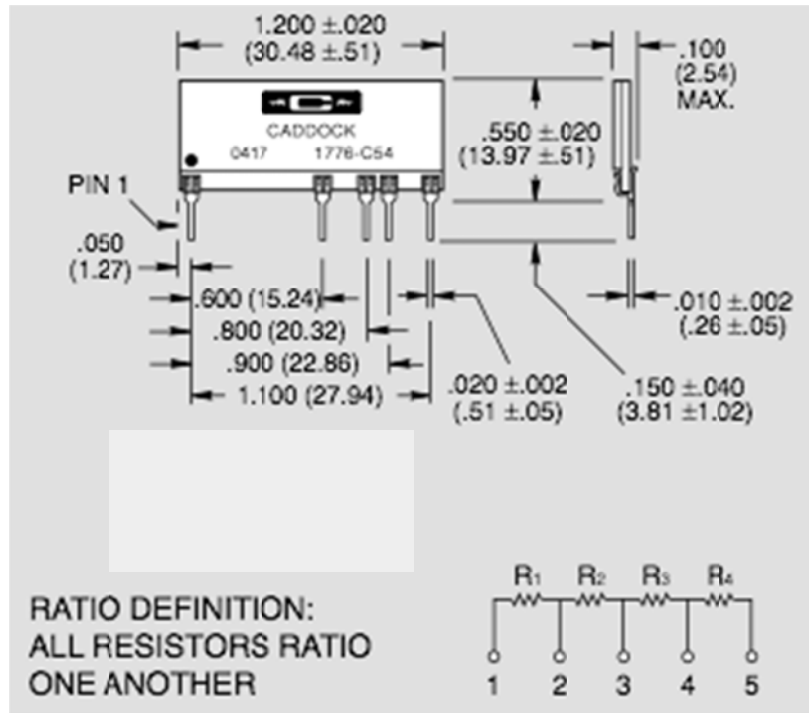


Figure 2-10: Caddock Electronics Voltage Divider

The output was attached to pins 3 and 5 so that the DAQ would see  $\pm 4.8\text{V}$  from the voltage and frequency voltage divider (a  $10\text{k}\Omega$  total resistance). It is noted that a capacitor can be added later for filtering if the signal is too noisy.

#### 2.4.8 Unique Safety Requirements

Unique safety requirements were encountered due to the nature, size and voltage levels of the equipment. Not only is the system different than traditional industrial applications because it utilizes automotive equipment, but it also functions in an educational atmosphere. In this environment the system has two different users: researchers, who need flexibility, and students who may not be experienced with

electrically and mechanically dangerous equipment. Both of these users require different safety measures. Relative to traditional safety standards, the system needs to have ground fault detection, multiple E-stop switch locations, and thermal management. The insulation or ground fault detection device is discussed in the next section. Emergency stop buttons are located throughout the test center in three different areas to ensure that the user is always within ten feet of an E-Stop. In typical industrial environments E-stop switches are included and installed in covers and doors of the purchased system but since the components were sourced from an automotive supplier, these switches were added during the lab design and construction. More specifics of the E-stop system are detailed in section 3.4.10. In addition to this safety, light towers were installed to provide visual verification if a breaker is closed and the system is live. This will visually notify users not to open breakers, control boxes, make electrical connections or perform repairs when the system is energized.

The battery management system provided by Artisan monitors each cell performance to determine battery safety and health. These values are communicated to the Powertrain Control Module graphical user interface (PCM GUI). The PCM GUI monitors the battery SOC and prevents operation if the battery SOC is not within the defined operating range. For example, if the battery were fully charged when the GAS controller commands a charging operation, which could over-charge the battery, the PCM would cancel the command in order to preserve battery health and proper use. The PCM GUI software has limits defined for cell over/under voltage, over/under temperature, and charge/discharge rate.



#### **2.4.8.1 Insulation Monitoring Device**

Battery subsystems present unique safety challenges, particularly guarding against short circuits between battery supply lines and ground. The system is equipped with a ground fault circuit interrupter (GFCI), which engages when the system is not operational. If for any reason the battery becomes grounded, the GFCI disconnects/opens the battery contacts and sounds appropriate alarms. Note that the GFCI system is operational only when the battery is not connected to and operating as part of the system.

The Bender IR155 was chosen because it provides a clear “ok” – safe or “not ok” unsafe output. The IR155 monitors the insulation resistance between the insulated and active high voltage lines of battery and the reference (chassis) ground. Its design for compact size, temperature, and vibration makes it ideally suited for hybrid vehicle applications. Figure 2-11 (image from: [http://www.iso-f1.de/downloads/iso-F1-IR155-32xx-electric-vehicles\\_DB\\_en\\_20101202.pdf](http://www.iso-f1.de/downloads/iso-F1-IR155-32xx-electric-vehicles_DB_en_20101202.pdf)) shows the Bender IR155 GFCI used in the lab.



**Figure 2-11: Bender IR155 Ground Fault Circuit Interrupter**

#### 2.4.8.2 Insulated Connectors

Since the lab is designed to operate in two independent modes, GAS and dyno, a safe way to switch between the two was required. To convert to GAS mode, the inverter connections need to be unplugged from the motor and attached to the LC filter. These interconnections would be difficult to produce using interlocked breakers and switches, opening the possibility that the system could be started in an invalid configuration. Instead, the connections are performed using colored cabling and shielded quick disconnect cam-lock connectors from Marinco Electrical. These connectors, which are also utilized for event power and expeditionary military operations, safely handle the high current and voltage demands and allow safe interconnect while minimizing the risk of a short circuit.

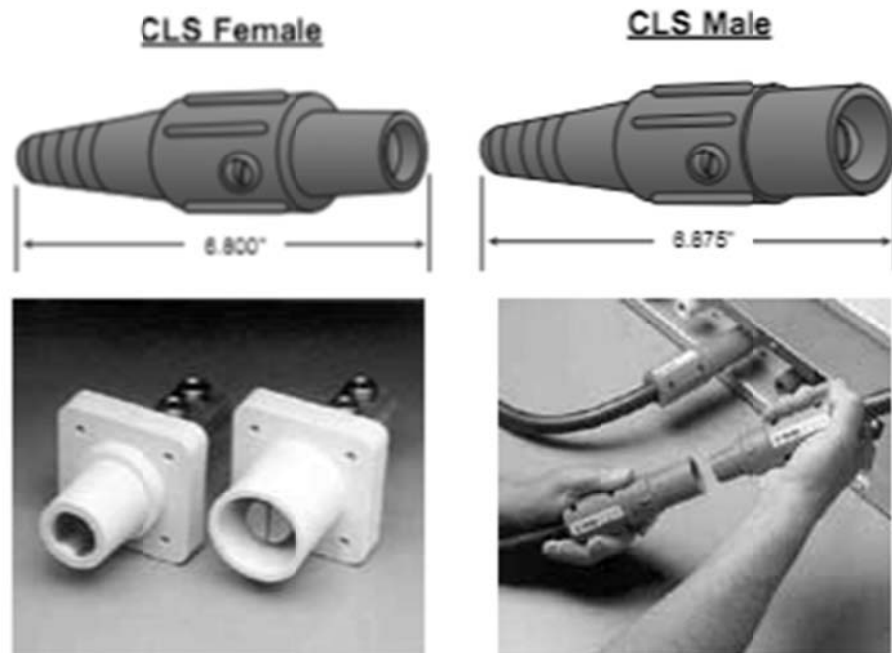


Figure 2-12: Cam Connectors by Marinco. Clockwise: Female Cam Connector, Male Cam Connector, and Demonstration of Installation, Panel Mounts

Figure 2-12 (images from: <http://www.beckelectric.com/store/pc/Marinco-Information-c266.htm>) illustrates the different cam connectors. They have a male or female plug to prevent unintended connections. The system was designed such that the user only matches the proper colors. The polarity and color of the plug were designed so that only one arrangement is possible. Color-coding was selected to minimize the chance of inadvertently connecting incompatible power leads. DC leads are color coded as black ( $V^-$ ) and red ( $V^+$ ). The AC connections would normally use the industrial standard of red-white-blue for 208 V<sub>AC</sub>. However, this would create the potential to interconnect a red DC line with phase A of the 208 AC lines. Therefore, all AC lines are color-coded using the 480 V<sub>AC</sub> standard of brown-orange-yellow for the three phases. With the use of these insulated connectors, users of the lab can quickly, safely, and with confidence, change between the two lab set-ups.

## **2.5 Check Out and Verification**

This section describes overall lab construction (Section 2.5.1), a step-by-step overview of the system operation (Section 2.5.2), and results of the system verification tests (Section 2.5.3).

### **2.5.1 Finalized System Construction**

A 3D CAD model was utilized to layout the lab. Figure 2-13 illustrates this model with call-outs to the specific components of the lab.

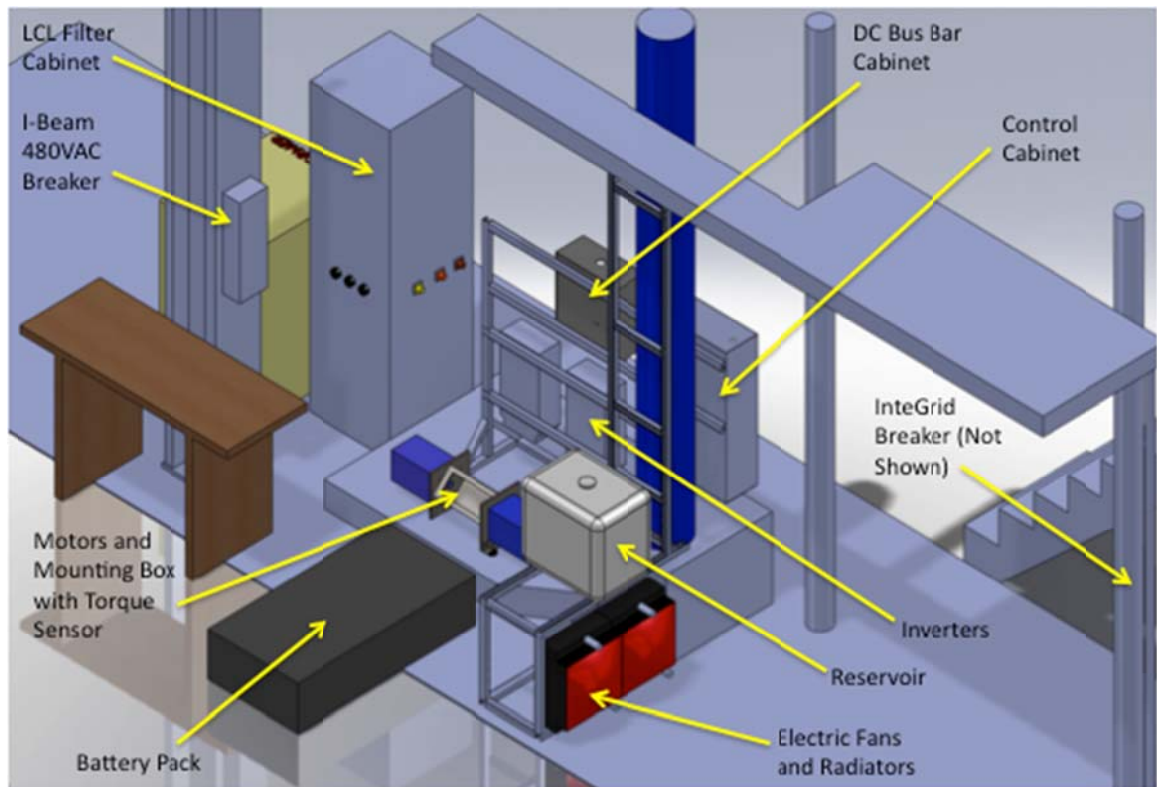


**Figure 2-13: Overview of Components and Their Locations in 3D CAD Model**

The CAD model illustrates key components; conduits and cabling are not shown. During construction each conduit was sized according to the required wire size and fill ratio as dictated by the local electrical code.

Figure 2-14 shows the completed construction of the GAS portion of the eDTC lab with call-outs labeling the major components.

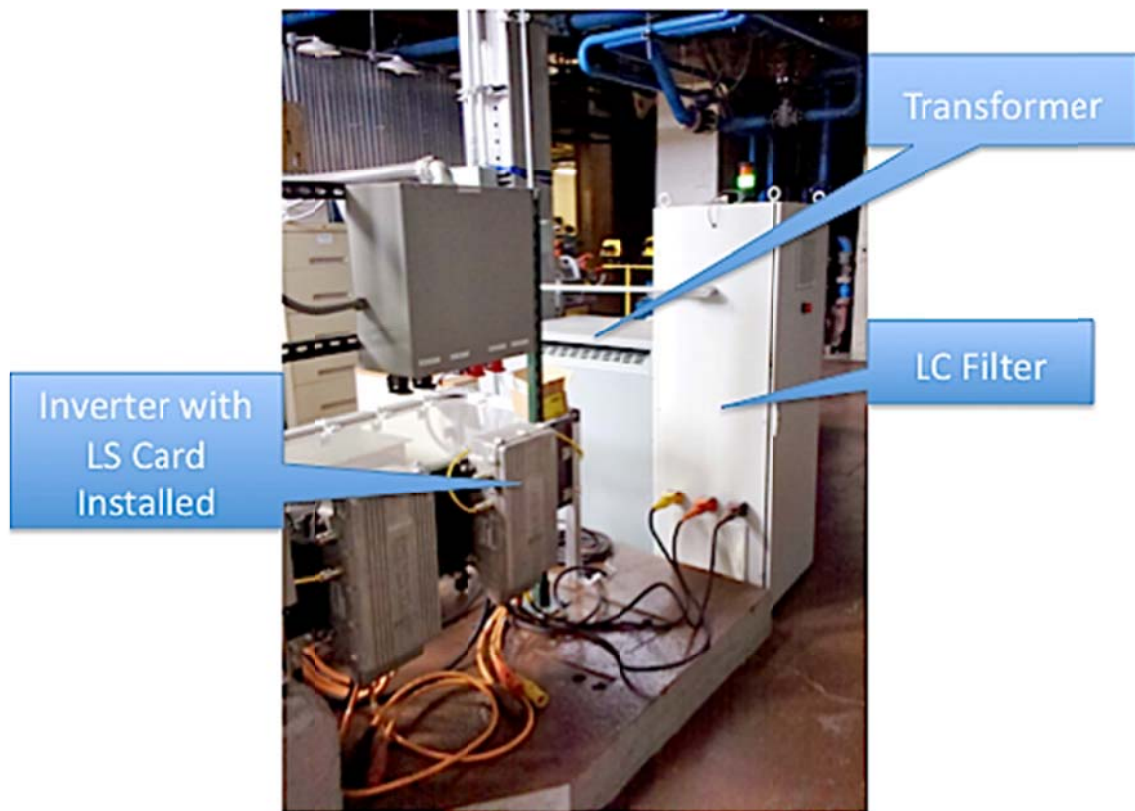


**Figure 2-14: Actual Layout of GAS Components**

Figure 2-15 shows the specific details of the components installed in the LC filter cabinet. The attenuator is used as feedback for the inverter to communicate with the filter and pre-charge circuit. Both the pre-charge and the main circuit contactors are housed in the one package labeled contactor.

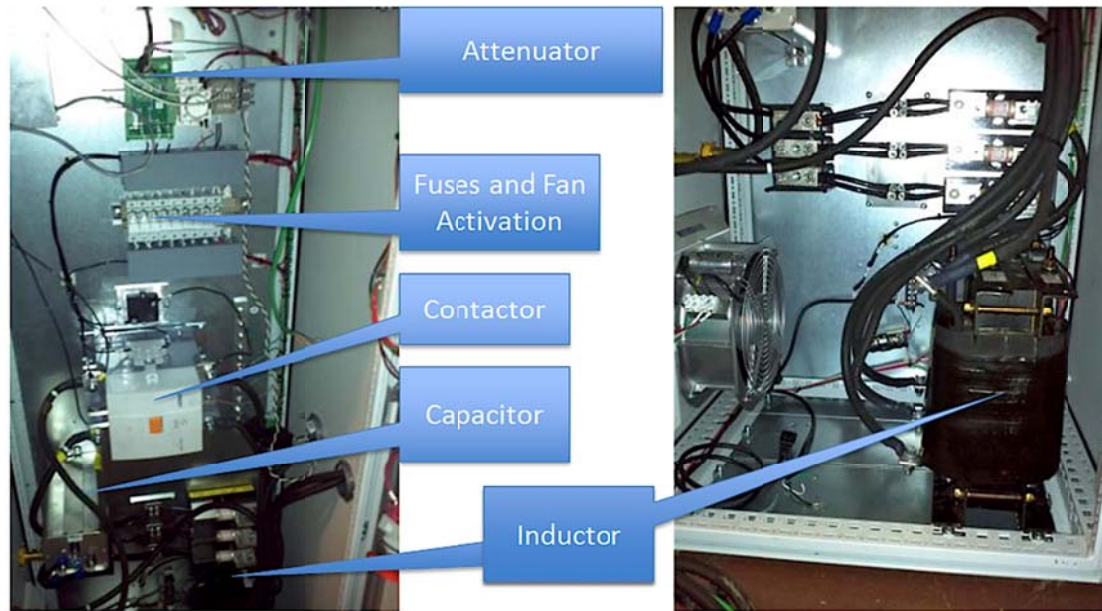


Figure 2-15: Actual Layout LC Filter Cabinet

### 2.5.2 System Operation

The system works by booting up the control computer and opening the PCM GUI software and the Parker SSD Drive control software, called DSE Lite. Then the user must confirm CAN communication is established with the software to ensure proper system checkout. Once these steps are preformed the user must perform safety checks to ensure that: no cables are improperly color matched, everything is properly connected, all shields and covers are closed, all E-stop switches are in the up (released) position. It is recommended that an experienced supervisor confirm the correct operational state before approving the testing procedure.

Then the *InteGrid* switchgear main service disconnects need to be switched on (closed) and the 480V<sub>AC</sub> “I-Beam” breaker can be switched to the ON position. The LC filter pre-charge switch MUST be in the off position before closing the LC filter breaker



to prevent the LC filter circuit from arcing. The filter cabinet fans and the radiator fans should be activated at this time. The pump for the GAS circuit must also be plugged in. At this point the breaker to the LC filter can be switched to the ON position. The user must ensure that the GAS inverter is communicating properly and seeing an AC bus voltage of 187V<sub>AC</sub>. When the proper voltage is observed, the LC pre-charge contactors can be switched ON to begin the pre-charge. After a few seconds, the main contactor will automatically close with a loud “thud.” After system checkout, the battery key-on switch may be turned to begin the battery pre-charge and full connection. The final step involves the user flipping the “ENABLE” switch for the GAS inverter on the desk control box (shown in Figure 2-16).

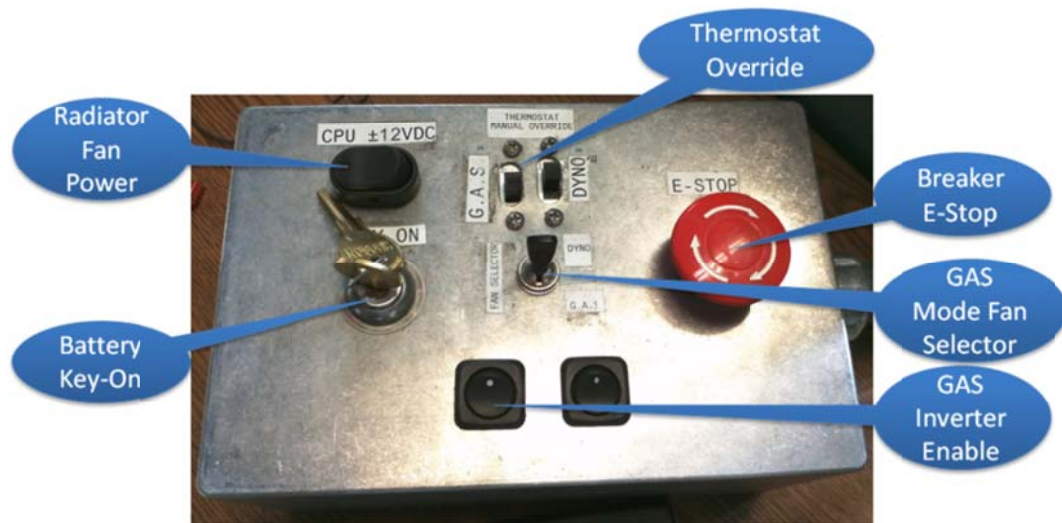


**Figure 2-16: Desk Control Box with Switch Callouts**

Using the DSE Lite software, the user can define current control mode, motor induction leakage, and current demand from the battery. By defining the current demand values the battery will charge or discharge accordingly. The user can monitor

various parameters including: real and reactive power, power angle, power factor, actual current, DC voltage, real and reactive current feedback, and synchronization frequency. An example of these parameters is shown in Figure 2-17, below.

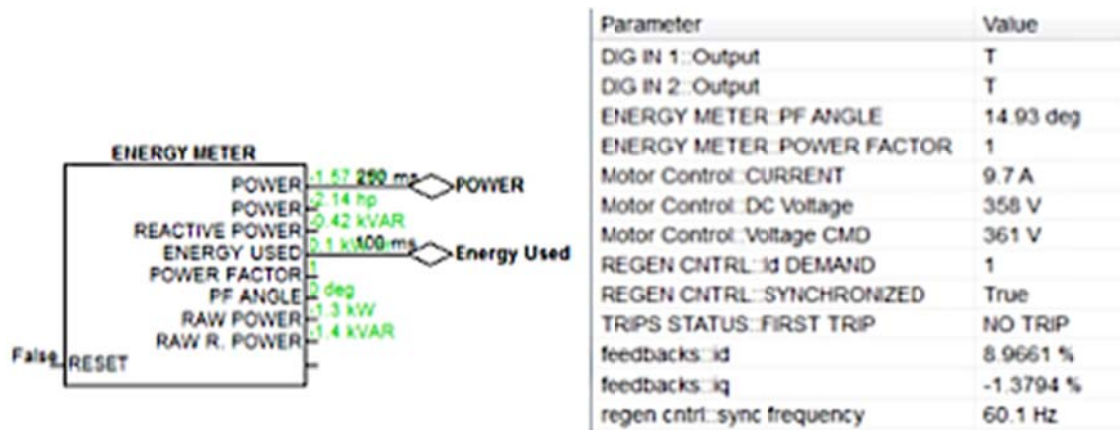


Figure 2-17: Display Parameters in DSE Lite with Arbitrary Values for Display Purposes Only

### 2.5.3 Testing Results

Operating the system to charge and discharge of the battery from the grid performed a final system checkout. Only manual current control was utilized. During manual control, the inverter current was set to +10A and -10A for consecutive ten second periods. Figure 2-18 is a screenshot showing the system synced to the grid and the battery discharging and then charging. In the background is the DES Lite inverter software showing grid synchronization, true current control mode, and 10A current limit. In the foreground is the PCM GUI showing battery voltage in the lower left corner. Notice the dip towards the end of the plot. This designates the discharge period of the testing. A more detailed view of event is shown in Figure 2-19.





Figure 2-18: Screenshot of DSE Lite in Background with PCM GUI BMS Monitor in Foreground

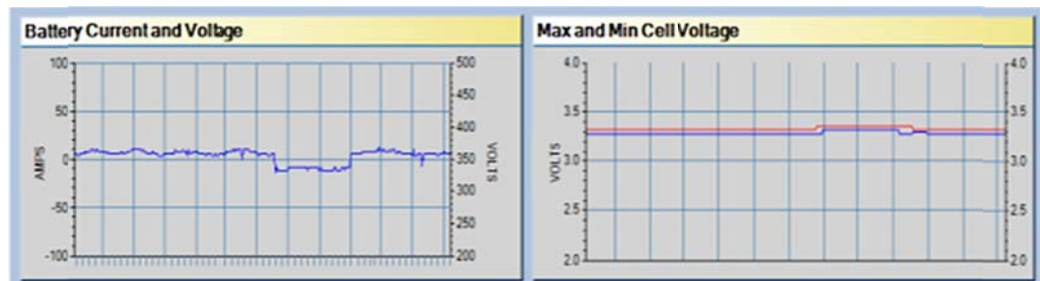
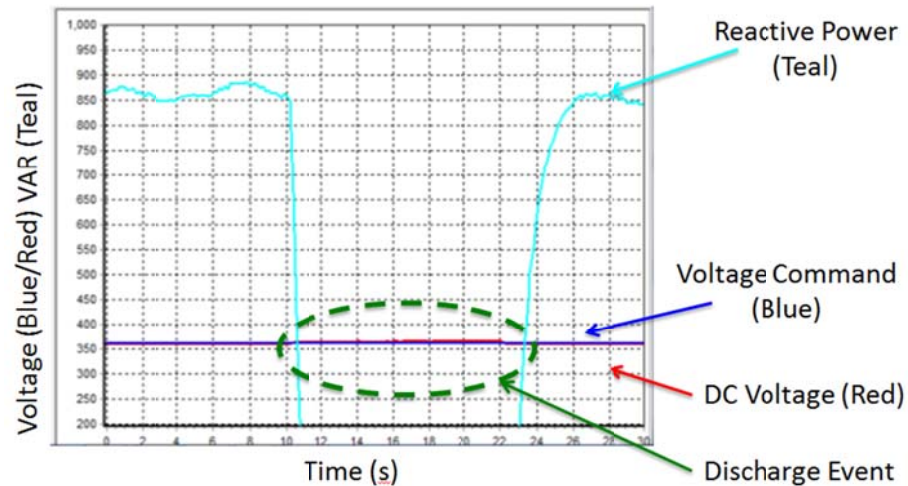


Figure 2-19: PCM GUI BMS Plot of Pack Current and Voltage vs. Time Plot (left) and Max and Min Cell Voltage vs. Time Plot (right)

During this testing the scope function of DSE Lite was utilized to monitor the reactive power of the system as well as the voltage command along with actual voltage (shown in Figure 2-20).



**Figure 2-20: Voltage and VAR vs. Time Plot for DC Voltage Command and Real as well as Reactive Power during the Discharge Event**

This system checkout verified that all power components were operational and functioning as intended. However, additional tuning will be required for future research applications. Several issues need to be noted. Referring to Figure 2-20, the reactive power fluctuates at the start of the test; this is due to sub-optimum software settings and poor DC voltage measurement at the battery. A slow ramp rate is also apparent at the end of the discharge test, when it takes several seconds for the reactive power to settle at the commanded level. It is currently believed that these issues can be resolved via software updates and further system configuration testing. AVS has committed to providing technical assistance with this fine-tuning during the next testing session.

### **3. Electric Vehicle Component Education through a Dynamometer**

This chapter focuses on the dynamometer portion of the eDTC. Sections include an introduction of to dynamometers (Section 3.1), an overview of the system (Section 3.2), the challenges that were presented with the system (Section 3.3), the design selection of each of the key components (Section 3.4), a system check-out (Section 3.5) and course work example (Section 3.6).

#### **3.1 Dynamometer Introduction**

A dynamometer (hereafter referred to as dyno) is a device used as a brake to test rotary machines. Dynamometers are utilized to test internal combustion engines, motors, generators and related machines. A dyno consists of a shaft coupling and a controllable loading mechanism, typically capable of independently controlling either torque or speed of the unit under test (UUT). There are many different kinds of dyno loading mechanisms, including: water brakes, eddy current brakes, electrical generators, fan, hydraulic resistance loads, and controllable mechanical friction loads. Each type has its own advantages and disadvantages, which needed to be considered based on the requirements of the lab. Since the eDTC lab has very tight space requirements, this limited many technologies. The electrical generator dyno type was pursued since it would be the simplest to implement and most compact. Using an electrical motor as the brake or absorber means that electrical power recovered from the dyno could be reused

by the system, thus requiring an external power to only provide power for the losses within the system.

### **3.1.1 Various Methods of Motor Testing To Date**

Many industrial and educational internal combustion engine (ICE) stands exist around the world, but their design is very different compared to an automotive electric motor test stand. The existing test benches have liquid cooling infrastructure, exhaust venting, emissions measurement equipment, fuel storage, plumbing, and safety precautions, as well as different sensors (O<sub>2</sub>, timing, thermocouples, pressure, mass air flow rates, etc.). However, only a few of these components and testing knowledge can be carried over to electric motor and GAS test stands. ICE test stands do not have inverters, batteries, or traction DC power supplies. In addition to the differences, some dynos (i.e. water brake dynos) do not have generators that can be used for regenerating power back on to the local utility grid. In general, test operators would prefer to sell power back to the grid. However, they are constrained by the utilities interconnection regulations and additional expensive infrastructure. For this reason, most dyno test stands today simply turn the used energy into heat and dissipate this energy during testing. This gives operators more flexibility at the expense of continuous power input.

In the eDTC lab, it was desired to not use the dyno to produce waste heat but rather minimize consumption by designing a regenerative solution. While the dyno set-up of this lab doesn't have grid regeneration, it does feature a regenerative loop that minimizes power consumption. This regenerative concept was selected to minimize power input and to reduce cost of components.

### **3.1.2 Uniqueness of this Set-Up**

The CSU eDTC test lab is unique because the majority of current test labs support only ICE testing. Few universities have full-scale traction motor testing, making it difficult for students to acquire hands-on experience with electric vehicle components and for researchers to perform physical testing. Many vehicle manufacturers, component designers, and even national labs have electric motor testing facilities or hybrid dynamometers, but few have an educational laboratory utilizing components of this scale. The unique contribution of the eDTC laboratory is providing an educational facility using full-scale automotive components in a flexible system configuration.

### **3.2 High-level System Overview of the Dynamometer Lab**

This section describes the architecture of the dyno laboratory at a high level, including the motor to test, the absorber motor, inverter drives for each motor, power supply, and torque sensing.

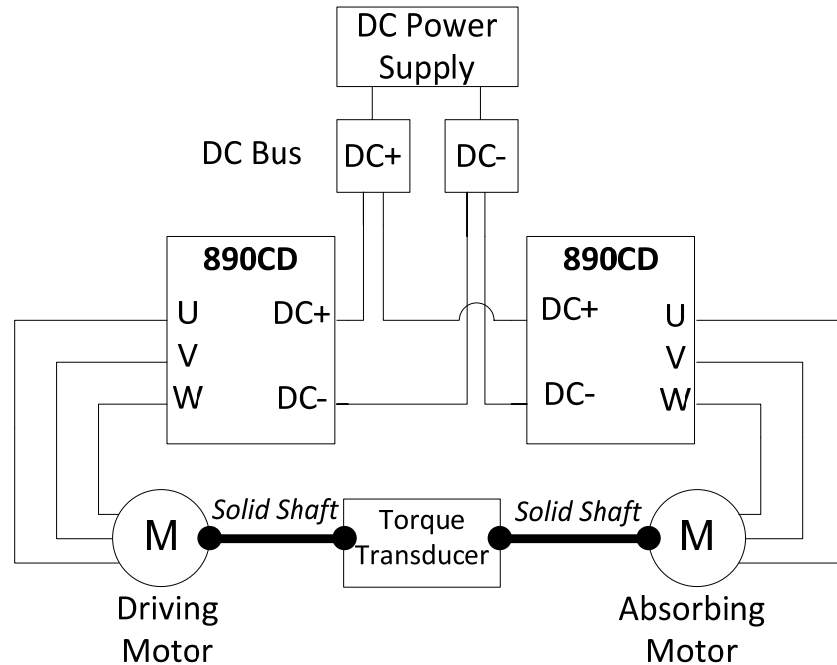


**Figure 3-1: Simplified Diagram of Dyno Set-Up**

Above, Figure 3-1, shows selected components and how they are interconnected. Starting from the top of the diagram:

- The DC power supply supplies make-up power to the system, i.e. the losses due to friction and impedance in the drives, motors and drivetrain. The DC power supply provides closed-loop control of the DC bus voltage.
- The DC bus provides a common DC bus for both the driving and absorbing motor-inverter pairs. The “driving motor” is the unit under test (UUT), while the “absorbing motor” loads the UUT.
- The UUT inverter (890 CD is the inverter model number) provides variable frequency and voltage, 3-phase, AC power to the UUT motor, which converts electrical power into mechanical rotational power.

Control of the UUT inverter can be modified to support education or research needs. Either speed or torque control are possible.

- The torque sensor monitors both the torque and speed of the UUT.
- The absorber motor loads the UUT, generating variable-frequency, 3-phase, AC, power to its inverter.
- The absorber inverter (also inverter model number 890 CD) absorbs power from the absorber motor and drives that power back onto the DC bus by adjusting its DC output voltage. Generally, the absorber will be controlled using the opposite parameter of the UUT inverter – speed if the UUT is controlling torque, and vice versa.

The only major component not shown in the figure is the power train control module (PCM), which facilitates communication between the control computer and inverters.

### **3.3 Design Challenges**

This section elaborates on the challenges in the design and construction of the dyno portion of the lab, and describes the selection of key components.

#### **3.3.1 Cogging and Other Vibration Effects**

Under certain high-load conditions, traction motors may exhibit significant cogging. In traction-drive test mode this cogging can excite torsional vibration modes in the drivetrain between the two motors. These vibrations may be amplified if the compliance in the couplings and the torque transducer create natural vibration modes

near the excitation frequency. The top design speed of the system is 8,000 RPM. Given that the motors have eight poles, the fundamental cogging frequency is 32,000 RPM or 533 Hz. To avoid resonance, an ideal solution would place the first vibration mode above 1066 Hz. Given that the mass of the UUT and absorbing motors is largely set by their size, the frequency requirement primarily impacts the selection of the torque sensor and shaft couplings.

### **3.3.2 Sizing of DC Power Supply**

The lab is not designed to utilize the battery as a motor power supply. Therefore a DC power supply was utilized to power the inverters during testing. Each motor is rated at 70kW. Therefore, if no regeneration is utilized, the lab must provide up to 70 kW to the UUT motor (plus losses), and must dissipate up to 70 kW generated by the absorber motor. However, the power supply demand can be greatly reduced if the power generated by the absorber is reused within the dyno, and the need for a 70 kW load bank can be entirely removed. In this architecture, only “make-up” power will be required to account for friction and impedance losses within the two motor/inverters. This regenerative set-up is achieved by placing both inverters on a shared DC bus. Therefore, the size of the make-up supply depends on the losses in the system.

To determine these losses, the worst efficiencies were used to calculate the maximum make-up power required for different power and speed situations. Figure 3-2 shows how the system was modeled for calculating power consumption based on the different efficiencies of the different components.



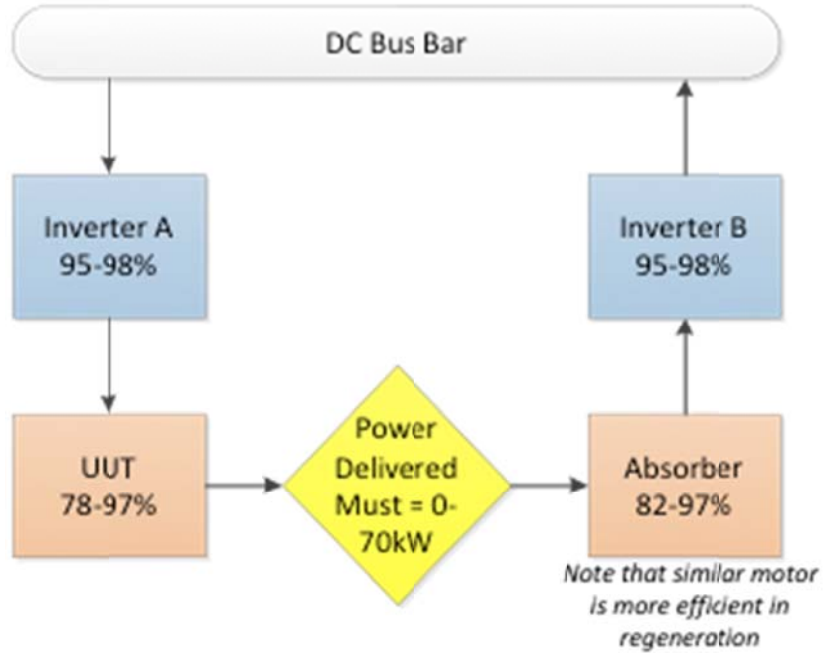


Figure 3-2: Schematic for Efficiency Calculations

The efficiency at each point was calculated by adding the losses at each point of system using equation 3:

$$\text{Make up Power} = \frac{P_{\text{Desired}}}{\epsilon_{\text{inverter}} * \epsilon_{\text{UUT}}} - (P_{\text{Desired}} * \epsilon_{\text{absorber}} * \epsilon_{\text{inverter}}) \quad (3)$$

where  $P_{\text{Desired}}$  is the power needed at the motor shafts and epsilon (  $\epsilon$  ) denotes efficiency for each component noted in subscript. Even though the motors are identical, AVS indicated that the efficiency of the absorber is better than the unit under test because the motors operate better in regeneration. However, in order to determine the worst case scenario, the better efficiencies of the motor in regeneration mode were neglected and the lower efficiencies (i.e. when the motor operates in positive torque) were used. Using the equation and known efficiencies, Table 3-1 was compiled.

**Table 3-1: Required Make-Up Power by the Power Supply Calculations**

<b>Power (kW)</b>	<b>Motor Efficiency</b>	<b>Inverter Efficiency</b>	<b>Total Efficiency</b>	<b>Make-up Power (kW)</b>
<b>At 833 rpm</b>				
10	94%	95%	80%	2.03
20	96%	95%	83%	3.37
30	97%	96%	87%	3.99
40	94%	97%	83%	6.74
50	92%	98%	81%	9.36
60	89%	98%	76%	14.36
70	87%	98%	73%	19.12
<b>At 2,000 rpm</b>				
10	89%	95%	71%	2.85
20	97%	98%	90%	1.93
30	97%	98%	90%	2.89
40	97%	98%	90%	3.85
50	96%	98%	89%	5.74
60	95%	98%	87%	7.99
70	94%	98%	85%	10.60
<b>At 4,500 rpm</b>				
10	79%	95%	56%	4.37
20	88%	98%	74%	5.29
30	94%	98%	85%	4.54
40	97%	98%	90%	3.85
50	97%	98%	90%	4.82
60	97%	98%	90%	5.78
70	96%	98%	89%	8.04
<b>At 7,500 rpm</b>				
10	78%	95%	55%	4.51
20	89%	95%	71%	5.70
30	96%	95%	83%	5.05
40	97%	98%	90%	3.85
50	97%	98%	90%	4.82
60	97%	98%	90%	5.78
70	96%	98%	89%	8.04

Table 3-1 shows that an estimated 19kW is needed in the worst case. With these estimations and a 25% factor of safety, it was determined that an existing 25kW power supply would provide sufficient make-up power. Re-using the existing 24 kW power supply reduced the cost of the system by \$4,150 – the cost of an additional 50 kW drive to provide makeup power.

### 3.4 Design of this Equipment

This section describes the key components incorporated in the dyno lab including: electric motors (Section 3.4.1), inverters (Section 3.4.2), DC power supply (Section 3.4.3), current sensors (Section 3.4.4), torque sensor and couplers (Section 3.4.5), mounting box for the motors, couplers, and torque sensor (Section 3.4.6), powertrain control module (Section 3.4.7), control computer (Section 3.4.8), data acquisition system (Section 3.4.9), and emergency stop circuit (Section 3.4.10). In each section, requirements are discussed, followed by the choice of components to meet the requirements. Figure 3-3 shows these major components and their integration in a more detailed view. Due to margin constraints, the size of the image is reduced thus making the lines difficult to see (for the full scale image please refer to Appendix A: Figure 0-9).

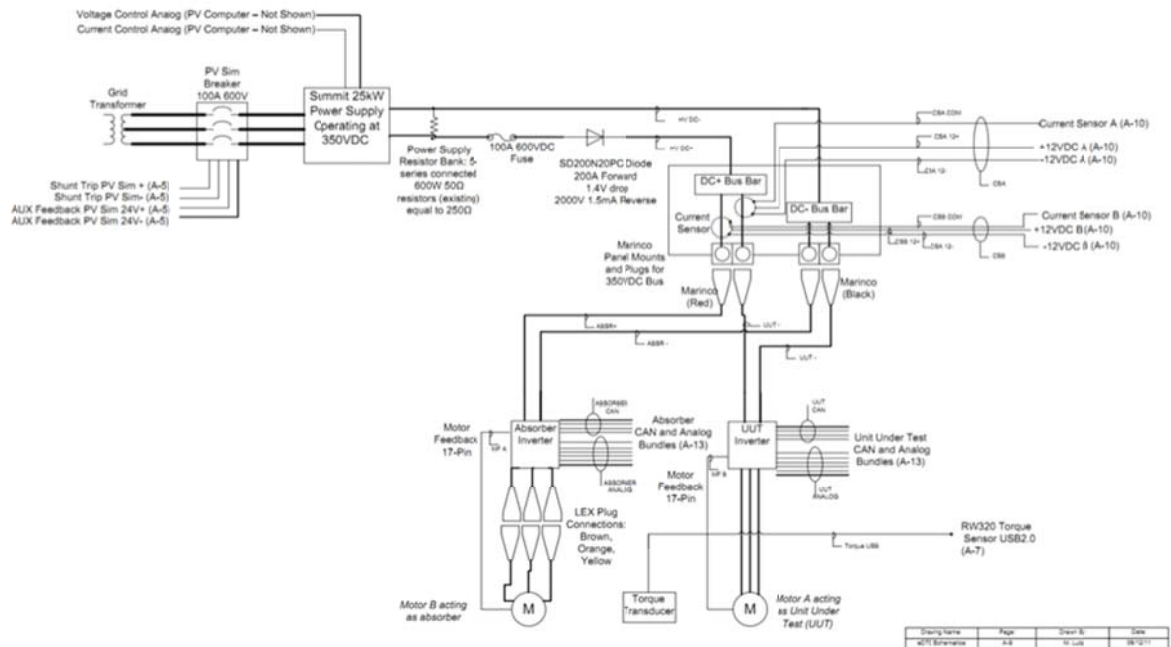


Figure 3-3: Schematic for eDTC Dynamometer Set-Up

Starting from the left hand side of the figure:

- The service disconnect provides power to the Summit™ DC Power Supply.
- A diode prevents power flowing in reverse direction from the DC bus to the DC power supply.
- Both inverters are connected to the DC bus using Marinco insulated power connectors.
- Current sensors are shown within the DC bus bar area to monitor the current flow to each inverter from the DC bus.

### **3.4.1 Electric Motors**

For this lab, both a UUT motor and an absorber motor (acting primarily as a generator) are needed. Since the lab will function as a test bed for any automotive-based electric motor, the choice of motors is not particularly crucial. Motors were chosen for the dynamometer lab from Artisan Vehicle Systems because the automotive-style motors could be procured at below market cost and be pre-package to work together with AVS inverters and powertrain control module (PCM), as well as an open-source control system. The chosen motor pair is the Parker GP150WC motors packaged and sold by AVS. They are surface mounted, three-phase, permanent magnet synchronous motors with 8-poles, 70kW peak output, 8000rpm maximum speed, and 138Nm maximum torque. Figure 3-4, Figure 3-5, and Figure 3-6, courtesy of AVS, illustrate the torque, power, and efficiency curves of the selected motors. The high performance to weight ratio and compact packaging of these motors is typical of automotive motors.

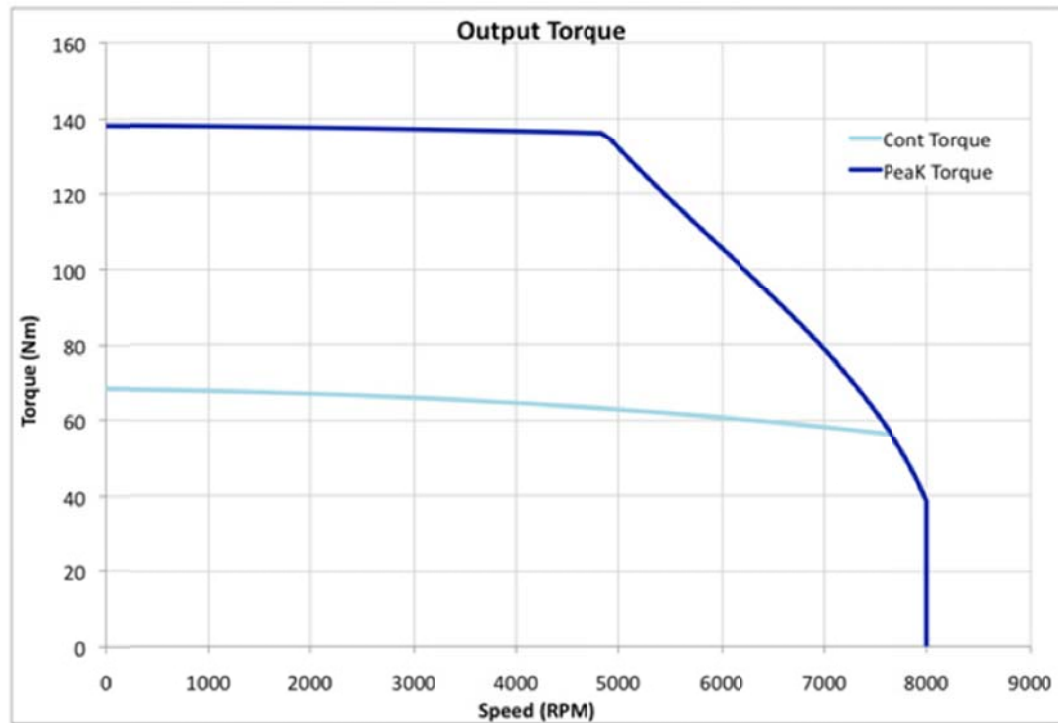


Figure 3-4: Output Torque of GP150WC Motor from Artisan Vehicle Systems

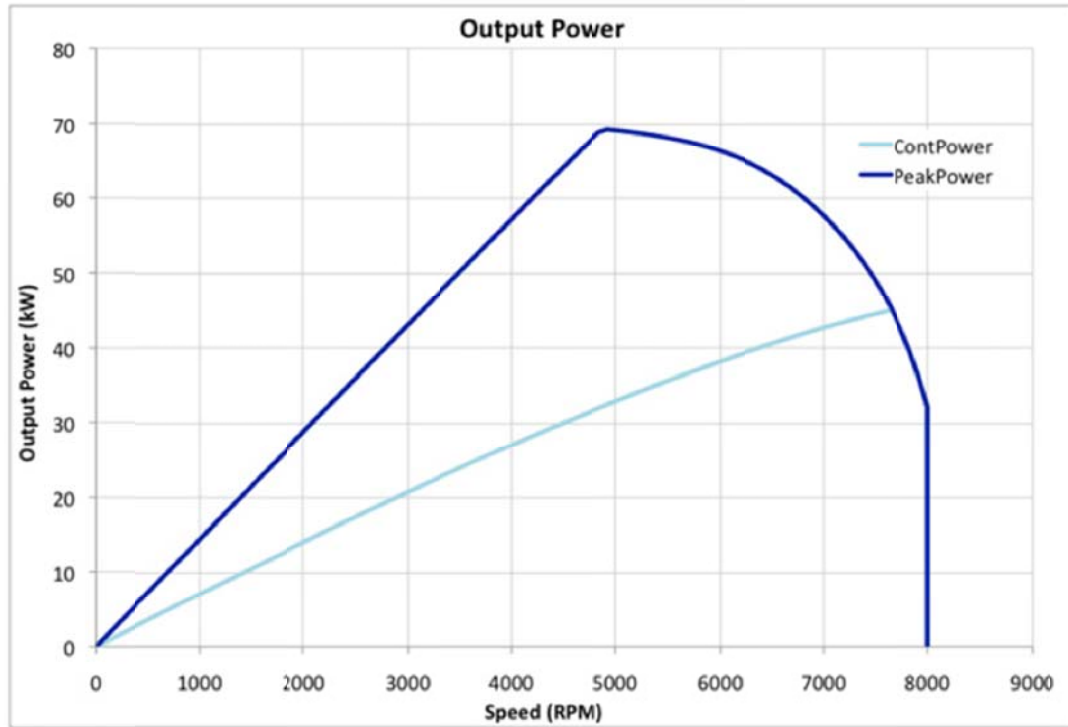


Figure 3-5: Output Power of GP150WC Motor from Artisan Vehicle Systems

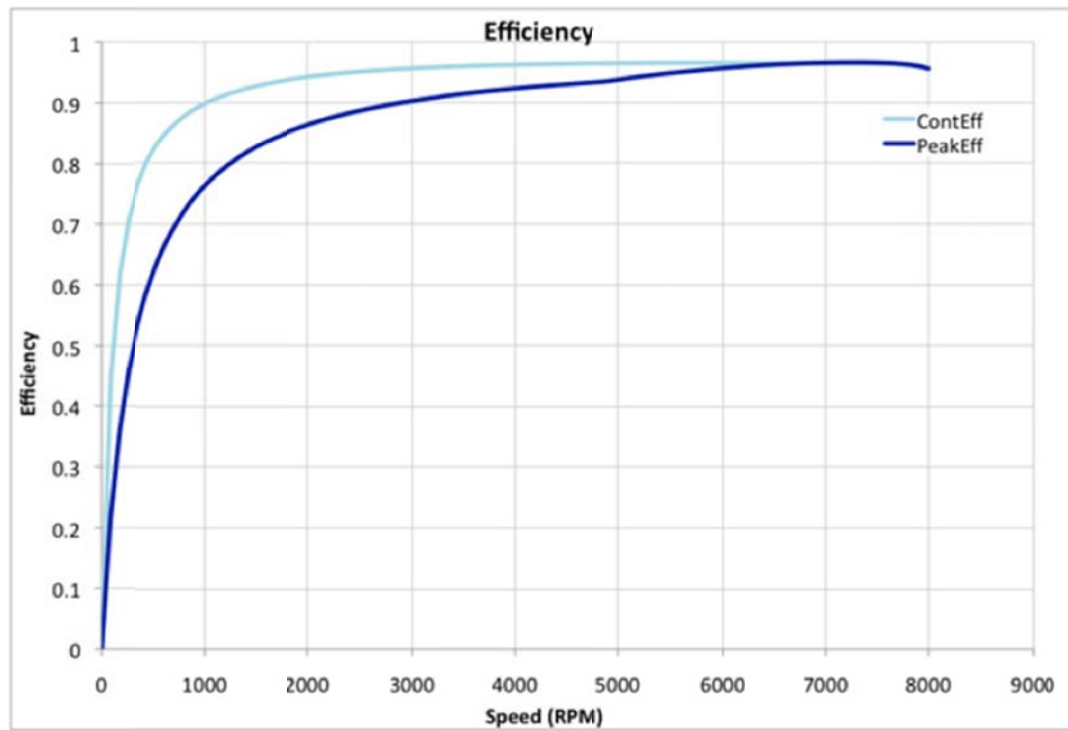


Figure 3-6: Efficiency Curve of GP150WC Motor from Artisan Vehicle Systems

### **3.4.2 Variable Frequency Drive**

Variable frequency drives (VFD) or inverters are needed in AC synchronous motor applications to provide speed control. The VFDs match the 3-phase power required by the motors to the DC power available on the DC bus. Improper frequency selection could potentially lead to significant motor slip causing stalling or damage to the motor or VFD.

The choice of the VFDs was constrained by requirements for the GAS operation mode, described in Section 2.4.1. While the UUT VFD is not utilized in GAS mode, the absorber VFD is reused as the line inverter for GAS mode. To convert from GAS to dyno mode, the user must disconnect the battery and LC filter from the DC bus, and connect the UUT VFD to the DC bus. Additionally, the user must replace the “line synchronization” (LS) with the resolver card necessary for dyno speed control, and the data harness must be swapped appropriately. Detailed instructions of this procedure can be found in Appendix E. Finally, the software on the inverter must be re-programmed to support dyno mode.

### **3.4.3 DC Power Supply**

The eDTC utilizes an existing 25kW DC power supply from the *InteGrid* Laboratory, a Summit™ 57000007D from Advanced Energy Incorporated. This supply provides floating DC output, which means it is insensitive to the direction of DC current flow when operational. However, in emergency shutdown events, the supply must be protected from a potential current surge caused by discharge of output capacitance of the VFDs. To provide this protection, a Vishay SD200N20PC diode was installed in the

DC power lines to prevent current backflow. The diode supports a 200A forward current with a 1.4V drop, and has reverse voltage protection to 2000V. Figure 3-7 shows the inline installation of the diode on the DC positive wire in the DC disconnect enclosure.

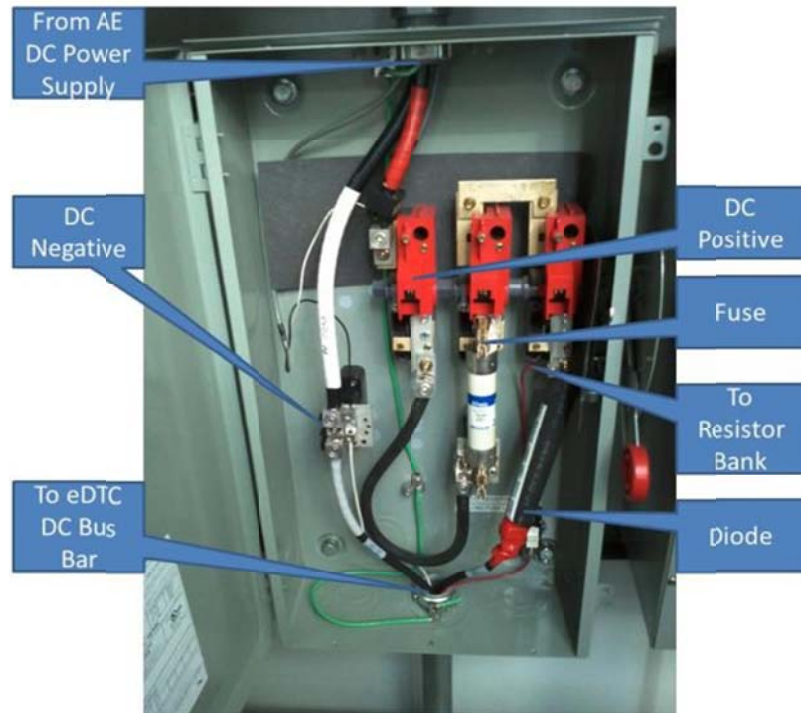


**Figure 3-7: DC Disconnect Internals Showing Diode Installation**

Currently, there is no capacitance across the DC bus, other than the output capacitance of the VFDs. This produces a very “stiff” DC bus, which may excite high frequency modes or control instabilities. A capacitor may be required to damp these modes if issues are observed; no estimation of the capacitor requirements was completed during this work.



### 3.4.4 Current Sensor

To measure the VFD power, it is necessary to measure both the DC bus voltage and the current on each VFD connection. Voltage measurement was described in the GAS description, above (Section 2.4.7). Current measurement is described below.

The three most common types of current sensor are: shunt, current transformer, and Hall-effect sensors. Current transformers are only suitable for AC current measurements. Current shunts are often susceptible to noise, may have heating issues at high current levels, and often require galvanic isolation to prevent floating DC-mode signals for damaging data acquisition equipment. Modern Hall-effect sensors, however, gain noise immunity by using built-in amplification, and, because they are indirect sensors, provide both galvanic isolation and virtually no heating at high current levels. “Hall effect sensors are broadly deployed because of their dc current sensing capability, galvanomagnetic isolation, and zero circuit insertion loss” (Zhou, 2003).

Within the Hall-effect measurement type there are two different groups based on their measurement control loop. These two groups are defined as open or closed loop sensors. Open loop Hall-effect current sensor designs internalize the current carrying conductor, allowing the manufacturer to optimize the current sensor package’s size and thermal characteristics. Measurement of open loop sensors usually has a more limited range of linearity and cannot compensate for offset and residual field errors. The closed loop Hall-effect sensors, on the other hand, act as transformers that use a reference voltage, which allows for higher accuracy than open loop control sensors. The disadvantages to closed loop sensors include larger size and higher cost. The closed loop

sensor is typically more accurate because the output of the Hall-effect element is connected to a secondary coil, which generates a field to cancel the primary field's current. The amount of cancelling is proportional to the coil ratio between the two

(Dickinson & Milano, 2002)

Another consideration is the measurement signal. All Hall-effect sensors need an amplifier to increase the signal, but some closed loop sensors are designed to work with a data acquisition system that measure the delta voltage and interprets this as current flow. This allows for reduced component count, cost, and complexity.

Based on the above knowledge, the requirements for the current sensor selection were: 425A peak measuring ability, sensor size must be smaller than the allotted space in the junction box (6"x2"x6"), closed loop for accuracy, and lowest cost relative to other closed loop options. The Honeywell CSNS300M current sensor was chosen because it has +/-12VDC reference voltage requirement, 600A max measurement, closed loop control, and ease of panel mounting. Figure 3-8 shows the final current sensor selection installed in the high voltage DC bus bar cabinet.



**Figure 3-8: DC Bus Cabinet with Current Sensors Shown on Right**

The sensor needs measurement resistors to tune the sensor's output. The measurement resistance was chosen as 51 Ohms because the range of the suggested resistance was 5 to 95 Ohm at 200A or 5 to 50 Ohm at 300A max. This suggestion is also at a rated  $\pm 15\text{VDC}$ , whereas the lab will be using  $\pm 12\text{VDC}$ . During initial set-up, if the measured values have poor resolution, a different resistor will be used.

### **3.4.5 Torque Sensor and Coupler Selection**

#### **3.4.5.1 Objectives**

The eDTC needed to purchase a torque sensor that could be used in an electric motor dynamometer to measure the torque in the system between the motor under test and the absorber motor. The torque sensor requirements included: price, torsional stiffness, sampling rate, non-contact measurement, operational speed of 8000rpm, and capable of withstanding 138Nm of torque. Due to the significant effect that cogging and vibration can have on measurements, finding the best sensor depended on: max measuring speed, max torque limit, cost, torsional stiffness, and moment of inertia. The following sub-section describes the method used to make the selection.

#### **3.4.5.2 Method**

Several torque sensors were investigated as valid sensors for the eDTC dynamometer application. These were tabulated below (Table 3-2) based upon the selection parameters. In total, eleven sensors were considered for evaluation. In order to narrow down the results, sensors over \$5,500, rotational speeds below 10,000 rpm and sampling rates slower than 1kHz were ignored.

**Table 3-2: Compilation of Torque Sensors Considered for Selection**

Company	Model	Max RPM	Max Torque (Nm)	Torsional Stiffness, Kc (Nm/rad)	Mass Moment of Inertia (kgm <sup>2</sup> )	Sampling Rate	Measurement Method	Price	Notes
Binsfeld	TorqTrack Revolution	Motor speed	Motor torque	As rigid as mounting shaft	Shaft inertia	4.8kHz	Inductive Strain Gauge	\$5,657	One coupling needed
Datum	M420-S2-A	8K	250	Not Given	Not Given	RS232	Non-contact Strain gauge	\$2,178	Keyway mount
Datum	FF420-S1	10K	250	Not Given	Not Given	20kHz (option)	Non-contact	\$4,824	Flange mount
Futek	TRS805-4	8K	200	6.0E4	4.0E-4	1kHz	Non-contact Strain gauge	\$6995	Max rpm!
HBM	T22	12K	200	13.8E4	1.8E-4	Not given	Non-contact	Not given	Only sell to Europe
Interface	T2-200-AXA	12K	200	6.70E4 * for neck part of sensor	1.0E-4 drive 0.9E-4 test side	10kHz	Non-contact	\$4724	Includes speed & angle option
Magtrol	TM 312	10K	200	3.82E4	4.85E-4	Not given	Non-contact Optical	\$6,700	Over-priced
S. Himmelstein	MCRT 28003T (2-3)	8,5K	226	2.94E4	10.59E-4	Not given	Non-contact Strain gauge	\$3,995	Heavy
S. Himmelstein	MCRT 86004V (2-3)	13.5K	225	181.00E4	1.32E-4	3kHz	Bearingless Rigid	\$8,000	Artisan used this
Sensor Tech	E200 ORT-13	12K	200	Not given	Not given	50kHz	Non-contact Optical	\$8429	Most expensive
Sensor Tech	RWT320-FB	12K	225	3.56E4	1.43E-4	USB digital output 2kHz	Non-contact Surface acoustic wave	\$3,588	TorqView not included

Notice the special exceptions to the Binsfeld sensor. There is no torsional stiffness (Kc) and no mass moment of inertia (J) values for the Binsfeld sensor because it utilizes inductive strain gauge sensors built into a collar that is rigidly attached to the shaft. Many other sensors have no Kc or J values simply because the company didn't release any of this data.

In order to properly determine the best coupler for the system, the following parameters were used in the selection choices: torsional spring rate, clamping quality (self-centering and adequate strength), speed range, balancing quality, alignment capability, and price. The selection choices are tabulated in Table 3-3. During torque sensor research, it was recommended that the coupling should have at least three times the torsional stiffness of the sensor. This finding helped narrow down the selection. All the selected couplings below comply with this recommendation.

**Table 3-3: Coupling Selection Values**

<b>Company</b>	<b>Model</b>	<b>Max RPM</b>	<b>Max Torque (Nm)</b>	<b>Torsional Stiffness, Kc (Nm/rad)</b>	<b>Mass Moment of Inertia (kgm<sup>2</sup>)</b>	<b>Price Each</b>	<b>Notes</b>
DODGE	Para-flex	6K	200	N/A	N/A	-	Rubber membrane
Interface Single-Flex	950F300-M32-38	11.8K	250	28.0E4	1.22E-3	\$243	Recommended by Interface
R+W America	BKM-400-42-38	10K	400	17.0E4	0.62E-3	\$535	Final size depends on sensor
R+W America	BK2-200-105-42-38	10K	200	19.1E4	4.5E-3	\$372	Final size depends on sensor

In order to further narrow down the selection, modeling of different sensor-coupler combinations was completed in order to determine the system natural frequency. During this investigation, different methods for defining the model were determined. Figure 3-9 highlights this model with definitions of each of the components. Note that there are two methods of defining the model based on the placement of the

torsional stiffness of the torque sensor shaft. The red mass number 4 is the definition under investigation.

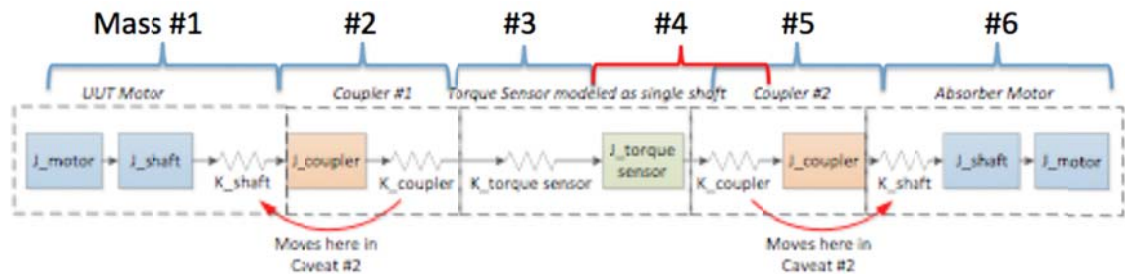


**Figure 3-9: Model Definitions Used to Determine System Natural Frequency with Mass Numbers Labeled above Different Components**

After modeling using both methods it was found that defining the system as first shown in Figure 3-9 makes most sense physically; therefore Caveat 2 is likely less representative of the physical system. Figure 3-10 illustrates the mode shapes of the system. More specific information on the modeling and detailed plot results can be found in Appendix D.

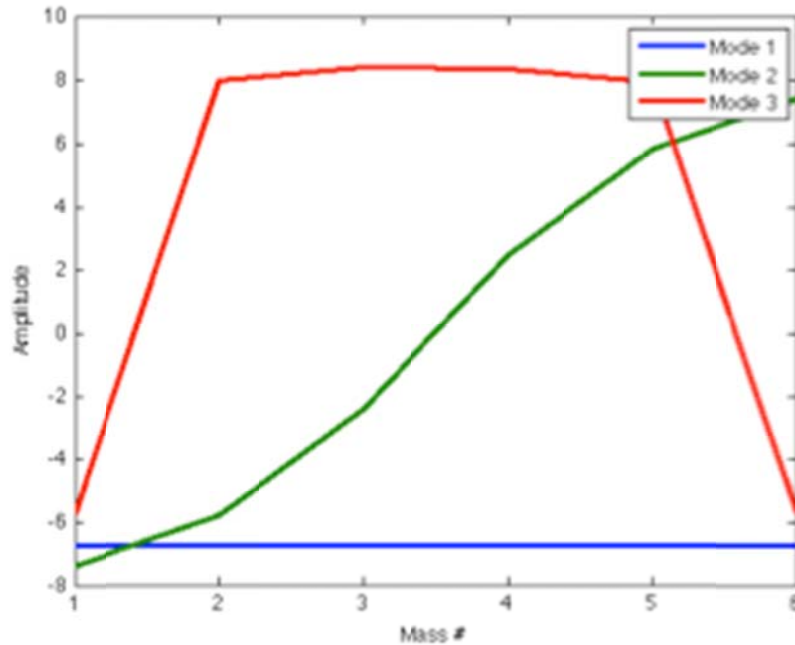


Figure 3-10: Amplitude at each Different Mass Number for the Three Different Modes

### 3.4.5.3 Results

The results of the frequency calculations provided interesting cost vs. performance trade-offs. As the plot below (Figure 3-11) demonstrates, almost all the sensors have a similar frequency range (330-415Hz) for the lowest vibration mode except the Binsfeld (600Hz), despite substantial variation in price. The plot also shows in a red dashed line, the cogging frequency of the motor at maximum speed. Notice that all but one sensor-coupler combination has a natural frequency lower than the cogging frequency, indicating that the system must transition through a natural frequency before reaching maximum motor speed.



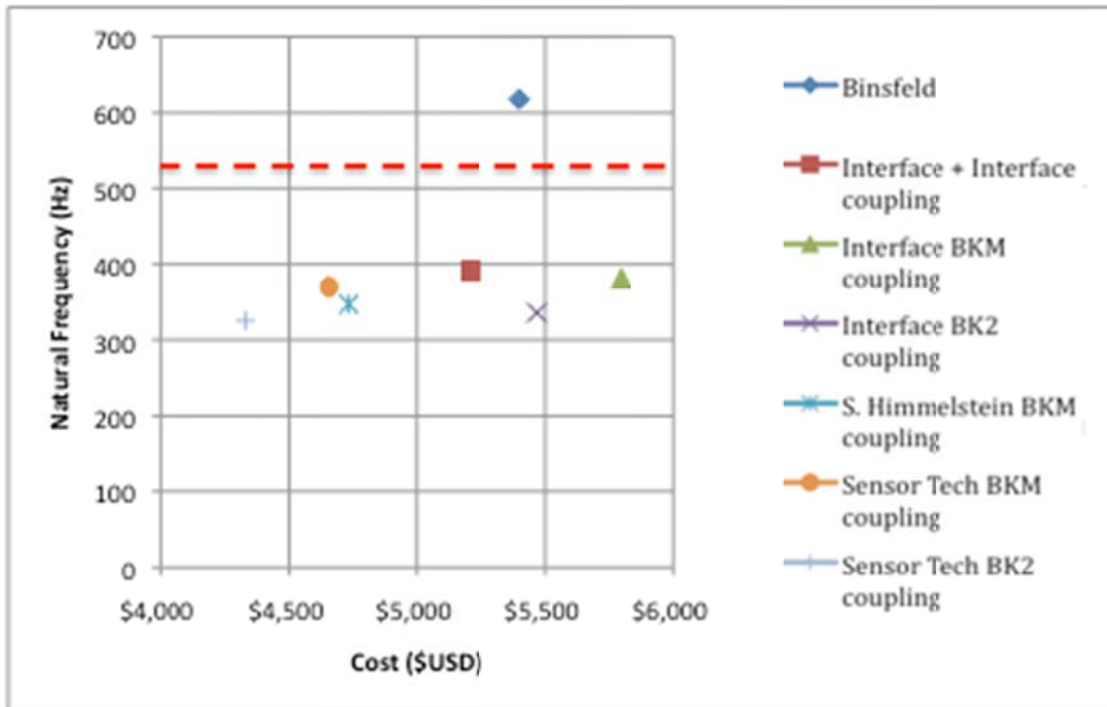
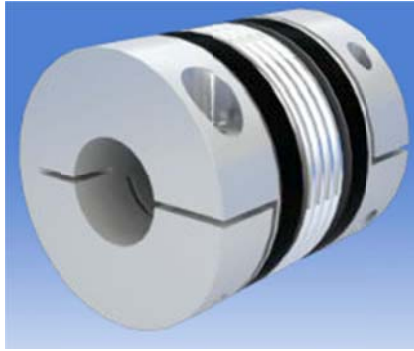


Figure 3-11: Visual Representation of Sensor and Coupling Cost vs. Natural Frequency Comparison with a Dashed Red Line Representing the Motor Natural Frequency

#### 3.4.5.4 Torque Sensor Selection

The selection of the torque sensor and coupler combination came down to a decision of price over performance. Figure 3-11 shows that all the options except the Binsfeld have the same natural frequency performance while having varying price. The Binsfeld solution exceeded the budget, therefore it was decided to purchase the lowest cost solution: the Sensor Tech RWT320 with BK2 couplings. Figure 3-12 and Figure 3-13 show the selected components.



**Figure 3-12: R+W America BK2 Bellows Coupling with Clamping Hub**



**Figure 3-13: Sensor Technologies RWT320 Torque Sensor**

The Sensor Technologies torque sensor utilizes a unique measuring technique based on measuring the resonant frequency change of Surface Acoustic Waves (SAW). It does this in a non-contact manner when strain is applied to a shaft inside the sensor. The applied torque causes a deformation of the quartz substrate of the SAW device, which in turn causes a change in its resonant frequency. The frequency signal measuring the resonant frequency is coupled via a non-contact RF rotating couple from the shaft to a fixed pick-up. It is the analysis of the difference in resonant frequencies between the two SAW devices, with electronic processing and calibration, that gives a precise indication of the torque transmitted by the shaft. SAW devices have a high immunity to magnetic fields allowing their use in motors, for example, where other analog

technologies are susceptible to electronic interference and are not suitable (Sensor Technology, 2011).

Since no sufficiently stiff combination could be found within the project budget, the system will be required to operate between the first and second harmonics during certain tests. To minimize vibration, users will be asked not to operate near the harmonic frequency for an extended period of time.

#### **3.4.6 Mounting Box for Torque Sensor and Two Electric Motors**

The design of an enclosure was investigated such that it will: protect users from entanglement, allow for proper shaft alignments, and secure the mounting of motors. Several different designs were considered and the selection was narrowed based on: ease of machineability (and thus cost), minimal welding distortion, maximal alignment between motor shafts, and sturdy mounting between motors and floor installation. These are highlighted below in Table 3-4.

**Table 3-4: Design Comparison for Different Mounting Box Designs**

<b>Design</b>	<b>Picture</b>	<b>Machineability</b>	<b>Alignment Tolerance</b>	<b>Cost</b>
A	Figure 3-14	Relatively simple: cut plate, buy box steel, weld up	Very poor. Alignment is dependent on floor, channels, boxes, and supports	Stock: high Machining: low
B	Figure 3-15	Difficult to fit height into large enough mill, little to no room for sockets for mounting bolts, narrow and shallow interior make it difficult for torque sensor	Better. Alignment is based on pocket location, flipping the piece over without a proper jig induces alignment errors	Stock: low Machining: medium
C	Figure 3-16	Simple design allows for more precision. Only three parts but water-jet, welding, and CNC machining required. Preventing “potato chip” warping of plate after welding heat is very difficult	Very tight. Machinist must design a jig to measure the piece from. However the first cut is the alignment pocket, which can be very precise and used to dimension all other geometry from	Stock: low Machining: medium-high

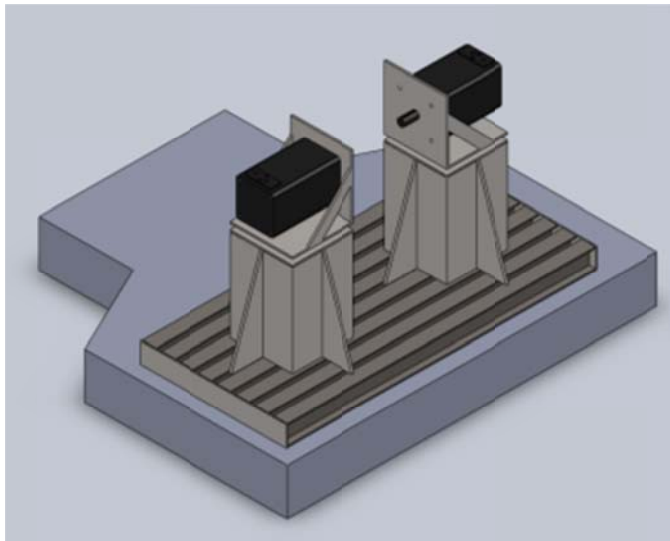


**Figure 3-14: Mounting Design Concept A. Motors Mounted on Reinforced Stands with Cantilevered L-Bracket Supports**

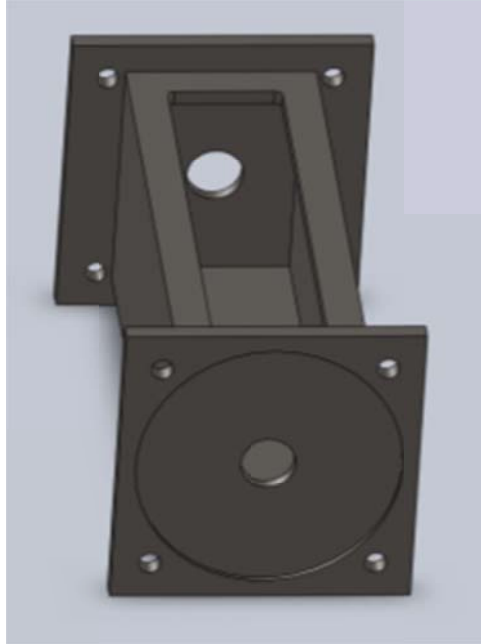


**Figure 3-15: Mounting Design Concept B. Square Box Mounted within Square Plate with Motor Mounting Holes**

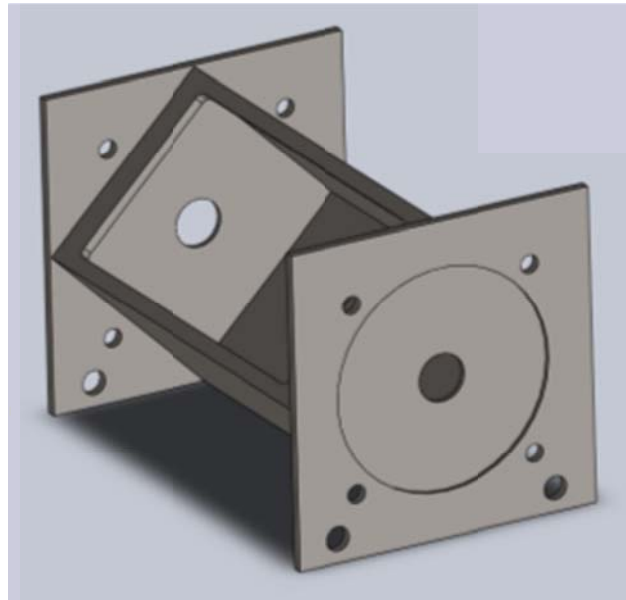


**Figure 3-16: Mounting Design Concept C. Square Box Rotated 45 Degrees to Allow for Most Interior Volume for Sensor and Couplers, Yet Still within Motor Mounting Holes**

Design C was the chosen design because it features the tightest alignment tolerances and allows for easy access to mounting bolts. Once this design was chosen,

stress calculations were performed using SolidWorks 3D CAD modeling software and its internal finite element analysis solver. Figure 3-17 shows the results of the simulation. This estimated model showed that loading the steel mounting plates would produce a von Mises stress of 3 ksi. This simulation helped estimate the thickness of the steel walls to determine if the motor max torque can damage the mounting box even under the worse loading moments.

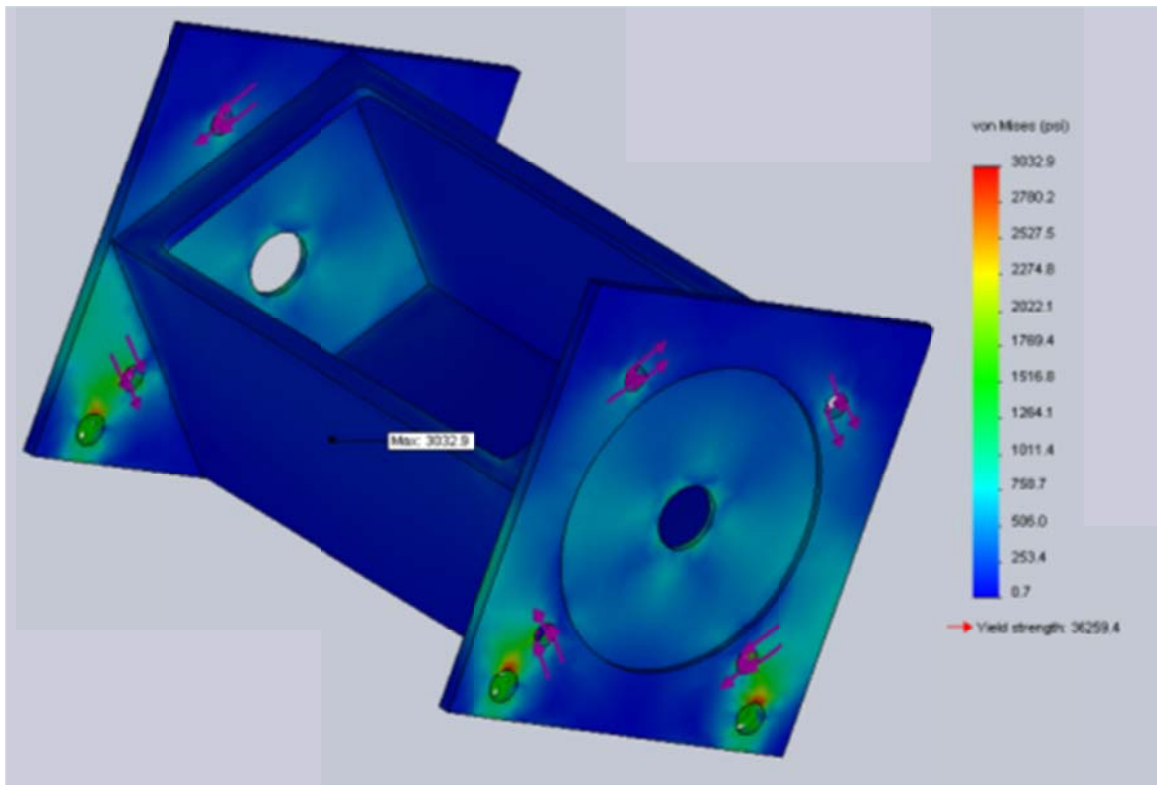


**Figure 3-17: Fundamental Finite Element Analysis of Design C with Concentrated Forces at the Motor Mounting Bolt Holes**

A challenge in Design C was allowing for sufficient tool space for installing the motor mounting bolts. Figure 3-18 shows the 3D CAD model of Design C and clearance for the socket and driver between the box and the bolt. After redesigning the box dimensions, the proper amount of spacing for a 9/16" nut and socket was found.

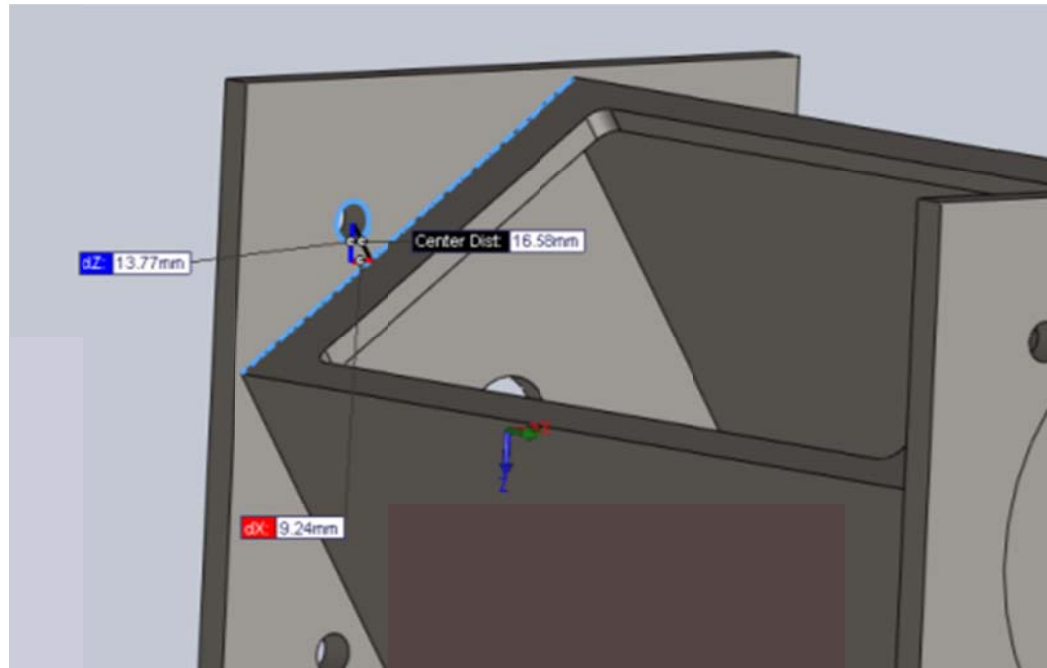


**Figure 3-18: CAD Model Showing Dimensions between Motor Mounting Bolt Hole and the Next Surface**

The other crucial design challenge was heat stress when welding the plate ends to the box. From a design perspective, welding on the interior of the box is ideal. However, welding technicians can't get tools in the tight corners. The manufacturing company agreed to perform the welds cautiously, in a staggered pattern to balance the heat. The resulting deformation could then be removed during machining.

Particular care was taken with the machining instructions. Since the design must produce tight alignment between the motors mounted on opposite ends of the box, it is critical to assure the alignment pockets on either end of the box are both parallel and axisymmetric. To minimize machining errors, the number of machining steps prior to milling the alignment pockets was minimized. The box was cut to length (with a slight amount of spare to account for the finishing of the plates), the access hole was cut using

a water jet, the end plates were welded on, and then both ends were machined to create the alignment pockets. All other features are based off of these pockets to ensure proper alignment. Machining was completed incrementally, utilizing a unique jig, built by the manufacturing company, to assure both ends of the box were properly aligned.

Many different options for attaching the mounting box to the floor were considered as well. Some options included building a framework of I-beams or box rails to slide the test rig on. However, since the rig doesn't need to be interchangeable like in most ICE dyno test stands, direct concrete anchors could be used. In order to reduce vibrations, rubber isolation dampers were added between the mounting box and the concrete anchors. Below, Figure 3-19, is a picture of the final design featuring the mounting box, angle bracket, and dampers.

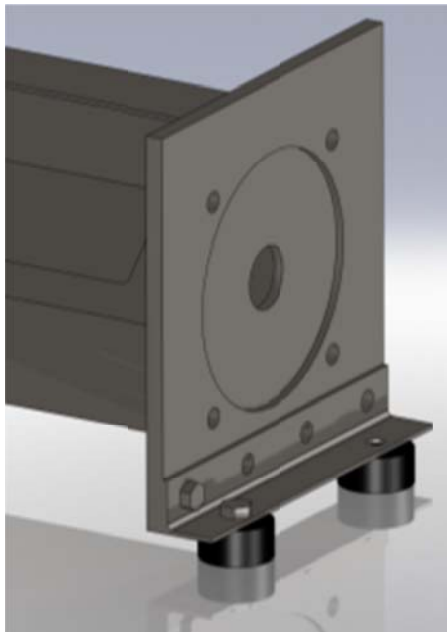


**Figure 3-19: 3D CAD Model of Design C with Mounting Feet Brackets and Bushings**



### **3.4.7 Powertrain Control Module**

The powertrain control module (PCM) was supplied by Artisan Vehicle Systems to provide communications between the inverters, batteries, and the user. The PCM is designed to be a plug-and-play solution by AVS. However, since this set-up is not a traditional application where the PCM only receives throttle input from the user, several communication modifications were made. Unlike vehicle control, the inverters in the lab can be controlled in two different methods (speed and torque control). The user then can select a multitude of different options to perform the desired test. These options include holding a set rpm for an extended period of time while incrementally increasing torque. This is very atypical for automotive use but standard for static laboratory testing.

### **3.4.8 Control Computer**

The following software was installed on the control computer: LabView, TorqueSense, Parker SSD DSE Lite, and the AVS PCM GUI. It is also equipped with math software to do analysis of results (Excel, MatLab, etc.) as well as modelers for control loops (MatLab Simulink), and 3D CAD modeling for designing layouts and building parts (SolidWorks). Fitted with this software, the computer functions as a way for the user to monitor the system and command the devices to perform in certain desired manners.

### **3.4.9 Data Acquisition System**

The data acquisition system (DAQ) chosen for the lab was based on cost, functionality, and expandability. As a main chassis, the National Instruments (NI)

CompactRIO (cRIO) with real-time controller and reconfigurable chassis (NI cRIO-9074) was chosen because it has: field-programmable gate array (FPGA), 8 slots for cards, up to 400 MHz real-time processor, 128 MB DRAM memory, and 256 MB of nonvolatile storage. In addition, the chassis was on sale because it will be replaced soon. One of the disadvantages to this model however, is that it is over-designed for its purpose in the lab. Since the chassis is FPGA based, this requires additional complex programming, which would have been avoided with a lower performance model. This adds more upfront programming to commission the lab but allows for flexible upgrading of the system in the future.

Proper cards were chosen for the cRio to handle the necessary I/O signals (digital in/out and analog in/out), required single power, and sampling rate required for the control system. For digital signals, the NI 9422 (8 channel, 24 to 60 V, 250  $\mu$ s C series sinking/sourcing digital input module) and NI 9472 (8 channel, 24 V Logic, 100  $\mu$ s sourcing C series digital output module) modules were chosen. Choice of the analog I/O cards was subject to time delays requirements, which were discussed in detail in section 2.3.4 and 2.4.7. The two analog modules NI 9215 (4 channel, 100 kS/s, 16-Bit,  $\pm 10$  V simultaneous sampling C series analog input module) and NI 9263 (4 channel, 100 kS/s, 16-Bit,  $\pm 10$  V, analog output module) were chosen because their sampling rate is greater than 1kHz required for AC voltage measurements.

Lastly, an NI 9853 2-Port, High-Speed CAN Module specifically for NI CompactRIO was selected in order for LabView to have CAN communications with all the key components in the system. This will allow the user to transmit and receive CAN

messages between the PCM, BMS, and the inverters. This is necessary for increased flexibility in communications between the devices and greater control of the system.

#### **3.4.10 Emergency Stop Circuit**

Typically, there are two ways to design an emergency stop (E-stop) circuit in industrial labs: series and parallel. In the series method, all switches have to be “ok” in order for power to flow to the system. In a parallel design, all switches are independent, but if the user closes one switch then the E-stop bus is powered causing an emergency stop of the system. The eDTC lab utilizes the parallel system. Once a single emergency stop is signaled (push of an E-stop switch or digitally pushing the DAQ E-stop button),  $24V_{DC}$  flows to the trip bus, which immediately powers all shunt trips, enable signals, and contactors to the de-energized or open state. Figure 3-20 shows a simplistic flow diagram of the E-stop circuit design.

It is important to note that the E-stop system is completely independent of the control system and does not require any input from the control computer to operate. However, a signal from the control system can trip the E-stop system, if necessary. The system is reliable as  $24V_{DC}$  is supplied. Additional redundancy could be built into the system to prevent the system from failing should the 24V become disconnected. However, at this time it was deemed as unnecessary.

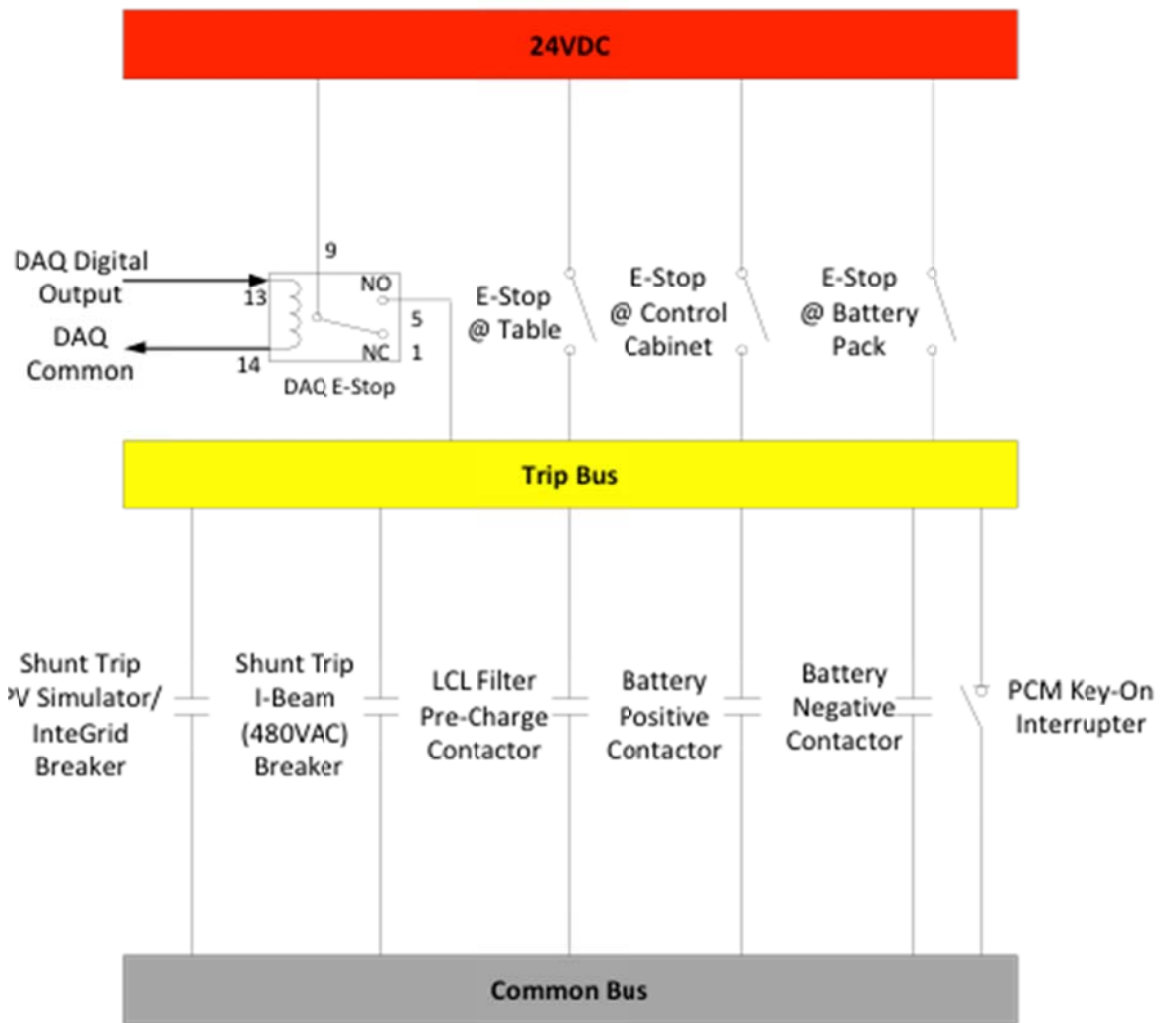


Figure 3-20: Simplistic Schematic of E-stop Logic

### 3.5 Check Out and Verification

This final section of the dynamometer portion of the eDTC lab discusses the final construction and implementation of the key components of the lab (Section 3.5.1) as well as an operational guideline for dynamometer users (Section 3.5.2). After these two subsections is the section on coursework examples (Section 3.6) to show how the educational objectives of the lab were met.

### 3.5.1 Implementation and Construction

The completed test center was a successful integration of motors, inverters, DC power supply, regenerative DC bus bar design, torque sensor, and liquid cooling circuit. Figure

3-21 illustrates the conceptual lab layout in a CAD model. The figures following (

Figure 3-22, Figure 3-23, Figure 3-24, and Figure 3-25) illustrate the lab as built with key components labeled.

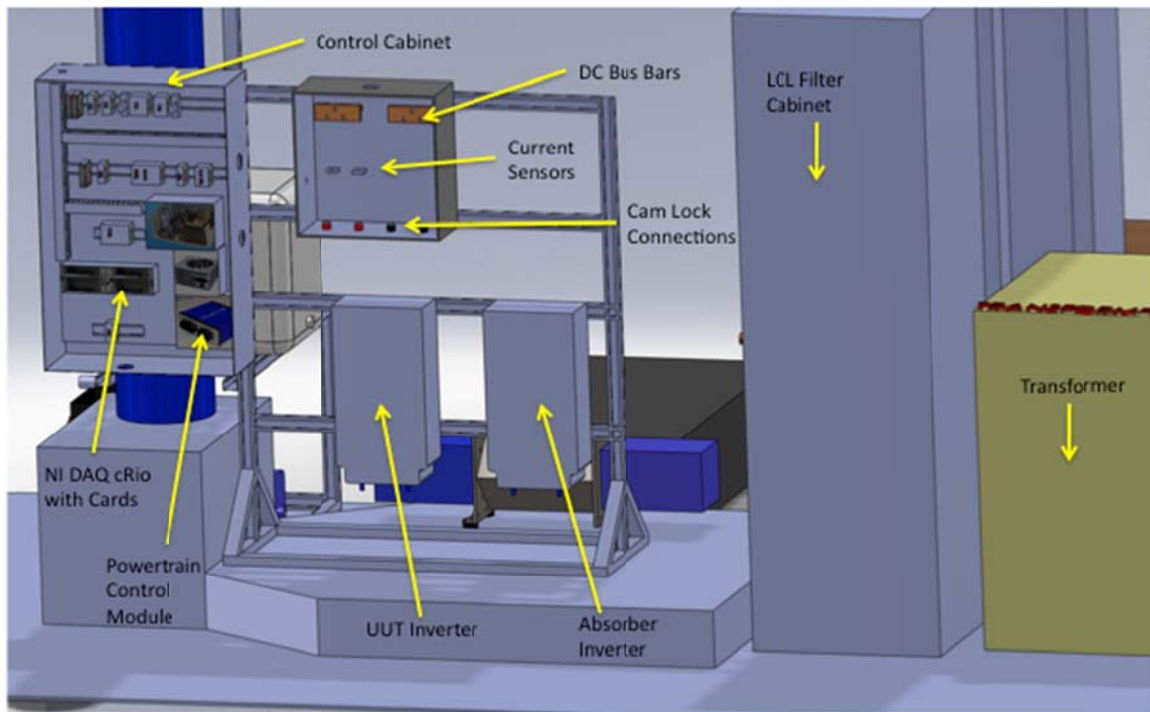


Figure 3-21: 3D CAD Model Detailed Layout with Component Call-Outs

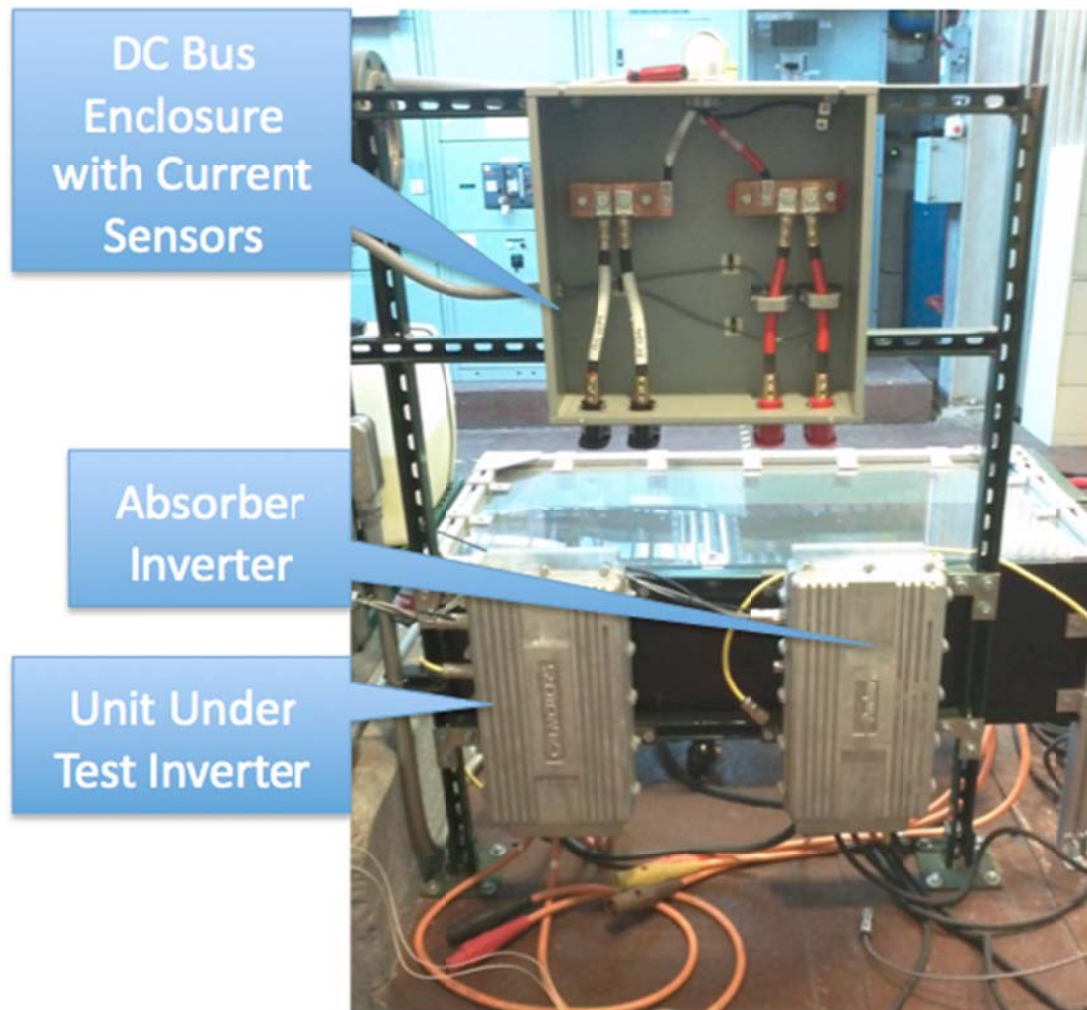


Figure 3-22: Inverter Rack with DC Bus Bar Cabinet

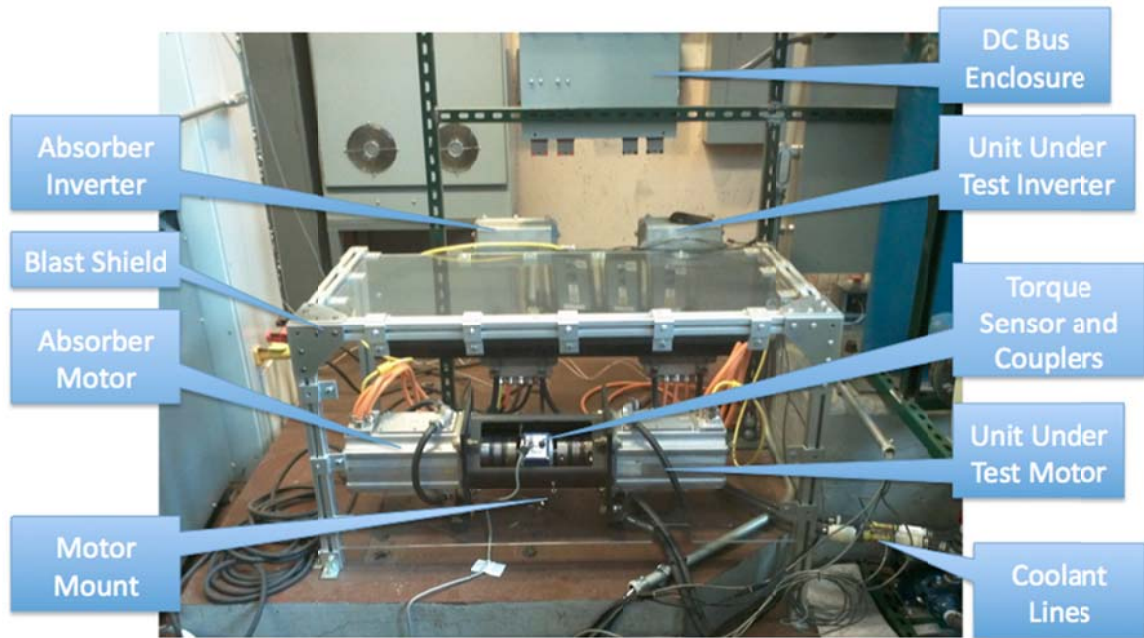


Figure 3-23: Dyno Rig with Key Components Called Out

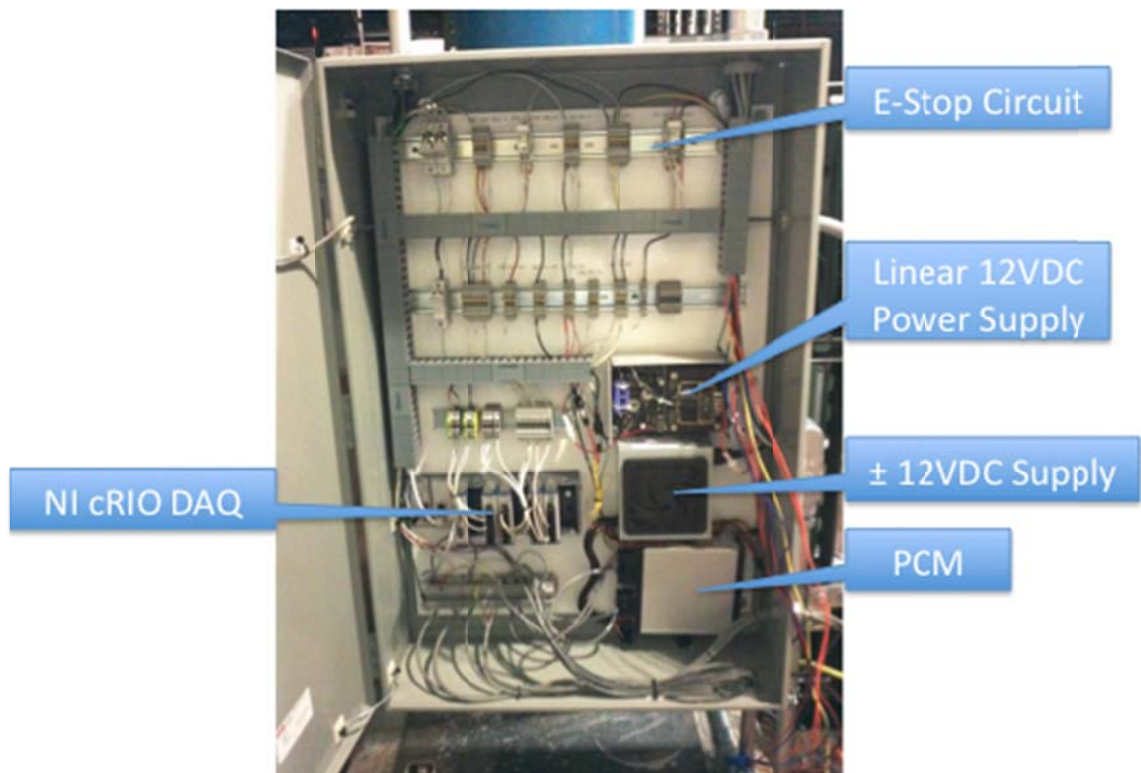


Figure 3-24: Control Cabinet Layout



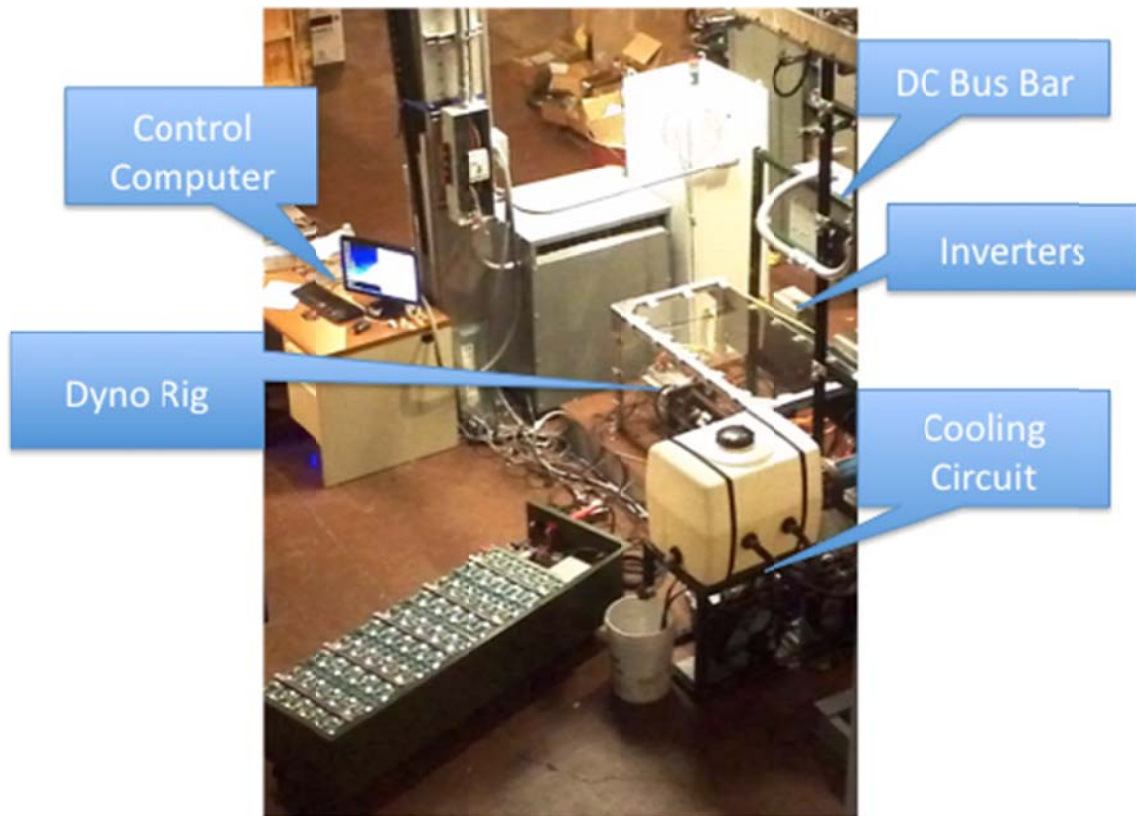


Figure 3-25: Physical Layout of Constructed Components

### 3.5.2 Motor Spin-Up and Coast Down Operation

To perform dyno testing, the user must first ensure all the connections between the DC bus bar cabinet, inverters, and motors are properly made. All the E-stop buttons need to be in the open, twisted up, off position. The user must obtain permission from *InteGrid* to have control of the AE Summit DC power supply and power on the *InteGrid* control PC. Using the AVS PCM GUI software on the eDTC control computer and DSE Lite software, the user can control the absorber inverter and motor. Depending on the set-up there can be two ways to operate the dyno. One way is to have an additional control computer to communicate solely with the unit under test motor and inverter via the DSE Lite software and manual control. This method could be substituted with a virtual



PC application that allows two DSE programs to run simultaneously on one PC. The other method is to have the NI cRIO DAQ communicate via CAN to the PCM and inverters, which can, in turn, communicate with both inverters. The first method is the only implemented method at this time.

To start the system, the user must set the *InteGrid* DC power supply control computer to command a bus voltage of 350 V<sub>DC</sub>. At the eDTC control computer, the user may turn the enable key to begin testing the dyno. While monitoring the program on the eDTC control computer (either LabView, AVS PCM GUI, or DSE Lite) the user can define speed set points on the absorber and then “throttle” up or down the torque request of the UUT motor. While performing different tests, the user can opt to record data via the PCM GUI, which will save data as a .csv file for a later use.

When the user is finished performing the desired tests they must spin the motors down to a stop by reducing the set points and switching the enable switch to the OFF position for both inverters. After this, the *InteGrid* control PC must properly shut down the DC power supply and open the service disconnects for all power equipment.

### **3.6 Course Work Examples**

This section illustrates four different labs that professors will use to educate students using the eDTC laboratory. These labs include mapping the torque of the motors (Section 3.6.1), finding the efficiency of the lab (Section 3.6.2), understanding thermal effects (Section 3.6.3), and an introduction to grid-attached-storage (Section 3.6.4).

### 3.6.1 Lab #1: Map Torque versus Speed Curve

**Introduction:** The objective of this lab is to learn more about motor performance, in particular, the torque curve. Students will experience creating a torque map similar to the torque curve in Figure 3-26. To perform this test, the user defines a set speed for the absorber motor and identifies the maximum torque achievable by UUT at that speed. Since the motors are directly coupled, both will operate at the same speed at all times, except for minor vibrational variations. The UUT is operated under torque control – i.e. the user commands the UUT to output a defined torque. The absorber is operated under speed control – i.e. it is commanded to always maintain a set speed. When the user changes the UUT’s commanded torque, the UUT attempts to produce that torque, while the absorber attempts to maintain a set speed. Since the absorber is controlled so that it can always produce more torque than the UUT, the speed may vary briefly before quickly returning to the commanded level.

During this test, the user will define 16 different speeds and record the max torque that results for each. Students must plot these max points and compare them to the torque curve below courtesy of [www.artisanvs.com](http://www.artisanvs.com).

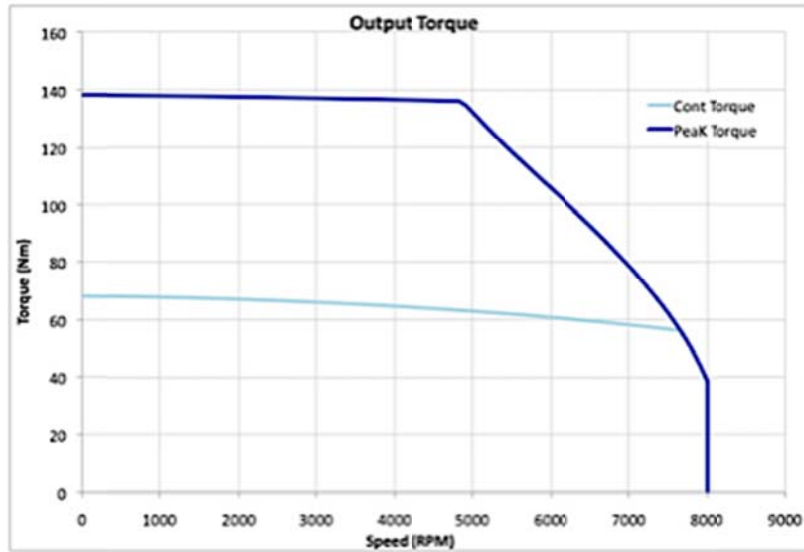


**Figure 3-26: Torque Curve at Continuous and Peak Torque**

### **Learning Objectives:**

1. Understand dynamometer controls
2. Learn how to measure the output torque of a motor
3. Gain experience with an electric motor torque curve and performance

### **Lab Operations:**

1. Check with the lab instructor that all the proper connections are made between motors, inverters, and DC bus cabinet. Plug-in the torque sensor power, Eagle 12V CPU power, and the LPS power plugs. Ensure all cabinets and covers are closed, E-stop switches in the OFF position (up), pumps and fans are turned on and water is flowing, and nothing is obstructing the spinning motion of the motor shafts
2. In the *InteGrid* PV Simulator area, switch on the power and log into the control computer. Open PV\_Manual\_Operator.vi (found on the desktop) and follow the

powering on instructions (screenshot shown in Figure 3-27). Set the command voltage to 350VDC

3. Return to the eDTC. Open the Motor\_Map.vi (example screen shot is shown in Figure 3-28), SSD Drives: DSE Lite, and Calmotors GUI (also known as AVS PCM GUI)
4. Set the absorber speed to 1,000rpm and switch on the enable switch on the desk control box
5. Define the UUT inverter torque to 10% and switch on the enable switch
6. Quickly accelerate to 200% torque and let the motor stabilize for five seconds and record the torque value
7. Ramp the torque back down to 0%
8. Change the absorber speed to 1,500rpm
9. Monitor the winding temperature at all times to assure that it is within 5°C of the initial winding temperature. If the temperature increases, wait until it cools sufficiently
10. Quickly accelerate the UUT to 200% torque and let it stabilize for 5 seconds.  
Record the torque at this point
11. Ramp the torque back down to 0%
12. Repeat steps 6-9 with 500rpm increments until you reach 8,000rpm
13. Plot your results on a Torque vs. Speed graph and submit to the instructor

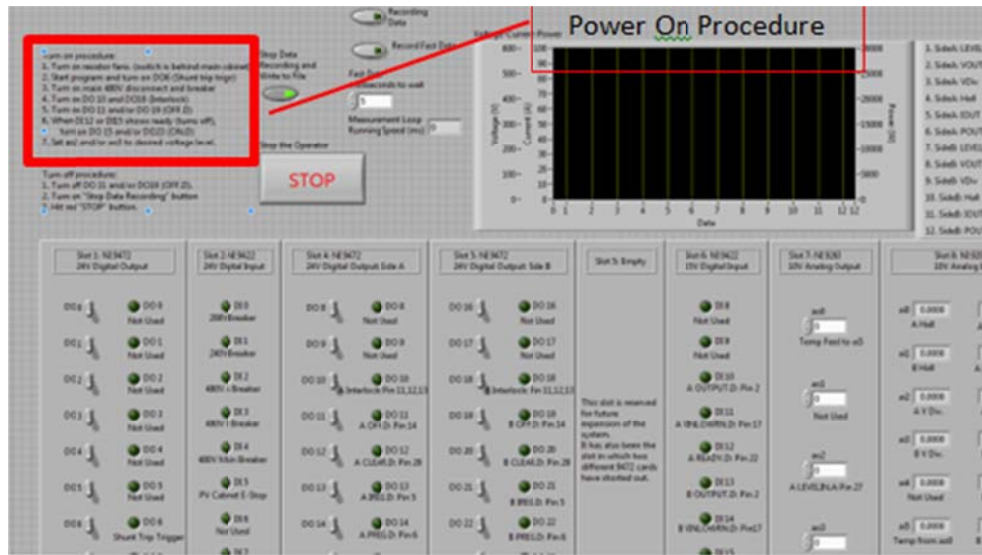


Figure 3-27: PV Simulator Screenshot of Manual\_Voltage.vi

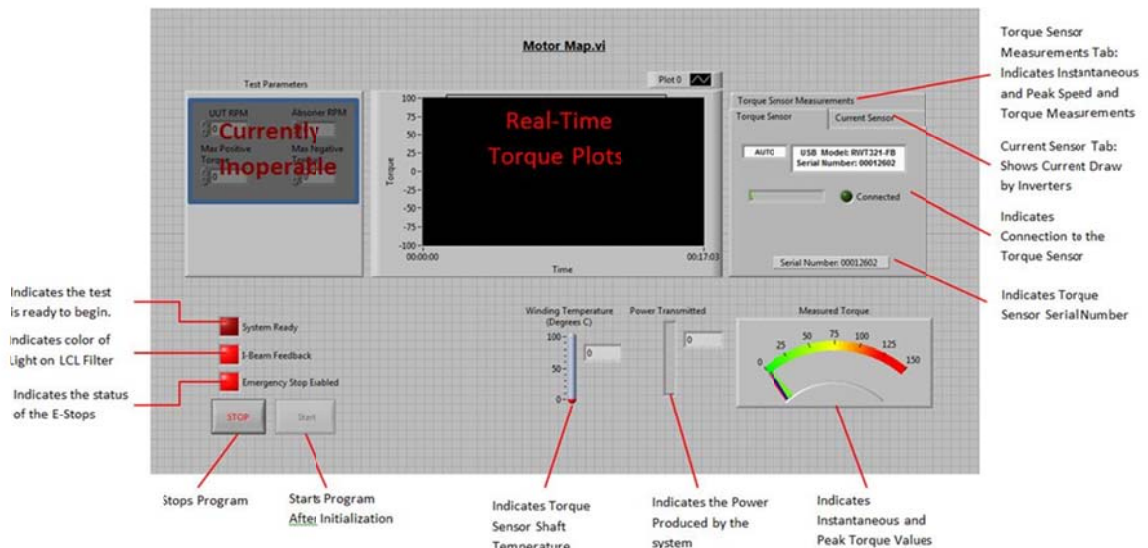


Figure 3-28: Screenshot and Explanations of Motor\_Map.vi

**Homework:** Now that you have seen how a dyno works, explain what is going on in “real world” applications. Explain the analogy between the absorber and road load. During the testing of the motor, why did the torque drop off at a certain speed? Explain

why electric motors behave in this manner. Are there different ways to control electric motors to change the impacts of the motor torque curve? Explain your reasoning.

Hand in your plot from in-lab and your essay answers to the questions above to your lab instructor before the beginning of the next lab.

### **3.6.2 Lab #2: Map Motor Efficiency Lab**

**Introduction:** The purpose of this lab is to better understand the efficiencies of an electric motor. As you learned in-class, there are many parts of an electric motor, which are subject to friction, heat, and electrical losses. This lab exercise investigates these losses at a system level.

To investigate efficiency, you will compare the electrical power input into the UUT inverter, the mechanical power transmitted to the absorber via the shaft coupling, and the electrical power returned to the system by the absorber. Given measurements at three points, it is possible to isolate the efficiency of subsets of the laboratory: The efficiency of UUT inverter/motor, and the efficiency of the absorber inverter/motor. Since one motor is operating exclusively in traction mode, and the other exclusively in regenerative mode, it is possible to assess the efficiency of the same motor model in both modes simultaneously. Figure 3-29 shows the estimated efficiencies for each component in the system.

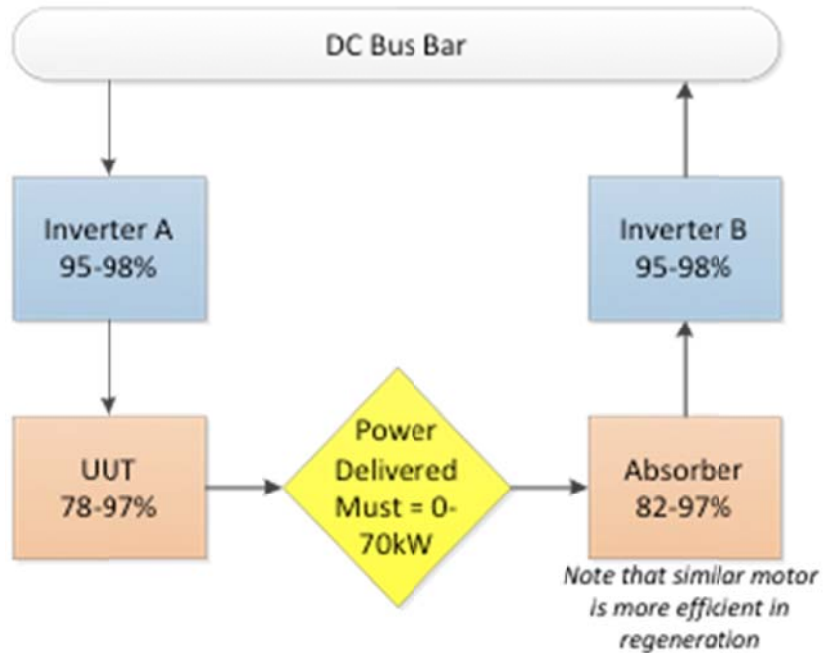


**Figure 3-29: Flow Schematic with Efficiencies at Each Component**

Your goal of this lab is to measure actual losses, explain their origin, map how efficiency varies with speed and torque, and what impact efficiency has on vehicle operation. To complete this, you will map the efficiency of the absorber or UUT. Figure 3-30 (courtesy of [http://www.uqm.com/propulsion\\_specs.php](http://www.uqm.com/propulsion_specs.php)) is an example motor efficiency map that you will produce at the end of the lab.

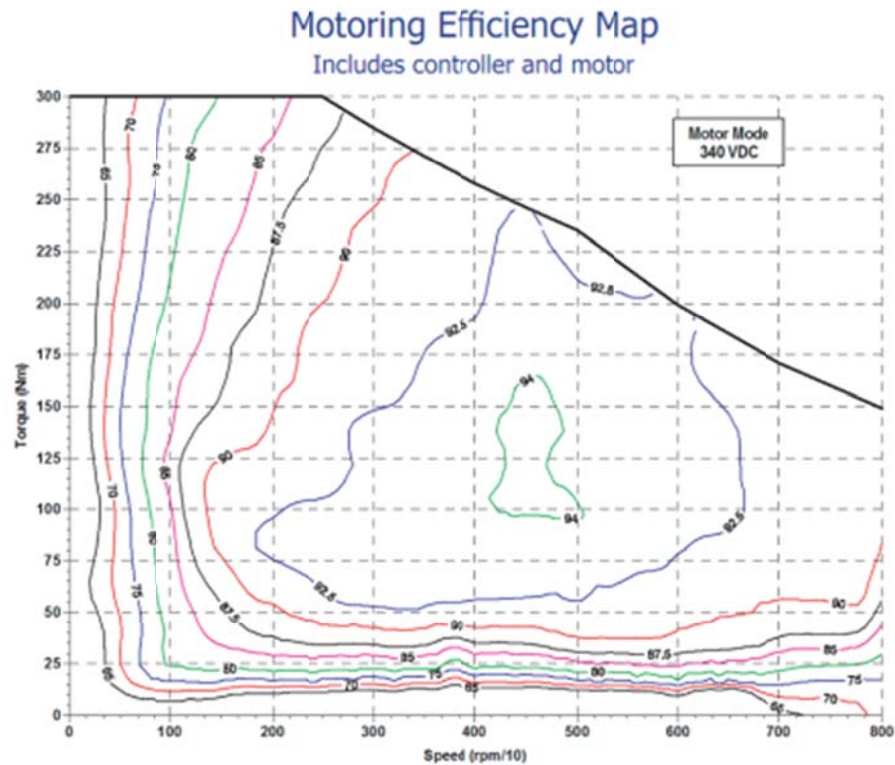


**Figure 3-30: Example Motor Efficiency Map**

### Learning Objectives:

1. Understand the power flow within the lab components
2. Get a hands-on perspective of efficiencies of a motor
3. Make a motor efficiency map

In most test labs the power for the dyno motor is typically supplied from a battery pack to simulate actual vehicle testing. However, in the case of the eDTC lab, the power comes from a controllable DC power supply. The DC supply sets the DC bus voltage seen by both the UUT and absorber inverters, in much the same way that a battery pack sets the DC bus voltage in a vehicle. Since the absorber is “regenerating” power onto the DC bus, the DC supply only provides “make up” power for losses in the



UUT and absorber. By regenerating the absorbed power back onto the DC bus, the lab minimizes the energy consumed and reduces the size of certain components.

**Lab Procedure:**

1. Check with the lab instructor that all the proper connections are made between motors, inverters, and DC bus cabinet. Plug-in the torque sensor power, Eagle 12V CPU power, and the LPS power plugs. Ensure all cabinets and covers are closed, E-stop switches in the OFF position (up), pumps are turned on and water is flowing, and nothing is obstructing the spinning motion of the motor shafts
2. In the *InteGrid* PV Simulator area, switch on the power and log into the control computer. Open PV\_Manual\_Operator.vi (found on the desktop) and follow the powering on instructions. Set voltage to 350VDC – the emulated battery voltage – and the safety current limit to 50A
3. Return to the eDTC control computer. Open the Motor\_Map.vi, SSD Drives: DSE Lite, and Calmotors GUI (also known as AVS PCM GUI)
4. Set absorber speed to 1,000rpm and then switch the enable to on for the absorber inverter
5. Record winding temperature
6. Define the UUT inverter torque to 10% and switch the enable switch to the on position
7. Enable data logging

8. Slowly ramp up the UUT torque to 200% using intervals of 20% and pausing for 5 seconds between steps (the more systematic you are with this, the easier it will be to interpret your data)
9. Ramp torque down to 0%
10. Check the winding temperature. Is it within 5°C of the starting temp? If not, wait until it cools (the cooling loop should quickly cool the motors) If yes, proceed to the next step
11. Change the absorber speed to 1,500rpm
12. Repeat step 5
13. Ramp down torque to 0%
14. Repeat steps 5-7 until absorber speed is 8,000rpm
15. Ramp down torque to 0% and absorber speed to 0rpm
16. Switch off enable switches for both inverters, safely power down the DC power supply according to instructions, switch off all break disconnects
17. Open the data file showing absorber speed at each: torque, speed, voltage and current (for both inverters) of the system

**Homework:** Do the calculations using equation one (show below) to determine the system efficiency at each data point and create a plot of Torque vs. Speed with “islands” of efficiency in different colors like the example in Figure 3-30.

$$\eta = \left[ 1 - \frac{(Power_{in} - Power_{out})}{Power_{in}} \right] 100 \quad (1)$$

### 3.6.3 Lab #3: Investigate Temperature Effects on Electric Motors

**Introduction:** The purpose of this lab is to investigate the impact of the winding temperature on the performance of a motor operating in different states. You will determine how changes in winding resistance impact the motor output in four scenarios: steady state cold, steady state hot, acceleration, and regeneration. Be prepared to answer where the heat is being transferred to and why.

#### Learning Objectives:

1. Understand the impact of temperature on motor performance
2. Get a hands-on perspective of motor operation in different conditions

#### Lab Procedure:

1. Check with the lab instructor that all the proper connections are made between motors, inverters, and DC bus cabinet. Plug-in the torque sensor power, Eagle 12V CPU power, and the LPS power plugs. Ensure all cabinets and covers are closed, E-stop switches in the OFF position (up), pumps are turned on and water is flowing, and nothing is obstructing the spinning motion of the motor shafts
2. In the *InteGrid* PV Simulator area, turn on the power and log into the control computer. Open PV\_Manual\_Operator.vi (found on the desktop) and follow the powering on instructions. Set voltage to 350VDC
3. Open the Motor\_Map.vi, SSD Drives: DSE Lite, and Calmotors GUI (also known as AVS PCM GUI)

4. Set the absorber speed to 1,000rpm, switch the enable absorber switch to on, and record the initial winding temperature
5. Switch the UUT inverter enable switch to on after setting the torque to 5%
6. Slowly accelerate to 75% torque and wait until the system stabilizes
7. Note the temperature over 1 minute
8. Bring the torque down to 0%
9. Quickly accelerate to 75% torque and wait until the system stabilizes and record the temperature in both the UUT and absorber motors
10. Bring the torque back down to 0%
11. Let the windings cool down to the initial temp before moving on to the next step
12. Change the absorber speed to 5,000rpm
13. Quickly accelerate to 200% torque
14. Record how the temperature of the winding responds to this input over time
15. After about 30 seconds, return to the torque to 0% and the absorber speed to 1,000rpm
16. Note the change you see in the temperature
17. Return both torque and speed to 0 and wait for the system to come to a stop.  
  
Let the coolant flow until the winding temperature is at the initial temperature when you started the lab

**Homework:** Discuss the effects of time and load in terms of temperature in the UUT and absorber motors. Present the data you collected in a manner that you best think describes the heat transfer.

Consider automakers performing these tests to determine how to best cool the motor. When do you expect the motors to experience different heating characteristics? Low torque up a hill, driving in reverse, highway cruising? Describe what will happen in each one of these cases and a few of your own based on the results you have gathered from this lab. Can you model the temperature characteristics of the motor at different speeds and at different length durations? Organize these findings and hand them into the lab director before the start of the next lab.

#### **3.6.4 Lab #4: Intro to Grid-Attached-Storage Lab**

**Introduction:** The purpose of this lab is to give students an initial contact with grid-attached-storage to understand the relationship between grid demand and allowable battery charge and discharge rates. Students will experience how a storage device, such as an automotive pack battery, interfaces with the grid.

“Grid-attached-storage” (GAS) involves connecting a storage device – in this case a battery – to the utility grid and controlling the charge and discharge rate of the storage to meet objectives such as grid stabilization, frequency regulation or peak reduction. For example, a battery could be utilized for peak shaving – charging during periods of low electricity consumption (typically when electricity cost is low) and discharging during periods of peak electricity consumption (typically when electricity cost is high).

This lab focuses on the basic requirements to control a battery GAS system connected to the power grid. Students will monitor the behavior of the battery while changing commanded charge and discharge levels.

**Learning Objectives:**

1. Understand grid-attached-storage components
2. Get a hands-on perspective of GAS current control methods
3. Witness the effects of battery performance with short pulse demands

**Lab Procedure:**

1. Open the PCM GUI and DSE Lite programs at the eDTC control PC
2. Check with the lab supervisor that all the proper connections between the inverter, battery, and transformer have been made. Ensure all safety checks are in place: no cables are improperly color matched, everything is properly connected, all shields and covers are closed, all E-stop switches are in the off position
3. Plug in the GAS water pump and close the priming valve to properly activate the cooling loop. Plug in the Eagle 12V power supply plug and turn on the GAS electric fan at the desk control box
4. Check that the battery is properly communicating with the PCM via CAN
5. Before moving to the next step, ensure that the LC filter pre-charge e-stop switch in the LC filter cabinet is in the off or twisted up position. Strict adherence to this will reduce the risk of arcing and damage to the LC filter
6. Follow *InteGrid* connection instructions to energize the 480V<sub>AC</sub> main tie breakers

7. Close the 480V<sub>AC</sub> I-Beam breaker on, turn on the LC filter fans, and close the LC filter knife switch on, letting the pre-charge circuit come online
8. Turn on the inverter through the ENABLE rocker switch via the control box by the eDTC control PC
9. Turn the battery key-on at the control desk box to the on position. You should hear the battery contactors switch the battery pre-charge on and then close the rest of the contactors
10. Once the system is synchronized with the grid, manual current control can begin
11. Using DSE Lite increase or decrease the current set-points in 1% increments following the control provided by your instructor
12. While manually controlling the current set points, monitor the battery SOC to assure that the battery pack remains within its operational SOC limits
13. Take notes of how the controller responds, battery pack behaves, and the time required for the system to respond to commanded changes in current output
14. Power down the system by commanding the PCM to open the battery contacts, turning the key to the off position, disabling AFE (absorber inverter ENANBLE rocker switch off), opening/switching off the LC filter breaker, and lastly the 480V<sub>AC</sub> breaker
15. To safely store the lab: unplug the battery connections, communication cable (Deutsche 23-pin connector). Unplug all the other power devices in the eDTC lab (water pumps, Eagle 12VDC CPU power supply, linear power supply (LPS), etc.)

**Homework:** Hand in a discussion and a controller model to your lab supervisor before the start of the next lab. In your discussion, consider the following questions:

- How do the asymmetric charge and discharge limits impact the control algorithm for the GAS system?
- Given that a fully charged or discharged battery system can no longer provide full control functionality to the grid, what control architecture would you propose to maintain the SOC of the battery while still responding to grid control requirements?
- Given the step response characteristics of the system, what is the maximum allowable control frequency for the system?

One application of GAS is to “firm” output from a renewable power plant, such as a wind farm or photovoltaic system. The concept behind firming is to control charging/discharging of the GAS system so that the combined output of the renewable plant and GAS system maintains a constant, forecasted value. The second part of this homework is to design a controller for renewable firming. As you witnessed, the lab currently uses manual set-point control for real and reactive power commands. Your objective is to design a control algorithm to firm the output from a renewable power plant. Your instructor will provide a time series output from a renewable power plant. In the next lab, you will test your algorithm simulation and controller (pending instructor approval) by uploading it to the inverter software controller to verify its robustness.



## **4. Summary and Conclusions**

The eDTC lab at Colorado State University is a test bed that advances the knowledge and training of engineers for a sustainable future. It allows for educating the next work force in electrical mobility and provides researchers with the components to test the implications of grid-attached-storage. The results from the lab will inform how utilities and electrified vehicles interact as well as the repurposing EV batteries for GAS systems.

This thesis described the need for understanding grid storage and its implications, what challenges are accompanied with designing a test bed of this scale with automotive-grade components, why different components were chosen over alternatives, and a brief demonstration of the system operation. The goals of the design were accomplished and a successful lab was constructed.

### **4.1 Future of the eDTC**

This is an exciting time for the eDTC lab because there are several new uses designated for the GAS and dyno portions of the lab. First, new graduate students will design new control algorithms for GAS for testing in both simulation and class environments. Second, used batteries from Altairnano and A123 were donated to CSU specifically for battery second use testing at the eDTC. Testing protocols and performance of these batteries is of great importance to industry and national labs.

Third, EcoCar2 teams will begin drive cycle testing using the dyno portion of the eDTC. This will provide real world results and validation to the modeling currently being evaluated. Finally, beginning spring 2011, the new ENGR580a1 class will utilize the course exercises designed in this thesis. With these and many more exciting projects, the eDTC has begun to show its importance and usefulness to both researchers and university students.

## WORKS CITED

- Blooming, T., & Carnovale, D. (2007). *Application of IEEE Std 519-992 Harmonic Limits*. IAS Atlanta Section. Appleton, WI: IEEE.
- Bredenberg, A. (2011, April 25). *Battery Storage: Smoothing Out the Wrinkles of Renewable Energy*. Retrieved May 22, 2011, from Thomas Net News: [http://news.thomasnet.com/green\\_clean/2011/04/25/battery-storage-smoothing-out-the-wrinkles-of-renewable-energy/](http://news.thomasnet.com/green_clean/2011/04/25/battery-storage-smoothing-out-the-wrinkles-of-renewable-energy/)
- Brockman, J. (2008, July 22). *Plug In, Drive On: The Promise of Next-Gen Hybrids*. Retrieved May 14, 2011, from NPR: <http://www.npr.org/templates/story/story.php?storyId=92792068>
- Brooks, A. (2002). *Vehicle-to-Grid Demonstration Project: Grid Regulation Ancillary Service with a Battery Electric Vehicle*. AC Propulsion. CARB.
- Bureau of Transportation: Statistics. (2010, May 03). *Number of U.S. Aircraft, Vehicles, Vessels, and Other Conveyances*. Retrieved May 12, 2011, from Research and Innovative Technology Administration (RITA), BTS: [http://www.bts.gov/publications/national\\_transportation\\_statistics/html/table\\_01\\_11.html](http://www.bts.gov/publications/national_transportation_statistics/html/table_01_11.html)
- Coomb, H. S. (2011). *Renewable Sustainable Expeditionary Power*. U.S. Navy, Office of Naval Research. Arlington, VA: U.S. Navy.
- Cready, E., Lippert, J., & Phil, J. (2003). *Technical and Economic Feasibility of Applying Used EV Batteries in Stationary Applications*. Sandia National Laboratories. Albuquerque, NM: Department of Energy.
- Demand Energy. (2011). *Demand Energy - Renewables Firming*. Retrieved September 2011, from Demand Energy: <http://demandenergynetworks.com/applications/use-case-renewables-firming.asp>
- Denholm, P., & Short, W. (2006). *An Evaluation of Utility System Impacts and Benefits of Optimally Dispatched Plug-In Hybrid Electric Vehicles*. National Renewable Energy Laboratory. Golden, CO: Department of Energy.

Dickinson, R., & Milano, S. (2002, July 11). "Isolated Open Loop Current Sensing Using Hall Effect Technology in an Optimized Magnetic Circuit. Concord, NH, USA.

Duvall, M. (2008). How many plug in hybrids can a smart grid handle? *Plug-In 2008*. San Jose, CA: EPRI.

EPRI. (2011). *Plugging In: A Consumer's Guide to the Electric Vehicle*. Electric Powertrain Research Institute. Palo Alto, CA: EPRI.

Eyer, J., & Corey, G. (2010). *Energy Storage for the Electricity Grid: Benefits and Market Potential Assessment Guide*. Sandia National Laboratory. Albuquerque, NM: Department of Energy.

Gavine, A. (2011, January). Ticket to Ride: User-Friendly System. *Electric and Hybrid Vehicle Technology International* , p. 50.

Goggin, M. (2008). *Wind Power and Energy Storage Fact Sheet*. American Wind Energy Association. AWEA.

Gupta, P. (2009, August 26). *Utility wants to deploy largest grid battery ever*. Retrieved May 30, 2011, from Reuters: <http://www.reuters.com/article/2009/08/26/us-edison-battery-idUSTRE57P4PJ20090826?sp=true>

Hadley, S., & Tsvetkova, A. (2008). *Potential Impacts of Plug-in Hybrid Electric Vehicles on Regional Power Generation*. Oak Ridge National Laboratory. Oak Ridge, TN: Department of Energy.

Himelic, J., & Novachek, F. (2010). *Sodium Sulfur Battery Energy Storage and Its Potential To Enable Further Integration of Wind*,. Xcel Energy Renewable Development Fund. Denver, CO: Xcel Energy.

Hoevenaars, T. (2003). *Interpreting IEEE Std 519 and Meeting its Harmonic Limits in VFD Applications*. IEEE.

Jost, B. (2011, September 1). *Who Pays for Firming Up Variable Energy Resources?* Retrieved September 2011, from [http://www.powermag.com/renewables/wind/Who-Pays-for-Firming-Up-Variable-Energy-Resources\\_3977.html](http://www.powermag.com/renewables/wind/Who-Pays-for-Firming-Up-Variable-Energy-Resources_3977.html)

Kempton, W., & Tomić, J. (2005). Vehicle-to-grid power fundamentals: Calculating capacity and net revenue. *Journal of Power Sources* , 144 (1), 268-279.

Kempton, W., Tomić, J., Letendre, S., Brooks, A., & Lipman, T. (2001). *Vehicle to grid power: Battery, hybrid and fuel cell vehicles as resources for distributed electric power in California*. University of California, Davis, Davis Institute for Transportation Studies. Davis, CA: University of California.

Kempton, W., Udo, V., & Huber, K. (2008). A Test of Vehicle-To-Grid (V2G) for Energy Storage and Frequency Regulation in the PJM System. *Mid-Atlantic Grid Interactive Cars Consortium*.

Kintner-Meyer, M., Schneider, K., & Pratt, R. (2006). *Impacts assessment of plug-in hybrid vehicles on electric utilities and regional US power grids, Part 1: Technical Analysis*. Pacific Northwest National Laboratory. Richmond, WA: PNNL.

Kirby, B. (2004). *Frequency Regulation Basics and Trends*. Oak Ridge National Laboratory. Oak Ridge, TN: Department of Energy.

Levitan, D. (2010, October 14). *Rising Hopes that Electric Cars Can Play a Key Role on the Grid*. Retrieved May 22, 2011, from Yale Environment 360: [http://e360.yale.edu/feature/rising\\_hopes\\_that\\_electric\\_cars\\_can\\_play\\_a\\_key\\_role\\_on\\_the\\_grid/2328/](http://e360.yale.edu/feature/rising_hopes_that_electric_cars_can_play_a_key_role_on_the_grid/2328/)

Lutz, M., Zimmerle, D., Huff, B., & Bradley, T. (2011). Design and Construction of Grid Attached Storage Simulator. *ASME 2011 5th International Conference on Energy Sustainability & 9th Fuel Cell Science, Engineering and Technology Conference* (pp. 1-9). Washington, DC: ASME.

McGuinness, M., & Fields, C. (2011, May 18). *Majority of Consumers Ready to Consider Buying Plug-in Electric Vehicles, But Challenge Utilities with their Car Charging Demands*. Retrieved May 21, 2011, from Accenture: [http://newsroom.accenture.com/article\\_display.cfm?article\\_id=5205](http://newsroom.accenture.com/article_display.cfm?article_id=5205)

Miller, N., Zrebiec, R., Delmerico, R., & Hunt, G. (1996). Battery energy storage systems for electric utility, industrial and commercial applications. *Battery Conference on Applications and Advances, 1996., Eleventh Annual* (p. 235). Long Beach, CA: Dept. of Power Syst. Eng., General Electric Co.

Mitlitski, J. (2011, February 18). *Raising the Volt-Age: Is Obama's Goal of 1 Million Electric Vehicles on U.S. Highways by 2015 Realistic?* Retrieved May 12, 2011, from Scientific American: <http://www.scientificamerican.com/article.cfm?id=one-million-electric-vehicles-by-2015>

Moura, F. (2006). *Driving Energy System Transformation With "Vehicle-to-Grid" Power*. International Institute for Applied Systems Analysis.

Naughton, K. (2011, January 10). *Ford to Hire 7,000 Workers to Help Manufacture Electric, Hybrid Vehicles*. Retrieved May 12, 2011, from Bloomberg: <http://www.bloomberg.com/news/2011-01-10/ford-to-hire-7-000-workers-to-help-manufacture-electric-hybrid-vehicles.html>

Neubauer, J., & Pesaran, A. (2010). *HEV/EV Li-Ion Battery Second-Use Project*. National Renewable Energy Laboratory. Golden, CO: Department of Energy.

Neubauer, J., & Pesaran, A. (2010). Secondary Use of PHEV and EV Batteries – Opportunities & Challenges. *10th Advanced Automotive Battery Conference* (pp. 1-14). Orlando, FL: Department of Energy.

Norton, R. (2000). *Machine Design* (2nd ed.). Prentice Hall.

Pacific Gas and Electric. (2011). *Pacific Gas and Electric - Tariffs*. Retrieved September 2011, from [http://www.pge.com/tariffs/tm2/pdf/ELEC\\_SCHS\\_A-10.pdf](http://www.pge.com/tariffs/tm2/pdf/ELEC_SCHS_A-10.pdf)

Parks, K., Denholm, P., & Markel, T. (2007). *Costs and Emissions Associated with Plug-In Hybrid Electric Vehicle Charging in the Xcel Energy Colorado Service Territory*. National Renewable Energy Laboratory Report. Golden, CO: Department of Energy.

Quinn, C. (2011). *Evaluation of Distributed Energy Storage for Ancillary Service Provision*. MS Thesis, Colorado State University, Mechanical Engineering, Fort Collins, CO.

Quinn, C., Zimmerle, D., & Bradley, T. (2009). The Effect of Communication Architecture on the Availability, Reliability and Economics of Plug-in Hybrid Electric Vehicle-to-Grid Ancillary Services. *Journal of Power Sources*, 195, 1500–1509.

Reiter, C. (2010, 12 June). *BMW Seeks 2,600 New Employees by End of 2011 on Electric, Hybrid Systems*. Retrieved May 12, 2011, from Bloomberg: <http://www.bloomberg.com/news/2010-12-06/bmw-seeks-2-600-new-employees-by-end-of-2011-on-electric-hybrid-systems.html>

Sandia National Laboratories. (2010). *Electric Power Industry Needs for Grid-Scale Storage Applications*. Sandia National Laboratories. Department of Energy.

Sensor Technology. (2011). *TorqSense - How it Works*. (Sensor Technology) Retrieved June 11, 2010, from Sensor Technology: <http://www.sensors.co.uk/about-us/technology/torqsense/>

Sheets, A. (2011). *The ReGenerator: Alternative Energy for Expeditionary Missions*. Retrieved May 23, 2011, from Raytheon: Technology Today: [http://www.raytheon.com/technology\\_today/2011\\_i1/regenerator.html](http://www.raytheon.com/technology_today/2011_i1/regenerator.html)

Short, W., & Denholm, P. (2006). *A preliminary assessment of plug-in hybrid electric vehicles on wind energy markets*. National Renewable Energy Laboratory. Golden, CO: Department of Energy.

Sioshansi, R., Denholm, P., Jenkin, T., & Weiss, J. (2009). Estimating the value of electricity storage in PJM: Arbitrage and some welfare effects. *Elsevier , Energy Economics*, 269–277.

Slocombe, J., Wagner, L., Heber, A., & Harner, J. (1990). Test Equipment for Determining Performance of Electric Motors. *Applied Engineering in Agriculture* , 100.

Tomić, J., & Kempton, W. (2007). Using fleets of electric-drive vehicles for grid support. *Using fleets of electric-drive vehicles for grid support* , 168 (2), 459-468.

Turton, H., & Moura, F. (2008). Vehicle-to-grid systems for sustainable development: An integrated energy analysis. 75 (8), 1091-1108.

UC Davis. (2010). *Second Life Applications and Value of “Traction” Lithium Batteries*. University of California at Davis, Plug-In Hybrid Electric Vehicle Research Center. Davis, CA: UC Davis.

Uhlenbrock, R. e. (2010, May). Electric Drive Train Test – Quo Vadis? *ATZ Autotechnology* , 10, pp. 56-9.

Vazquez, S., & Lukic, S. e. (2010, December). Energy Storage Systems for Transport and Grid Applications. *IEEE Transactions on Industrial Electronics* , 57 (12), pp. 3881-3895.

Walawalkar, R., & Apt, J. (2008). *Market Analysis of Emerging Electric Energy Storage Systems*. National Energy Technology Laboratory. Pittsburgh, PA: Department of Energy.

Warrington, R., Kirkpatrick, A., & Danielson, S. (2010). *Vision 2030 - Creating the Future of Mechanical Engineering Education Phase 1 Report*. ASME Center for Education Task Force.

Williams, B. (2010). A Strategy for Overcoming Plug-in-hybrid Battery Cost Hurdles in California: Integrating Post-Vehicle Battery-to-Grid (B2G) Use Values. *TRB*

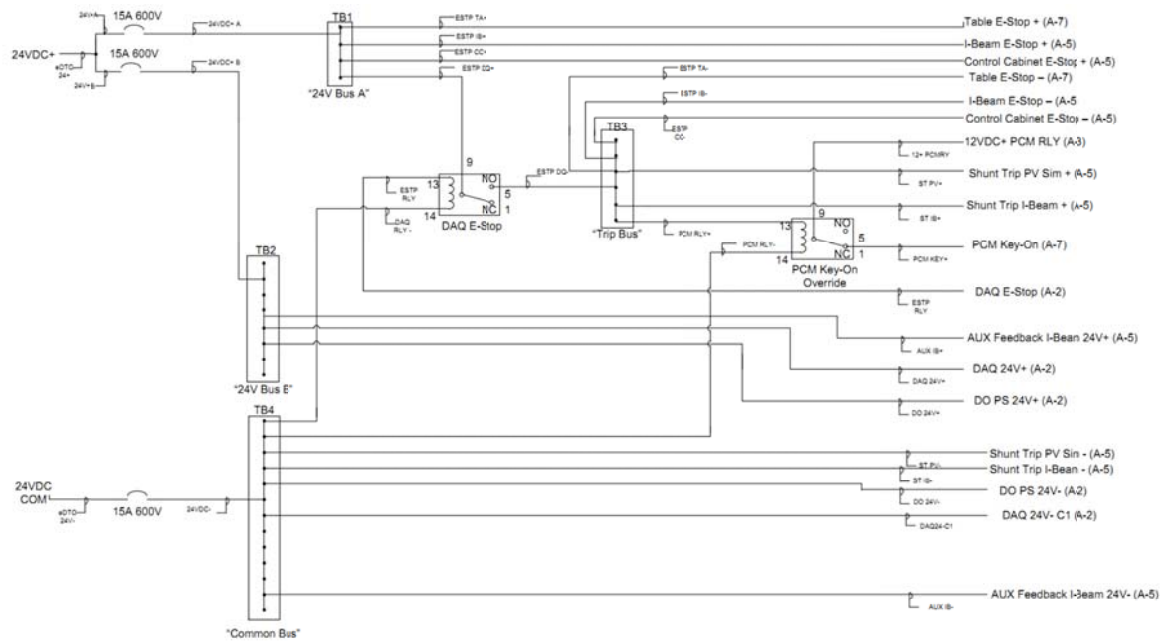
*Annual Meeting*. 538, pp. 1-28. Washington, DC: University of California: Berkley: Transportation Sustainability Research Center.

Wolkin, M. (2011, February 1). *Before Recycling, Electric Car Batteries Enjoy a Second Life*. Retrieved February 11, 2011, from Conversations for Accelerating the Transition to Sustainable Transportation: A Better Place Blog:  
<http://blog.betterplace.com/2011/02/before-recycling-electric-car-batteries-enjoy-a-second-life/>

Zhou, D. (2003, August 01). Testing Open and Closed Loop Current Sensors. Los Gatos, CA, USA.



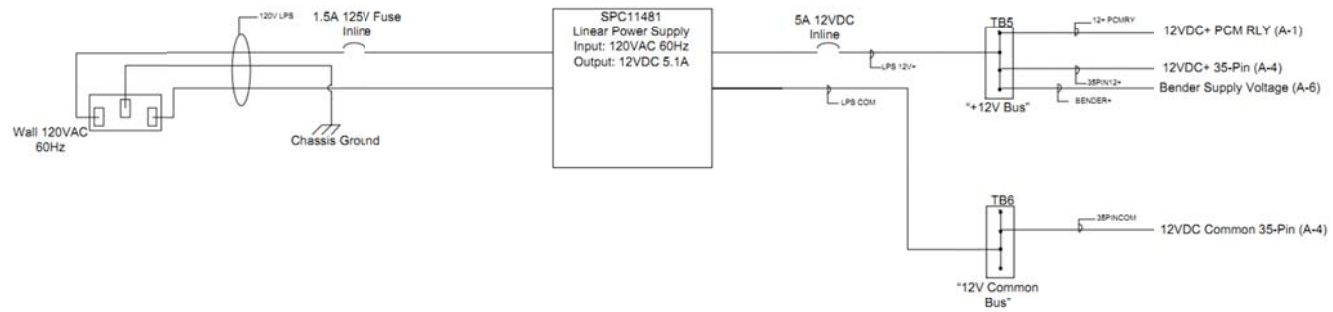
## Appendix A– Wiring Schematics



Drawing Name	Page	Drawn By	Date
4071C Schematic	A-1	10 LUT	08/2011

Figure 0-1: Control Cabinet Wiring

**Figure 0-2: DAQ Wiring**



Drawing Name	Page	Drawn By:	Date
407C Schematics	A-3	M. Lutz	06/12/11

**Figure 0-3: Linear Power Supply Wiring**

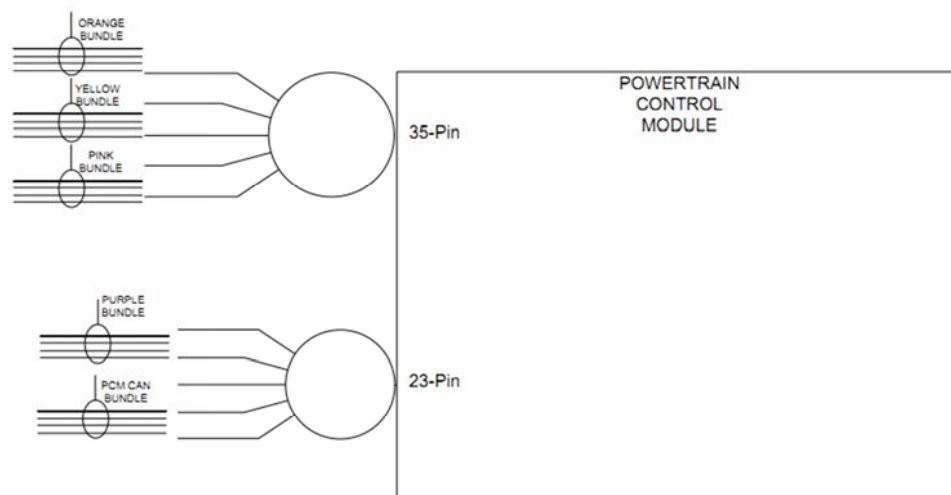


**Figure 0-4: Powertrain Control Module Wiring**

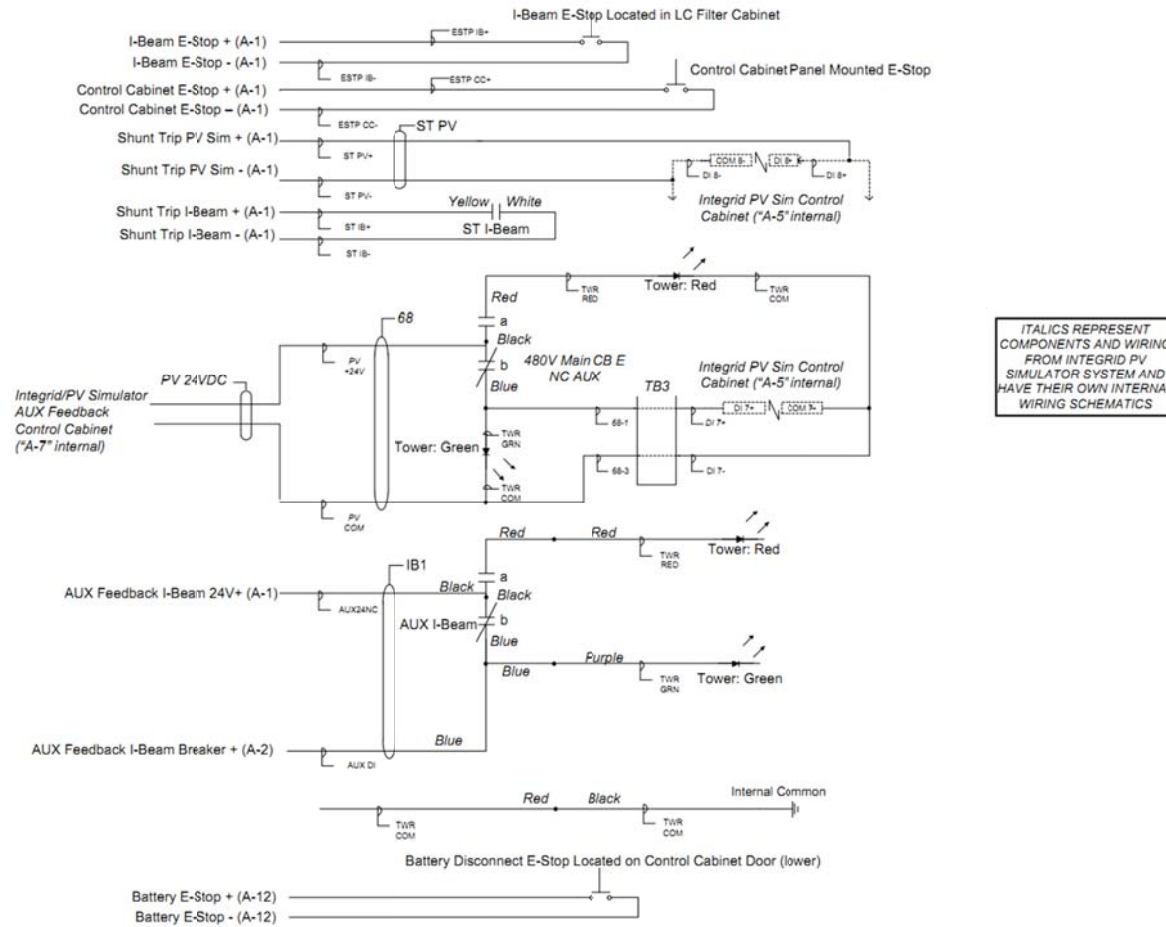
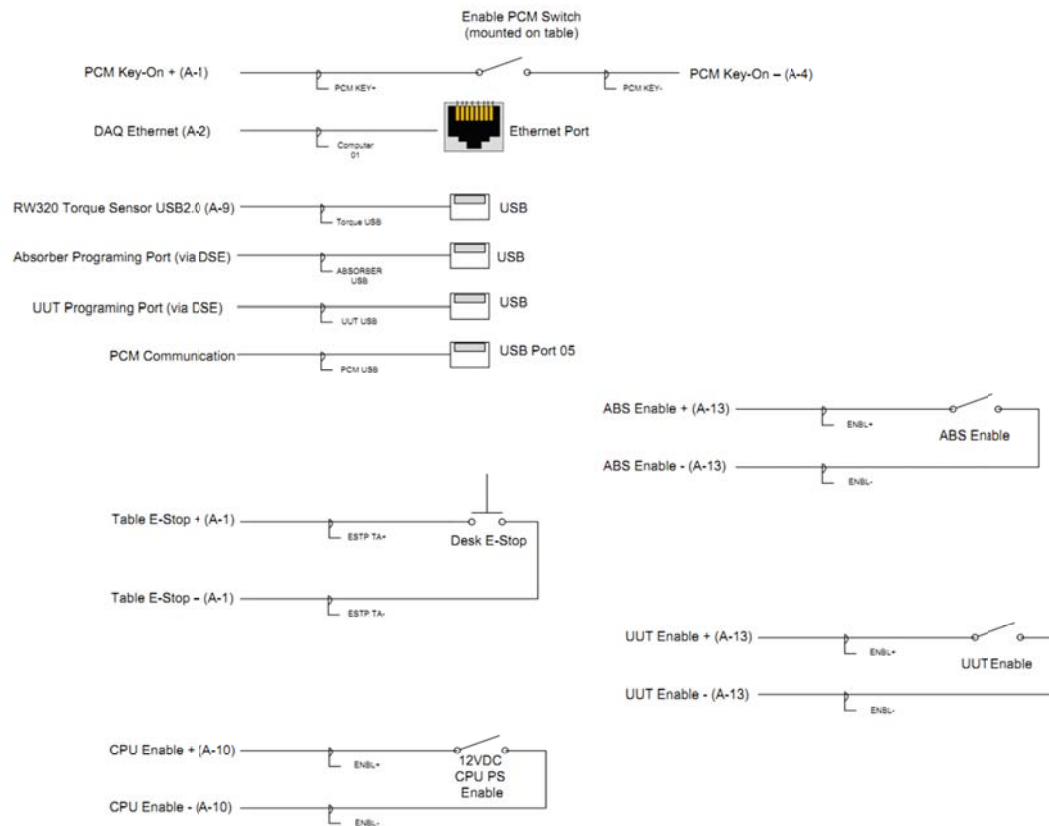


Figure 0-5: E-Stop, Breakers, and Light Tower Wiring

Drawing Name	Page	Drawn By	Date
427C Schematics	A-5	M. Lutz	06/13/11

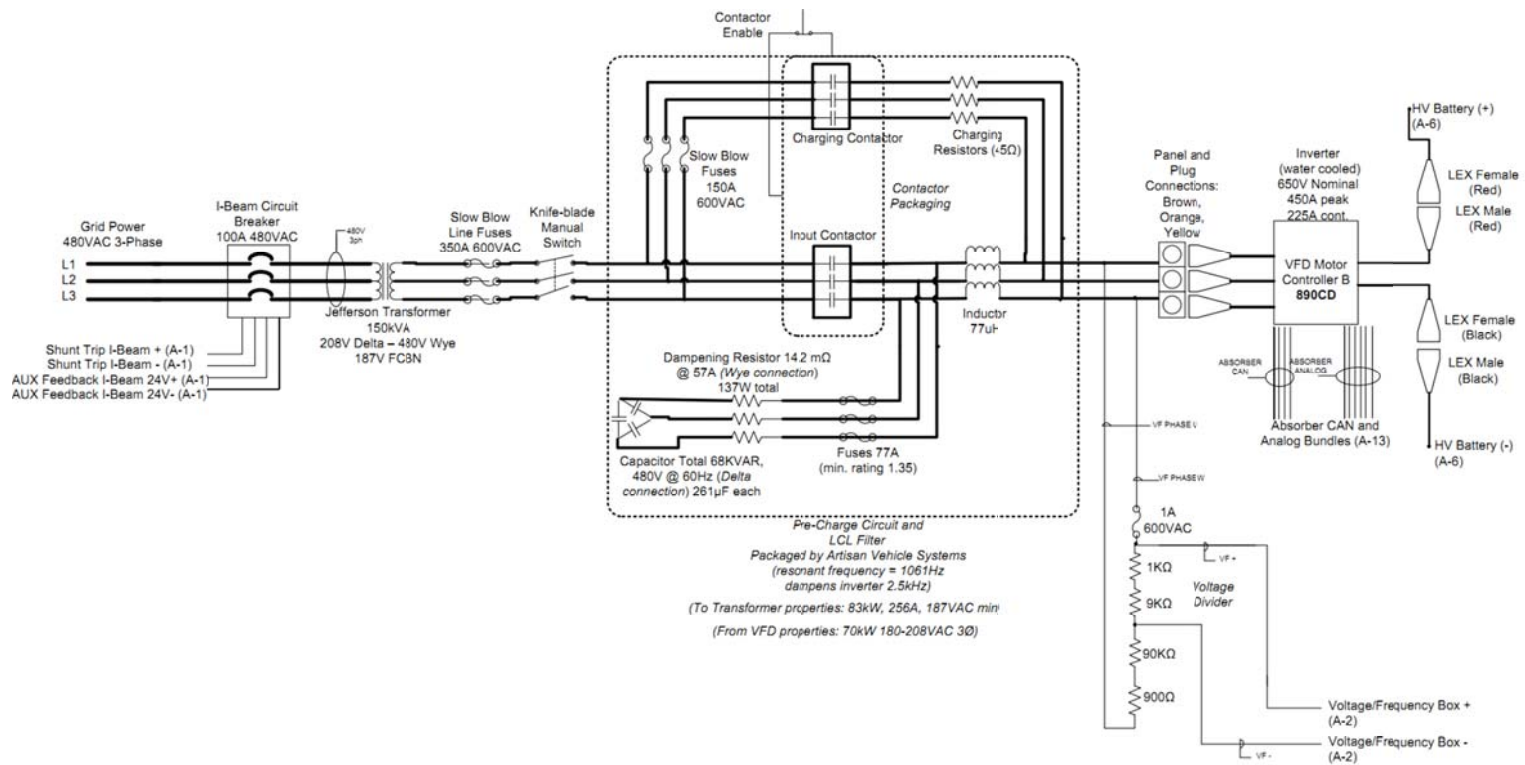
**Figure 0-6: GFCI and Battery Pack Wiring**



Drawing Name:	Page:	Drawn By:	Date:
EDTC Schematics	A-7	A. Luiz	06/12/11

Figure 0-7: Control Desk and Computer Wiring





Drawing Name	Page	Drawn By	Date
#DTC Schematics	A-8	W. Lucz	06/12/11

Figure 0-8: GAS Set-Up Wiring

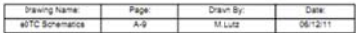


**Figure 0-9: Dyno Set-Up Wiring**

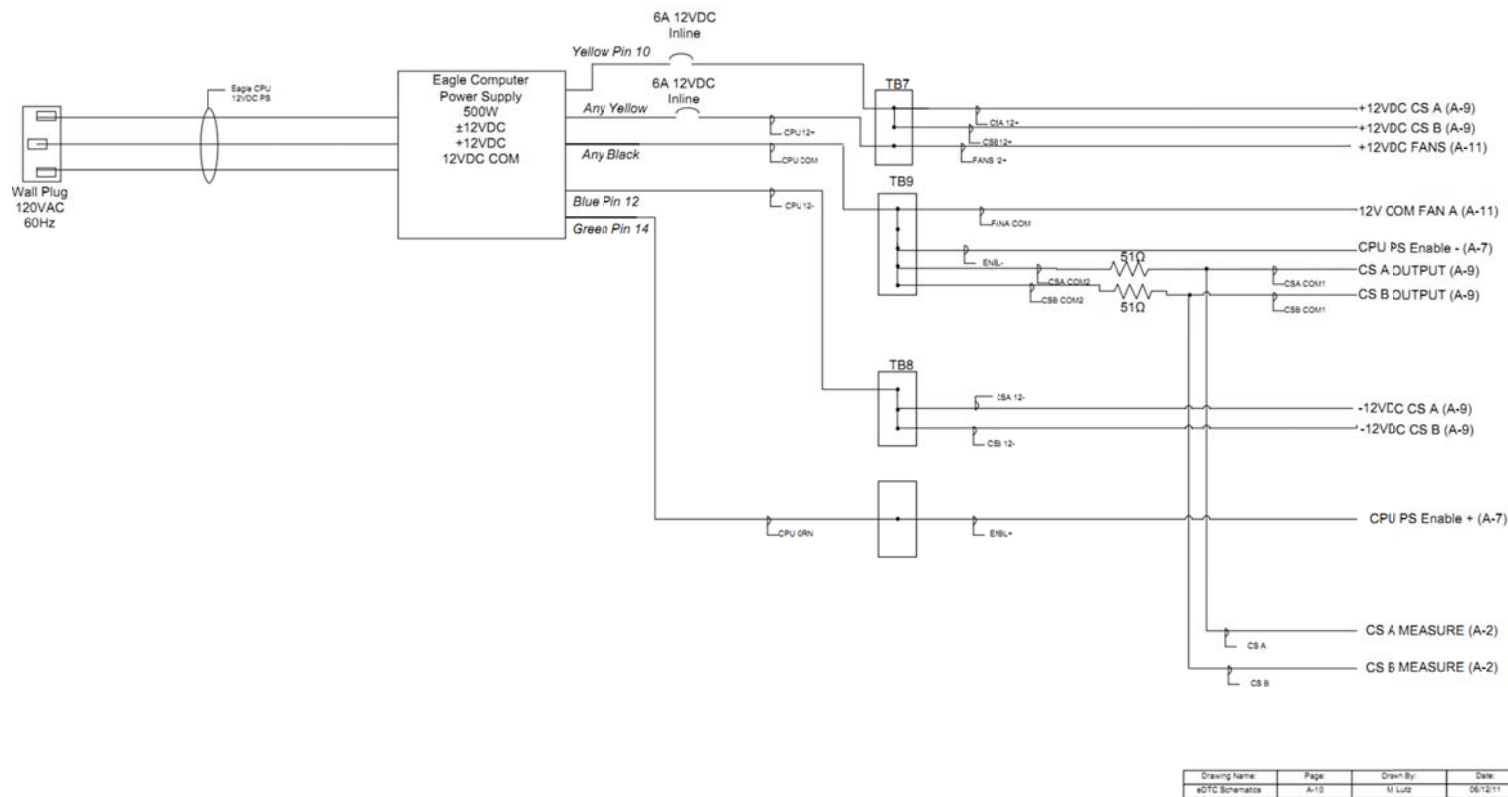
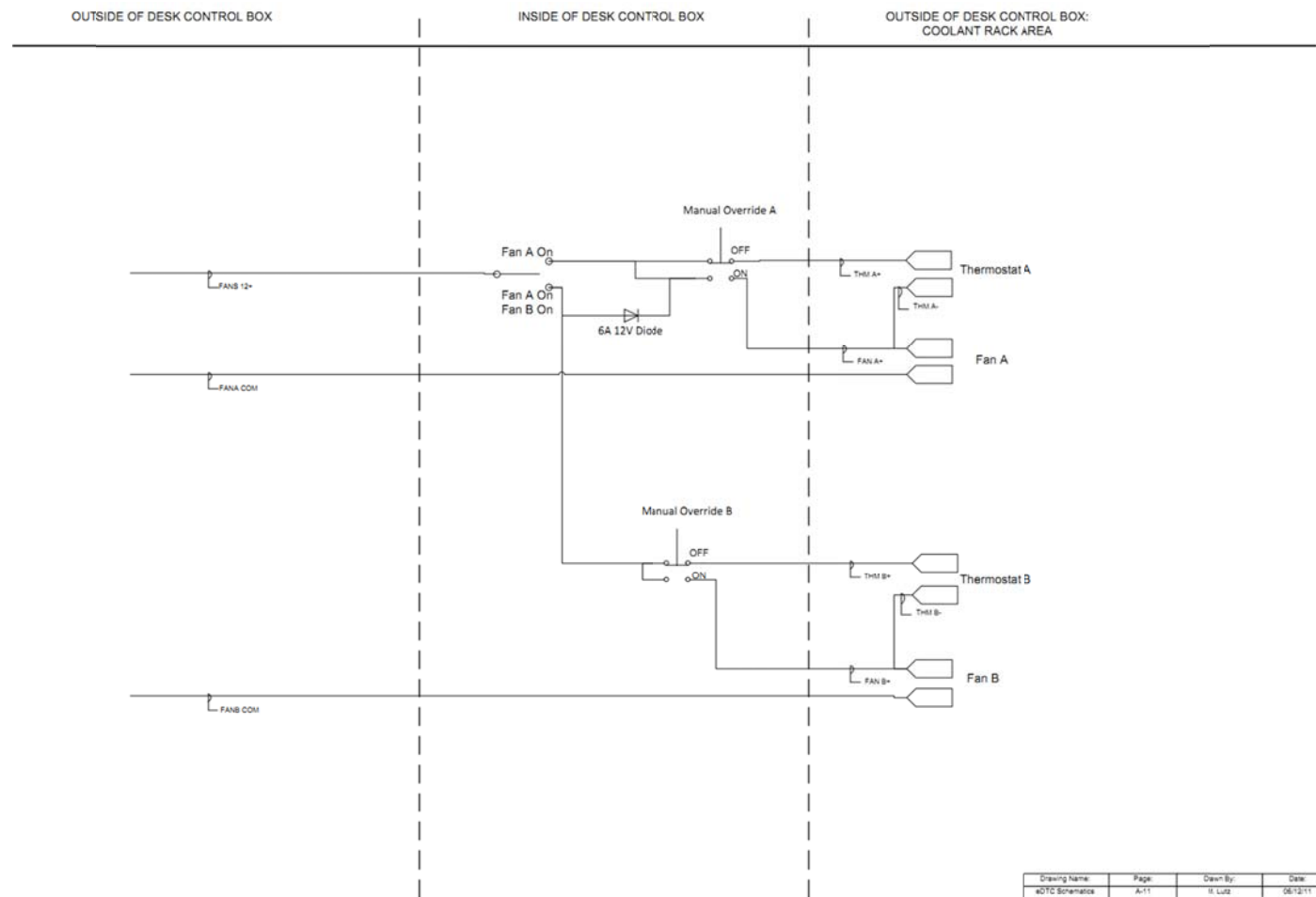
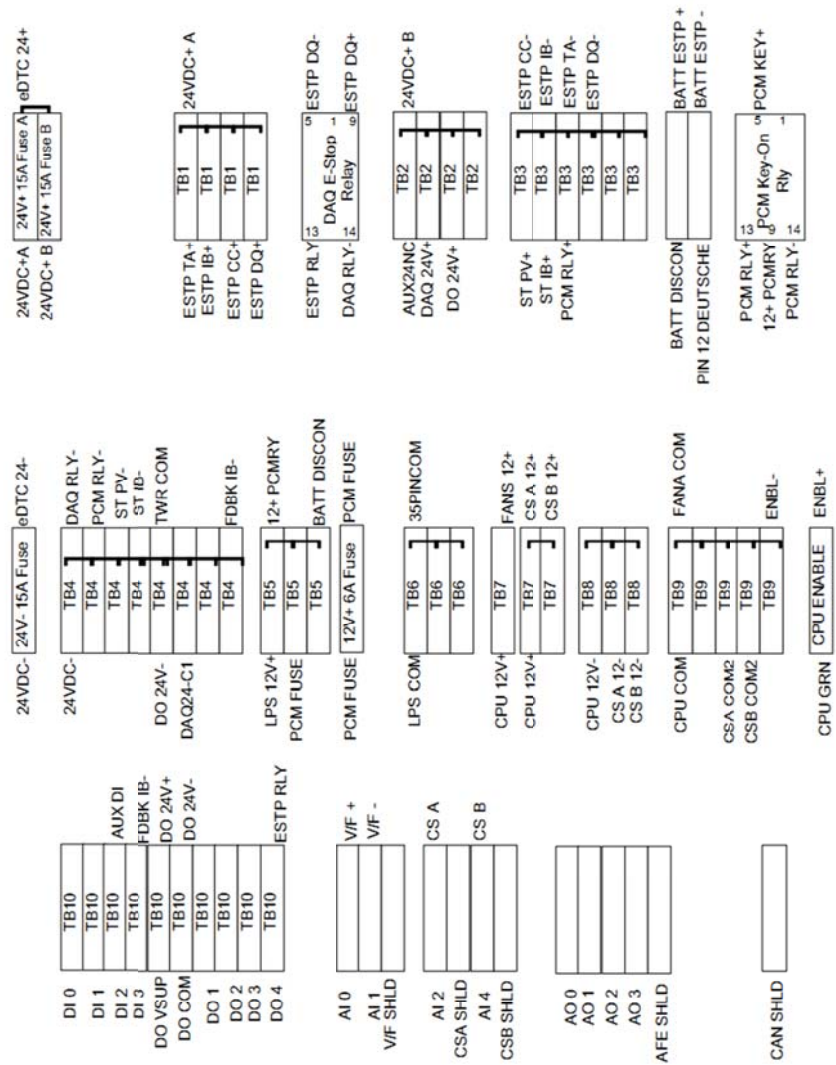


Figure 0-10: Eagle 500W CPU Power Supply Wiring



**Figure 0-11: Electric Fans Wiring**

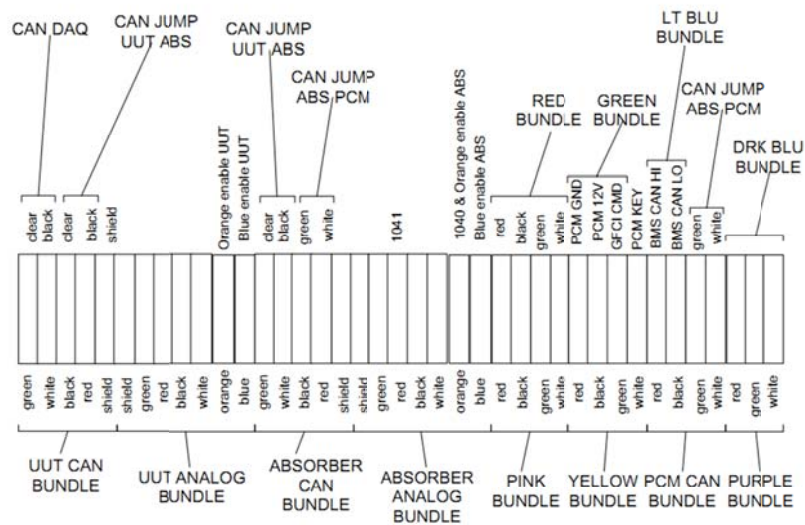
Figure 0-12:  
Terminal Block  
Layout in Control  
Cabinet



Legend

- Designates a jumper
- + Typically designates "to" but exceptions apply (such as high or positive)
- Typically designates "from" but exceptions apply (such as negative or common)

Drawing Name:	Page:	Drawn By:	Date:
eDTC Schematics	A-12	M. Lutz	06/12/11



Drawing Name:	Page:	Drawn By:	Date:
eTC Schematics	A-12 ONTD	M. Lutz	05/12/11

Figure 0-13: Terminal Block Layout in Control Cabinet (continued)

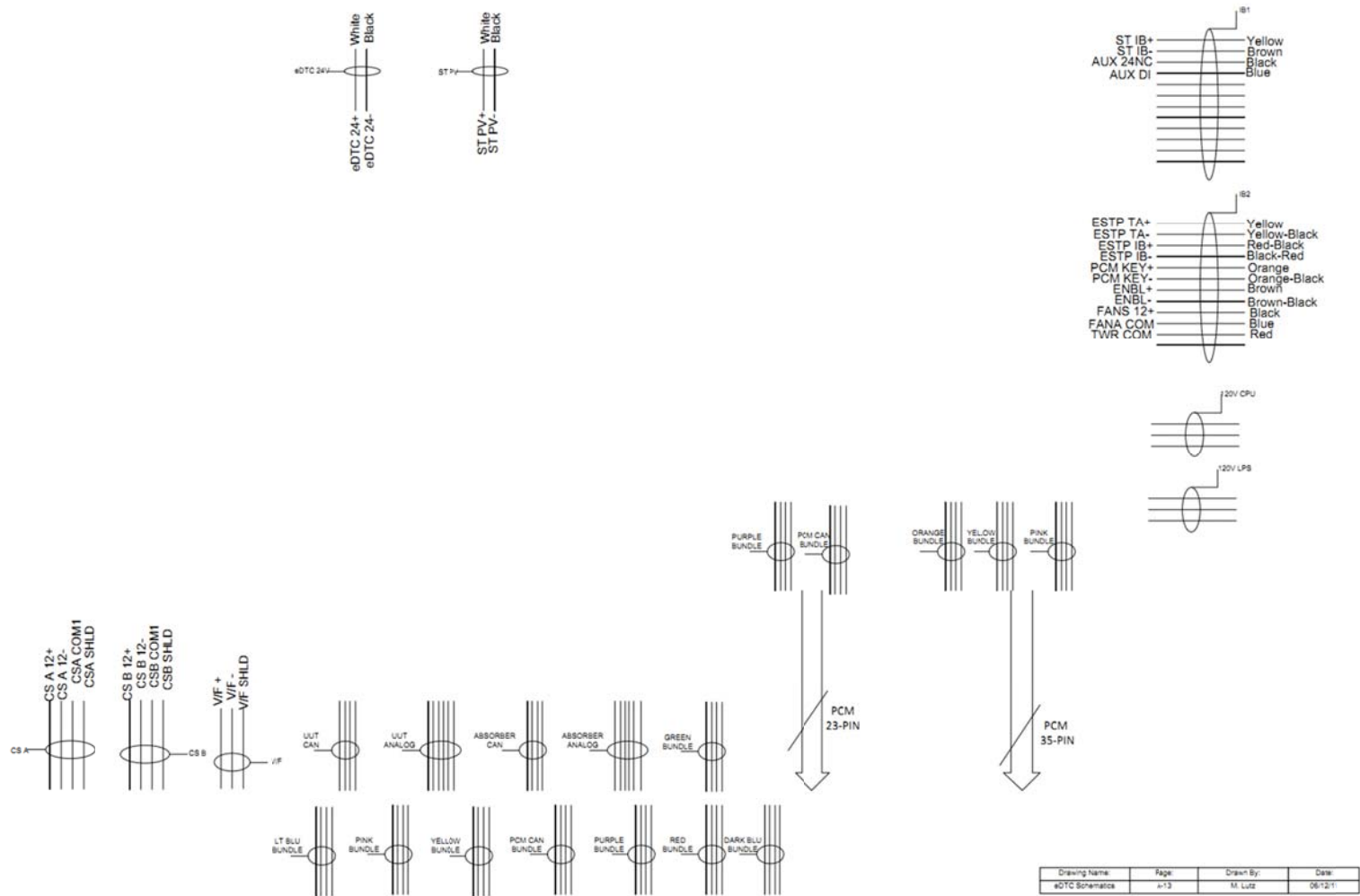


Figure 0-14: Wiring Bundle Distribution in Control Cabinet

## Appendix B— Artisan Vehicle Systems Pin-Out Listings




Table 0-1: PCM 35 Pin Assignments

35 pin Ampseal					
pin	CktMkr Lbl	Function	9S12XDP Pin	setup for	Vehicle Description
1	GND	Preferred GND supply in			
2	HBridge1_Out1	Hbridge/Motor Drive		up to 5A motor drive	
3	HBridge1_Out2	Hbridge/Motor Drive		up to 5A motor drive	
4	HBridge2_Out1	Hbridge/Motor Drive		up to 5A motor drive	
5	HBridge2_Out2	Hbridge/Motor Drive		up to 5A motor drive	
6	LAMP_1	Lamp driver 1	PM4	up to 500mA sink	Discharge Enbl (pumps, compressor, DC-DC)
7	LAMP_4	Lamp driver 4	PM7	up to 500mA sink	
8	LAMP_7	Lamp driver 7	PP6	up to 500mA sink	
9	Digital_In_2	Digital input 2	PT1	+12V in	isolation fault
10	Digital_In_5	Digital input 5	PT4	+12V in	interlock loop monitor
11	Digital_In_8	Digital input 8	PT7	+12V in	
12	RS232_0_TX	RS232 ch 0 tx		Serial Tx	RS232 Tx to GUI
13	GND	GND supply in		for high current application (>8A total)	
14	RELAY_01	Relay driver 1	PA0	up to 1.1A sink	Battery soft start (stage 1)
15	RELAY_03	Relay driver 3	PA2	up to 1.1A sink	Battery negative contactor (stage 1)
16	RELAY_05	Relay driver 5	PA4	up to 1.1A sink	Battery fan control (turn on when T>37C)
17	RELAY_07	Relay driver 7	PA6	up to 1.1A sink	Motor Controller Power Relay
18	LAMP_2	Lamp driver 2	PM5	up to 500mA sink	Charger relay
19	LAMP_5	Lamp driver 5	PP4	up to 500mA sink	
20	LAMP_8	Lamp driver 8	PP7	4.7K pullup to +5V, up to 500mA sink	
21	Digital_In_3	Digital input 3	PT2	+12V in	
22	Digital_In_6	Digital input 6	PT5	+12V in	Key On (triggers stage 1)
23	+5Vext	+5V for sensor power			
24	+12VRaw	Preferred +12V supply in			+12V PCM
25	+12VRaw	+12V supply in		for high current application (>8A total)	
26	RELAY_02	Relay driver 2	PA1	up to 1.1A sink	Battery positive contactor (stage 2)
27	RELAY_04	Relay driver 4	PA3	up to 1.1A sink	
28	RELAY_06	Relay driver 6	PA5	up to 1.1A sink	
29	RELAY_08	Relay driver 8	PA7	up to 1.1A sink	PCM Power Relay
30	LAMP_3	Lamp driver 3	PM6	up to 500mA sink	
31	LAMP_6	Lamp driver 6	PP5	up to 500mA sink	
32	Digital_In_1	Digital input 1	PT0	+12V in	charger connected
33	Digital_In_4	Digital input 4	PT3	+12V in	
34	Digital_In_7	Digital input 7	PT6	+12V in	
35	RS232_0_RX	RS232 ch 0 rx		Serial Rx	RS232 Rx from GUI

Table 0-2: PCM 25 Pin Assignments

25 pin Ampseal				
pin	CktMkr Lb	Function	9S12XDP Pin	setup for
1	CAN 0 L	CAN 0 low		
2	CAN 0 H	CAN 0 high		
3	Analog_Ou	Analog output 1		+10V full scale out
4	Analog_Ou	Analog output 4		+10V full scale out
5	Analog_Ou	Analog output 7		+10V full scale out
6	Analog_In-	Analog input 2	PAD01	+5V full scale in
7	Analog_In-	Analog input 5	PAD04	+20V full scale in
8	Analog_In-	Analog input 8	PAD07	+5V full scale in
9	+5Vext	+5V for sensor power		
10	RS232_1	RS232 ch 1 rx		
11	Analog_Ou	Analog output 2		+10V full scale out
12	Analog_Ou	Analog output 5		+10V full scale out
13	Analog_Ou	Analog output 8		+10V full scale out
14	Analog_In-	Analog input 3	PAD02	+60V full scale in
15	Analog_In-	Analog input 6	PAD06	+20V full scale in
16	CAN 1 L	CAN 1 low		
17	CAN 1 H	CAN 1 high		
18	RS232_1	RS232 ch 1 tx		
19	Analog_Ou	Analog output 3		+5V full scale out
20	Analog_Ou	Analog output 6		+10V full scale out
21	Analog_In-	Analog input 1	PAD00	+5V full scale in
22	Analog_In-	Analog input 4	PAD03	+10V full scale in
23	Analog_In-	Analog input 7	PAD06	+5V full scale in

Table 0-3: Absorber Inverter Feedback Cable Assignments for Dyno and GAS Set-Ups

Feedback Connector		RESOLVER CARD			LINE SYNC CARD			
		Signal	8902-RE Pin	Internal Cable	Signal	8902-LS Pin	External Cable - AFE	
1		REF SIN	3	BLACK	0V	X37.02	BLACK	1
2		SIN +	2	WHT	+15V	X37.03	RED	2
3		THERMAL DISCONNECT						
4		COS +	4	WHT	CH B	X37.07	GREEN	11
5		REF COS	5	BRN	CH B-	X37.06	YELLOW	12
6		THERMAL DISCONNECT						
7		+5V	6	WHT	CH A	X37.09	WHITE	14
8		WINDING THERM					BLUE	15
9		WINDING THERM					ORANGE	16
10		GND	7	RED	CH A-	X37.08	BROWN	17
11		shield	1	shield	shield	X37.01	shield	

131

Drive Connection		Signal	Range	Description	AFE SIGNALS	CSU MOTOR SIGNALS		
1		0V	FUTURE	0V reference for analog I/O	AGND	AGND	BLACK	
2		AIN3	FUTURE	0-10V, ±10V, 0-20mA, 4-20mA	Analog Input 3	Id Command	TORQUE LIMIT	GREEN
3		AIN4	FUTURE	0-10V, ±10V, 0-20mA, 4-20mA	Analog Input 4	Ic Command	SPEED LIMIT	WHITE
		AOUT1	FUTURE	±10V	Analog Output 1			
		AOUT2	FUTURE	±10V	Analog Output 2			
4		+10V	+10V	+10V output	+10V reference for analog i/o. Load 10mA maximum			
		-10V	-10V	-10V output	-10V reference for analog i/o. Load 10mA maximum			
5		DOU3 A	FAULT A	0-24V DC				
7		DOU3 B	FAULT B	0-24V DC	Relay Output: normally-open, volt-free, 24V DC 1A resistive load or use down to 1mA, 12V levels			
8		USER 24V	24V	0-24V DC	24V DC Output, 150mA maximum load	Switch Supply	24V	ORANGE
6		0V	DIG GND	0-24V DC	0V reference for USER 24V output			
9		DIN1	ENABLE	0-24V DC	Digital Input 1	Not Coast Stop	Enable	BLUE
10		DIN2	FUTURE	0-24V DC	Digital Input 2	Precharge closed		RED
		DIN3	FUTURE	0-24V DC	Digital Input 3			
		DIN4	FUTURE	0-24V DC	Digital Input 4			
		DIN5	FUTURE	0-24V DC	Digital Input 5			
		DIN6	FUTURE	0-24V DC	Digital Input 6			
		DIN7	FUTURE	0-24V DC	Digital Input 7			
	DINOUT1	FUTURE	0-24V DC	Digital Input/output 1				
	DINOUT2	FUTURE	0-24V DC	Digital Input/output 2				
11	SHIELD	SHIELD	SHIELD	CAN SHIELD				
12, 13	CANL	CANL	CAN	CAN Low Connections. Internally bussed.	CANL	CANL	BLACK GREEN	
14, 15	CANH	CANH	CAN	CAN High Connections. Internally bussed.	CANH	CANH	RED WHITE	
16	DOU4 A	FUTURE	0-24V DC					
17	DOU4 B	FUTURE	0-24V DC	Relay outputs are volt-free, normally open contacts. Rated to 240V 3A resistive load.				
	DOU5 A	FUTURE	0-24V DC					
	DOU5 B	FUTURE	0-24V DC	Relay outputs are volt-free, normally open contacts. Rated to 240V 3A resistive load.				
	DOU6 A	FUTURE	0-24V DC					
	DOU6 B	FUTURE	0-24V DC	Relay outputs are volt-free, normally open contacts. Rated to 240V 3A resistive load.				

Table 0-5: Deutsche Pin Battery Connector Assignments

PIN	COLOR	SIGNAL
1	ORANGE	PILOT
2	BLACK	NEG
3	BLUE	POS
4	BROWN	PRECH
5		
6		
7		
8		
9		
10		
11		
12		
13		
14		
15		
16		
17		
18	GREEN	CANL
19	PURPLE	CANH
20	BLACK	GND
21	ORANGE	12V BMS

Table 0-6: Colored Bundle Assignments and CAN Labeling

PIN	WIRE COLOR	SIGNAL	BUNDLE
1	Green	Pilot Monitor	Red
2	Black	NEG	Red
3	Red	POS	Red
4	White	PRECH	Red
5			
6			
7			
8			
9	Black	GFCI GND	Green
10	Red	GFCI POWER	Green
11	Green	ISO MONITOR	Green
12	White	BATT DISCON	Green
13		SHIELD	DRK Blue
14	Red	CUR SEN PWR	DRK Blue
15	Black	CUR SEN GND	DRK Blue
16	Green	CUR SEN SIG	DRK Blue
17	White	CUR SEN REF	DRK Blue
18	Green	CAN LO	LT Blue
19	White	CAN HI	LT Blue
20	Black	BMS GND	LT Blue
21	Red	BMS 12V	LT Blue

CAN RULES		
Direction	Signal	Color
TO	CAN HI	WHITE
TO	CAN LO	GREEN
FROM	CAN LO	BLACK
FROM	CAN HI	RED

Shown below is the geometric dimensions and tolerances for the motor mounting box.



## Appendix D–Natural Frequency MatLab Procedure

In order to further narrow down the results, an investigation of the natural frequency of the sensor and couplings in the system must be analyzed. The motor rotates at a maximum speed of 8,000rpm and thus the natural frequency needs to be above this in order to not experience resonance. According to Norton, “usual design strategy is to keep all forcing, self-exciting, frequencies below the first critical frequency by a factor of three or four” (Norton, 2000). Therefore it is crucial to determine the system natural frequency of the torque sensor and couplings to be greater than 32,000 rpm for safe operation. If the shaft system cannot be made higher than the required rotating frequency, then the motors must be able to accelerate rapidly enough through the resonance before the vibrations have a chance to build up amplitude. This allows the system to operate at a speed higher than resonance. Figure 0-15 (Source: [www.me.mtu.edu](http://www.me.mtu.edu)) illustrates the excitation at different dampening values for different frequency ratios. The purpose of this plot is to show that as the natural frequency of the system is approached ( $\omega/\omega_n = 1$ ), the displacement amplitude of the oscillations increases significantly depending on the zeta (dampening) value.



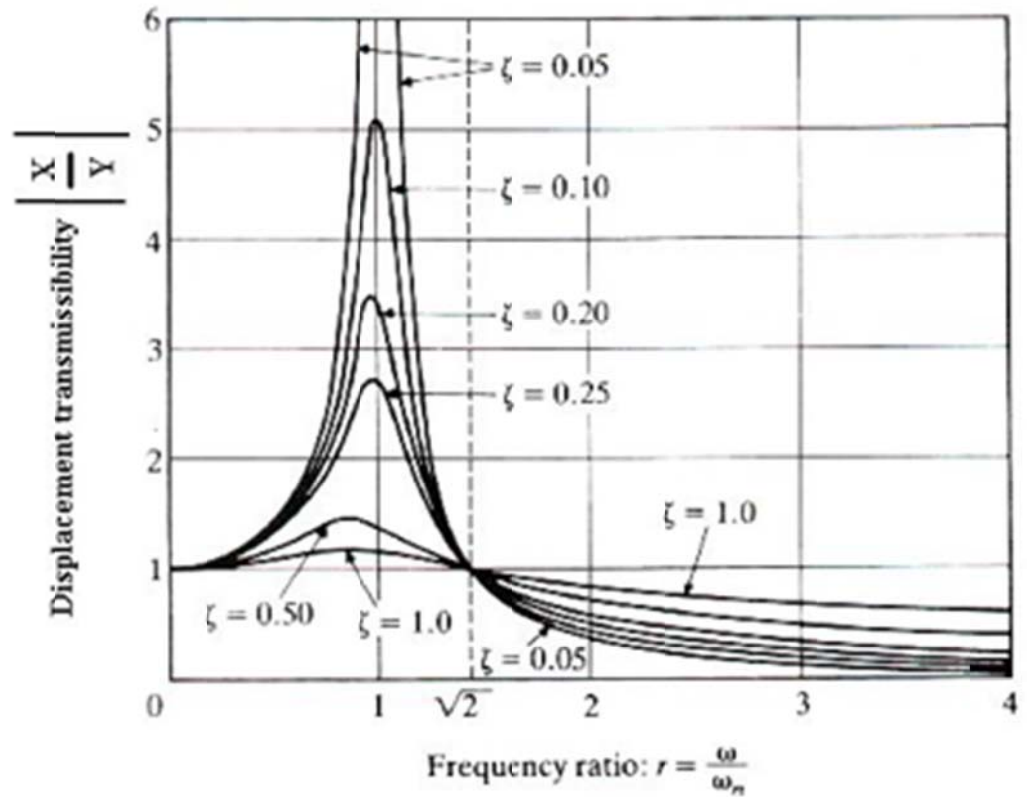


Figure 0-15: Natural Frequency Amplitude Response Plot

Utilizing Matlab, the different natural frequencies of the system for each torque sensor and coupling can be determined. The different mass moment of inertias and torsional spring rates were inputted into an m-file, which determined the natural frequency of the system with each sensor. The m-file represented the system as a spring-mass system shown below in Figure 0-16.

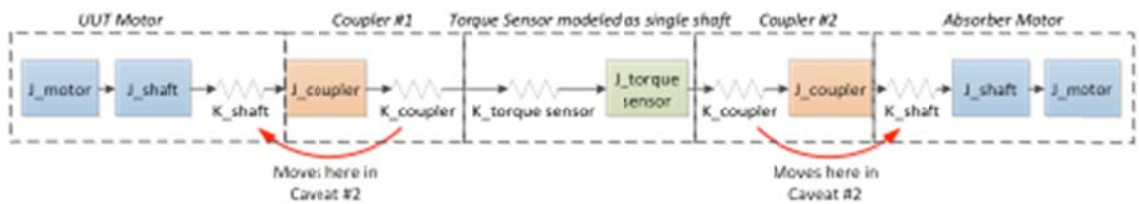


Figure 0-16: Spring-mass diagram for the Sensor Tech and R+W couplings set-up

Each mass moment of inertia (J) as well as torsional stiffness (K) is represented for the motor and motor shaft, coupling, torque sensor, and identical coupling and motor. The caveat to this analysis is how to model the spring representation of the coupling torsional stiffness. It can be modeled on either the motor shaft side or torque sensor shaft side of the coupler. Therefore an investigation will first be made between these two different scenarios defined as caveat #1 and caveat #2. Figure 0-16 uses arrows to highlight how the coupling spring could be modeled on either side. These two caveats are to be taking into account when analyzing the final natural frequency results. However, it is crucial to understand that there needs to be a spring between two masses so there must always be at least one coupler spring on one side of the torque sensor in order for the analysis to run. With this in mind, only the left side coupler spring was moved between caveat #1 and caveat #2 comparisons, leaving the right side coupler spring connected to the torque sensor side.

Using the tabulated values from Table 3-2 and Table 3-3, the first investigation (Sensor Tech RWT320 and R+W BK2 couplers) can be assigned to the above variables in Figure 0-16 for the scenario of the stiffest coupling and cheapest torque sensor (R+W BK2 and RWT320 respectively). Below are the MatLab variable constant definitions to the variables seen in Figure 0-16.

`%Mass Moments of Inertia:`

```
Jm = 6.271E-3; %kg*m^2 (motor rotor) Artisan GP150WC
Js = 1.295E-4 %kg*m^2 (motor shaft) calculated using
    stainless steel and actual shaft mass
Jc = 4.5E-3; %kg*m^2 (coupler) assuming R+W America
    BK2 coupler
```



Jts = 1.431e-4; %kg\*m^2 (torque sensor) assuming  
RWT320 Torque sensor

%Torsional Stiffness (spring constants):

Ks = 1.33E5; %Nm/rad (motor shaft) calculated assuming  
stainless steel

Kc = 1.91E5; %Nm/rad (BK2 coupler) given

Kt = 3.56E4; %Nm/rad (torque sensor) given

The Ks (motor shaft torsional stiffness) was calculated using G (Modulus of Rigidity) =  $73 \times 10^9$  Pa for stainless steel and the torsional stiffness equation:

$$K_s = J_{polar} * \frac{G}{L} = m_{shaft} * \frac{d^2}{8} = 1.295 \times 10^{-4} \text{ kgm}^2$$

where

$$J_{polar} = \frac{\pi * d^4 * m}{32} = 1.469 \times 10^{-7} \text{ kgm}^4$$

In order to calculate the shaft mass, the equation:  $m = \rho * v$ , where  $\rho$  is density and  $v$  is volume. The density of stainless steel was assumed to be  $7.90 \times 10^6$  g/m<sup>3</sup> for 304 stainless steel and the volume was calculated using

$$v = \frac{\pi * d^2 * L}{4} = \frac{\pi * (0.038 \text{ m})^2 * 0.0801 \text{ m}}{4} = 9.084 \times 10^{-5} \text{ m}^3$$

Using these values, the Ks for stainless steel of the motor shaft can be calculated as

$$K_s = \frac{1.469 \times 10^{-7} \text{ kgm}^4 * 73 \times 10^9 \text{ Pa}}{0.0801 \text{ m}} = 1.338 \times 10^5 \frac{\text{Nm}}{\text{rad}}$$

Once all the variables are assigned, the m-file relates the variables to the spring mass system shown in Figure 0-16. Note that some mass measurements appear to be in

kg, while others are in grams. These were converted to a common base in the calculation section of the simulation.

```
% Relate the physical values to the generic spring mass
system

J1 = Jm+Js

J2 = Jc;

J3 = Jts;

J4 = Jc;

J5 = Jm+Js;


% Caveat #1: Assuming the coupler "spring" is on the
torque sensor shaft "spring"

K1 = Ks;

K2 = 1/(1/Kc + 1/Kt);

K3 = Kc;

K4 = Ks;
```

However if both the caveats mentioned above are considered, the program can be re-run with the coupler spring on the other side with the code shown below.

```
% Caveat #2: Assuming the coupler "spring" is on the
motor shaft "spring"

K1 = 1/(1/Kc + 1/Ks);

K2 = Kt;

K3 = Kc;

K4 = Ks;
```

Continuing with the program code, the definition of the matrices for the Eigen vector of phi and lambda appear as:

```
% Define the matrices of coefficients
```



```
J_mat = [J1 0 0 0 0;  
          0 J2 0 0 0;  
          0 0 J3 0 0;  
          0 0 0 J4 0;  
          0 0 0 0 J5]
```

```
K_mat = [ K1 -K1 0 0 0;  
          -K1 K1+K2 -K2 0 0;  
          0 -K2 K2+K3 -K3 0;  
          0 0 -K3 K3+K4 -K4;  
          0 0 0 -K4 K4]
```

```
[phi,lambda]= eig(K_mat,J_mat)  
for i=1:5  
    nat_freq(i) = sqrt(lambda(i,i));  
end  
nat_freq_rpm = nat_freq*60/(2*pi)
```

The results from these calculations are tabulated in Table 0-7. Remember that Caveat #1 is when the torque sensor and coupling springs are together. Caveat #2 is when the coupler spring is paired with the motor shaft spring (on the left side of the torque sensor).

**Table 0-7: Sensor Tech with R+W Couplers Caveat Comparison Results**

<b>Natural Frequency At:</b>	<b>Caveat #1  n (rpm)</b>	<b>Caveat #2  n (rpm)</b>	<b>Difference (#1-#2)</b>
Mode 2	19,500	20,160	-660
Mode 3	67,570	55,130	12,440
Mode 4	72,450	70,950	1,500
Mode 5	379,920	384,510	-4,590

These results prove that the worse case, lowest natural frequency, occurs in Caveat #1: when the torque sensor and the coupling springs are paired instead of the motor shaft and the coupling springs being paired. It also shows that the only note worthy natural frequency is mode two since it is closest to the forcing frequency of 8 poles X 8000 RPM / 2 poles per rotation = 32000 RPM. The lowest mode, is, in fact, well within the operating regime.

The resulting amplitude plot of the mass at each mode is shown below (Figure 0-17 and Figure 0-18). These plots show that mode two has more vibration amplitude as the analysis moves down the length of the system. It must be noted however that without damping specified, the absolute magnitude of any mode is infinite, and thus cannot be compared. There are two notes on the following plots. First the scale of the x-axis shows half masses which is incorrect. This only appears due to the zoom of the axis and can be ignored for future mass plots. Second, the y-axis displays Amplitude with a

question mark. This is to only to remind the reader that this value is for determining which caveat s the best definition of the system to calculate natural frequency.

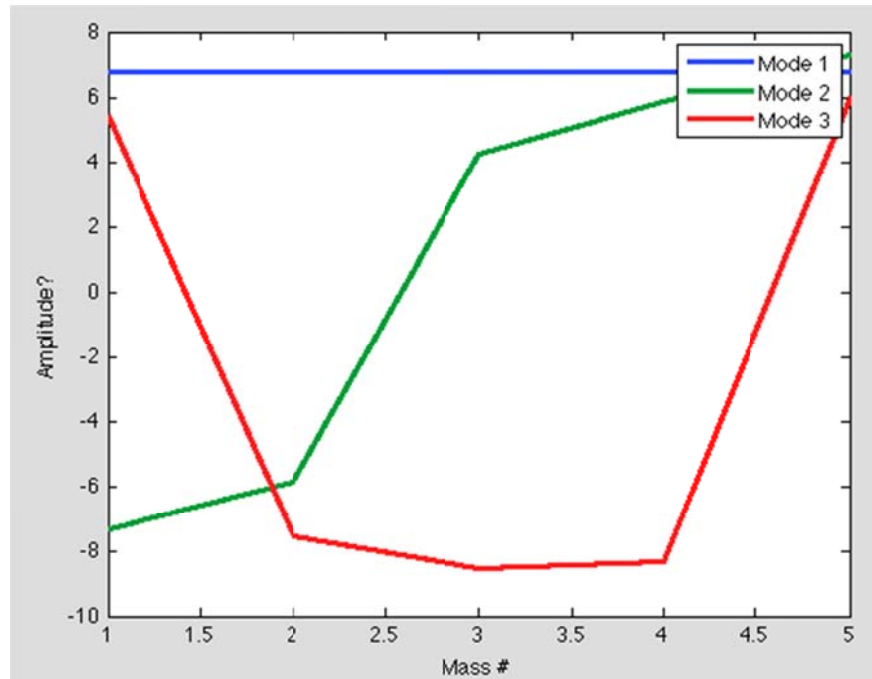


Figure 0-17: Caveat #1 Mode Amplitudes for Each Mass in the Spring-Mass System

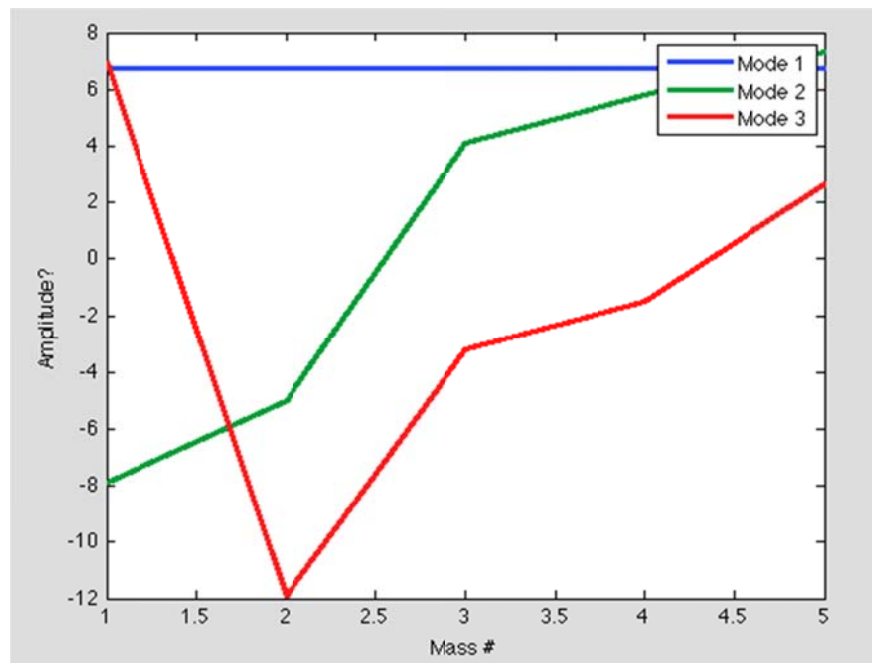
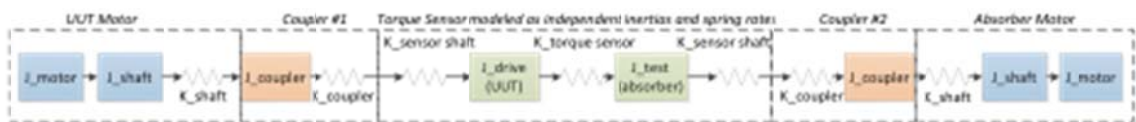


Figure 0-18: Caveat #2 Mode Amplitudes of Each Mass

The key take away from these plots is that moving the spring in the “caveat #2” case changed the shape of Mode 2 significantly. This does not make sense physically; therefore Caveat 2 is likely not representative of the actual system.

To investigate a different style sensor, the Interface torque sensor, modifications needed to be made to the Matlab m-file. The new mass-spring diagram, Figure 0-19, shows the Interface mass moment of inertias for the drive and test side. Interface uses a technology where a through shaft has a necked down portion in the middle and this measures the torque between the drive and test side. According to the Interface data sheet, the torsional stiffness is only of the neck component, thus the torsional stiffness of the shaft ends was calculated assuming stainless steel. The moment of inertias are different as well because the drive side has no measurement equipment attached whereas the test side of the sensor shaft has different measurement equipment attached.



**Figure 0-19: Mass-Spring Diagram of Interface Torque Sensor with Caveat #1 Shown (Coupler and Torque Sensor Shaft Springs Paired Together)**

Below is the set-up for the Interface m-file:

```
%Mass Moments of Inertia:

Jm = 6.271E-3; %kg*m^2 (motor) Artisan GP150WC

Js = 1.295E-4; %kg*m^2 (motor shaft) assuming stainless
steel

Jc = 4.5E-3; %kg*m^2 (coupler) assuming R+W America BK2
coupler
```

```
Jd = 1E-4; %kg*m^2 (driven/Unit Under Test (UUT) side  
of torque sensor) assuming Interface T2 Torque sensor
```

```
Jt = 9E-5; %kg*m^2 (test/absorber side of torque  
sensor)
```

```
%Torsional Stiffness (spring constants):
```

```
Ks = 1.33E5; %Nm/rad (motor shaft) calculated assuming  
stainless steel
```

```
Kc = 1.91E5; %Nm/rad (coupler) given
```

```
Kt = 6.7E4; %Nm/rad (torque sensor) given
```

```
Kst = 1.977E5; %Nm/rad (torque sensor shaft) calculated  
using stainless steel
```

```
% Relate the physical values to the generic spring mass  
system
```

```
J1 = Jm+Js;
```

```
J2 = Jc;
```

```
J3 = Jd;
```

```
J4 = Jt;
```

```
J5 = Jc;
```

```
J6 = Jm+Js;
```

```
% Caveat #1: Assuming the coupler "spring" is on the  
torque sensor shaft "spring"
```

```
% K1 = Ks;
```

```
% K2 = 1/(1/Kc + 1/Kst);
```

```
% K3 = Kt;
```

```
% K4 = 1/(1/Kc + 1/Kst);
```

```
% K5 = Ks;
```

% Caveat #2: Assuming the coupler "spring" is on the motor shaft "spring"

$$K1 = 1 / (1/Kc + 1/Ks) ;$$

$$K2 = Kst ;$$

$$K3 = Kt ;$$

$$K4 = Kst ;$$

$$K5 = 1 / (1/Kc + 1/Ks) ;$$

After running the file for both caveat #1 and caveat #2, Table 0-8 was produced to critique the difference in assumptions. A plot of the mode amplitudes at each location in the mass-spring diagram from Figure 0-19 is shown in Figure 0-20 and Figure 0-21. These figures are visual representations of the differences at each point in the system depending on which caveat is selected. It can again be determined that caveat #1 is the worst-case scenario for earliest natural frequency.

**Table 0-8: Interface Sensor with R+W Couplers Caveat Comparison**

<b>Natural Frequency At:</b>	<b>Caveat #1 ω n (rpm)</b>	<b>Caveat #2 ω n (rpm)</b>	<b>Difference (#1-#2)</b>
Mode 2	20,140	21,640	-1,500
Mode 3	67,320	51,700	15,620
Mode 4	72,880	61,900	10,980
Mode 5	308,360	439,350	-130,990
Mode 6	473,060	568,330	-95,270



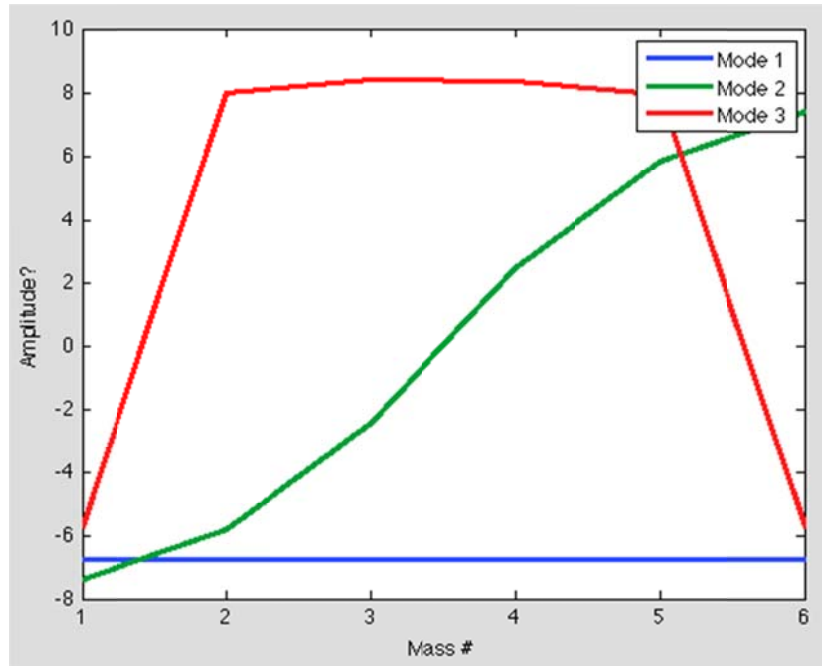


Figure 0-20: Detailed View of Caveat #1 with Only the First Three Modes Shown

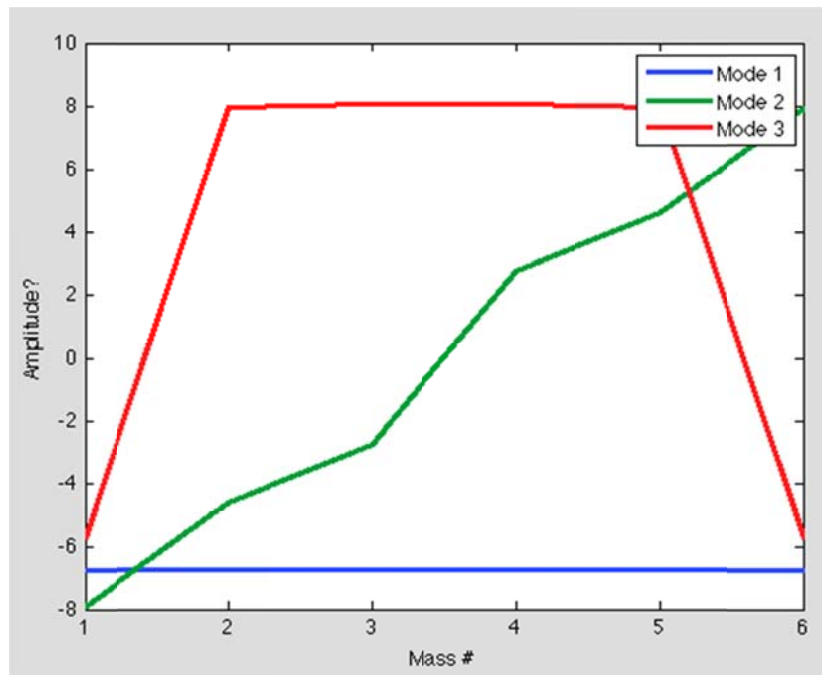


Figure 0-21: Mode Amplitude Plot of Caveat #2 for Interface Sensor

Looking at the different couplings available for the Interface set-up and their natural frequency effects on the system is another valuable study. Shown below (Table

0-9) is a table summarizing these findings. The three different couplings with their respective J and K terms were used for these calculations. Figure 0-22 and Figure 0-23 illustrate these findings for the first three modes.

**Table 0-9: Interface coupling comparison results (all using caveat#1)**

Natural Frequency At:	R+W BK2 coupling $\Omega_n$ (rpm)	Interface coupling $\Omega_n$ (rpm)	R+W BKM coupling $\Omega_n$ (rpm)
Mode 1	0	0	0
Mode 2	20,140	23,490	22,870
Mode 3	67,320	105,090	135,210
Mode 4	72,880	125,190	167,780
Mode 5	308,360	346,990	322,740
Mode 6	473,060	495,379	472,890

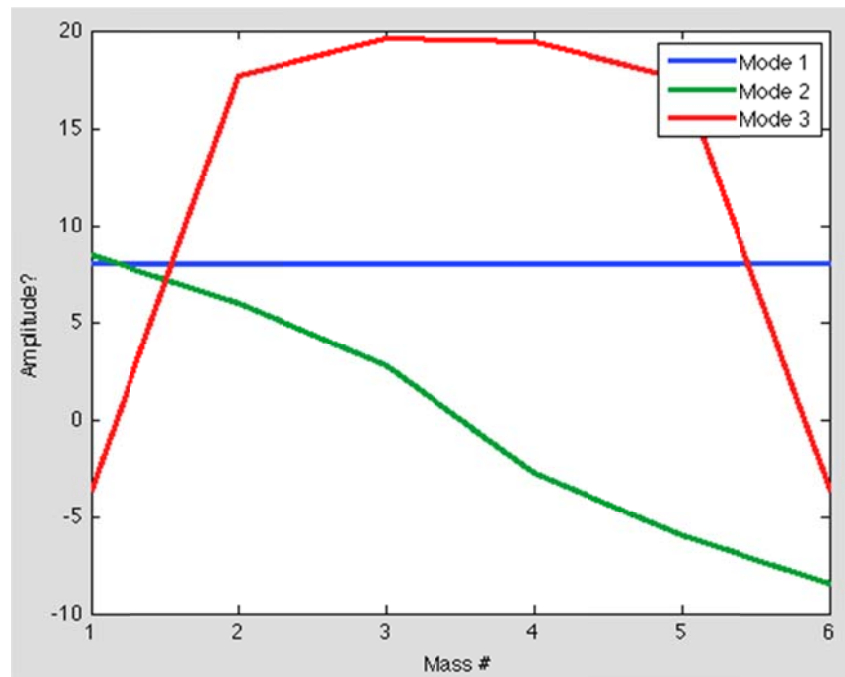


**Figure 0-22: Mode-Amplitude Plot of Caveat #1 with the Interface Sensor and the Supplied Interface Coupling**

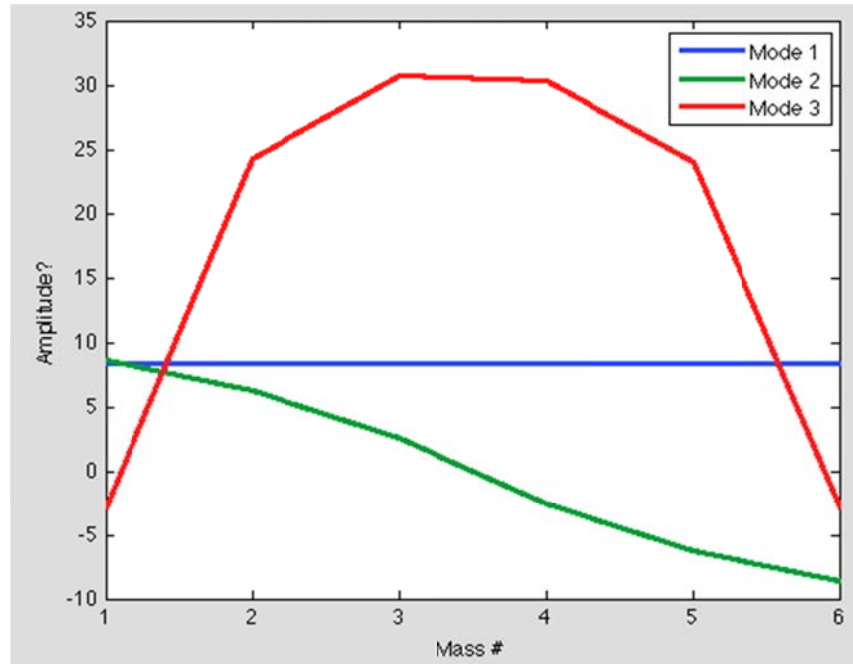


**Figure 0-23: Mode-Amplitude Plot for Caveat #1 with Interface Sensor and BKM Couplings**

The next sensor to investigate is the natural frequency of is the Binsfeld. This sensor uses a strain gauge that is mounted directly on the motor shaft and transmits the data inductively. Figure 0-24 pictorially illustrates the different sizes of Binsfeld sensors all with a non-contact collar.



Figure 0-24: Binsfeld Torque Sensors

Since the Binsfeld attaches directly to the shaft, only one coupler is needed and the sensor's inertia and spring constant can essentially be ignored. Figure 0-25 shows how the mass-spring model is changed for analysis.

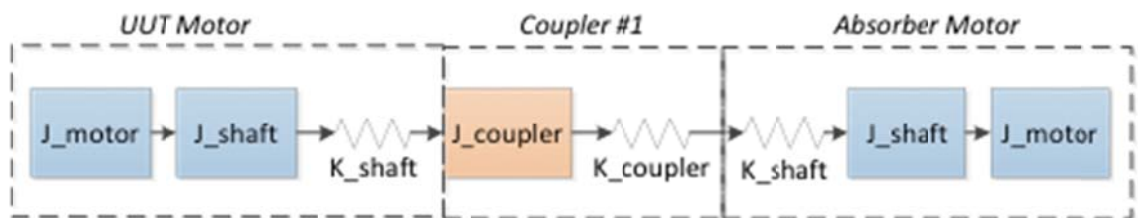


Figure 0-25: Spring-mass diagram of Binsfeld torque sensor set-up

After running the Matlab code for this new design, the following results seen in Table 0-10 were found. The results show that the second mode has the highest yet seen natural frequency.

**Table 0-10: Binsfeld natural frequency results**

	<b>Natural Frequency (rpm)</b>
Mode 2	37,070
Mode 3	76,950

There are some assumptions to the Binsfeld model that need to be mentioned however. The model assumes that the mass of the strain gauge collar on the shaft is negligible because it is made of nylon and is mounted solidly on one shaft. The shaft that has the sensor collar mounted to it would have a higher mass moment of inertia but this was neglected for simplicity. A better approximation would be to add the moment of inertia of the sensor collar to the coupler inertia. The assumptions used to calculate these frequencies allow for the values to be higher than they would be in the real-life application.

Table 0-11 summarizes the previous investigations into one table. Notice that the R+W BK2 and BKM couplers were each tried with different sensors for a more conclusive investigation.

**Table 0-11: Summary of Natural Frequency of Different Torque Sensors and Couplings (lowest reported natural frequency shown for each case)**

<b>Company</b>	<b>Model</b>	<b>Coupler</b>	<b>Natural Frequency (rpm)</b>	<b>Total Price</b>
Binsfeld	TorqTrack Revolution	(1) R+W BK2	37,070	\$5,902
Interface	T2-200-AXA	R+W BKM	22,870	\$5,794
Interface	T2-200-AXA	Interface Single-flex	23,490	\$5,210
Interface	T2-200-AXA	R+W BK2	20,140	\$5,468
S. Himmelstein	MCRT 28003T (2-3)	R+W BKM	20,810	\$4,739
Sensor Tech	RWT320-FB	R+W BKM	22,180	\$4,658
Sensor Tech	RWT320-FB	R+W BK2	19,500	\$4,332

## Appendix E– Instructions for Changing the Absorber Inverter from Line Sync Control to Resolver Control (GAS to Dyno Set-Up)

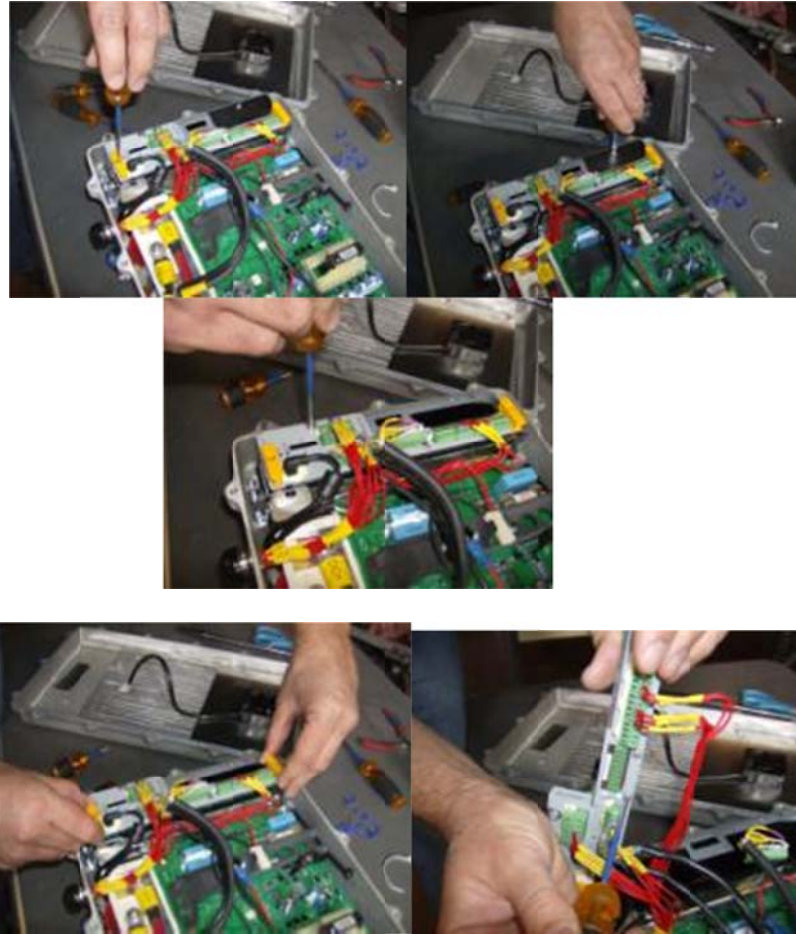
1. Unbolt cover (cover has dowel pins), disconnect fan on backside.



2. Cut the zip ties around the control box (if they were reinstalled by the last user)
3. Remove the pin-out harness from the line sync card



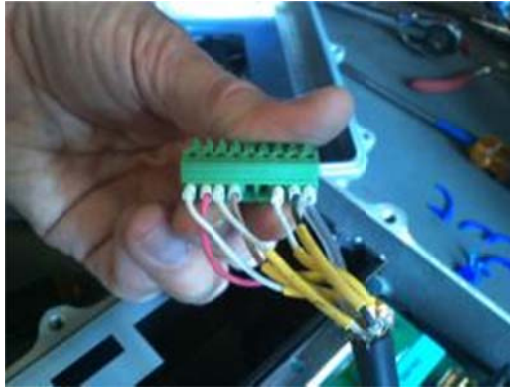
4. Unscrew the big screws on each side of the yellow tabs and the screw holding the empty aluminum cover plate on, to release the 8903-CB main Card. Pull it out very carefully as the wiring harness is VERY short. Take out the line sync card by removing the proper screws.



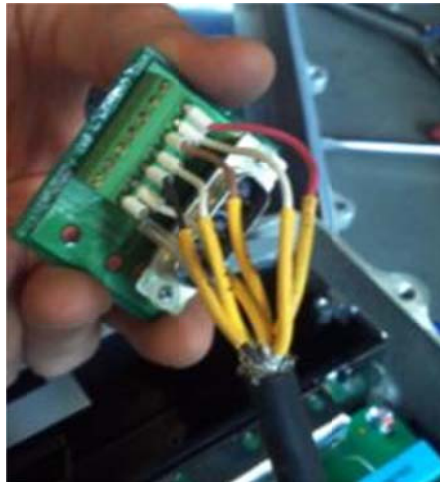
5. The little board is the feedback (resolver) card adapter.
6. Change the wires from the line sync card to the feedback (resolver) card adapter according to this wiring spreadsheet.

Resolver Card Pin	Internal Cable	Signal	Wire Label
3	BLACK	0V	1
2	WHT	+15V	2
4	WHT	CH B	11
5	BRN	CH B-	12
6	WHT	CH A	14
			15
			16
7	RED	CH A-	17
1		shield	

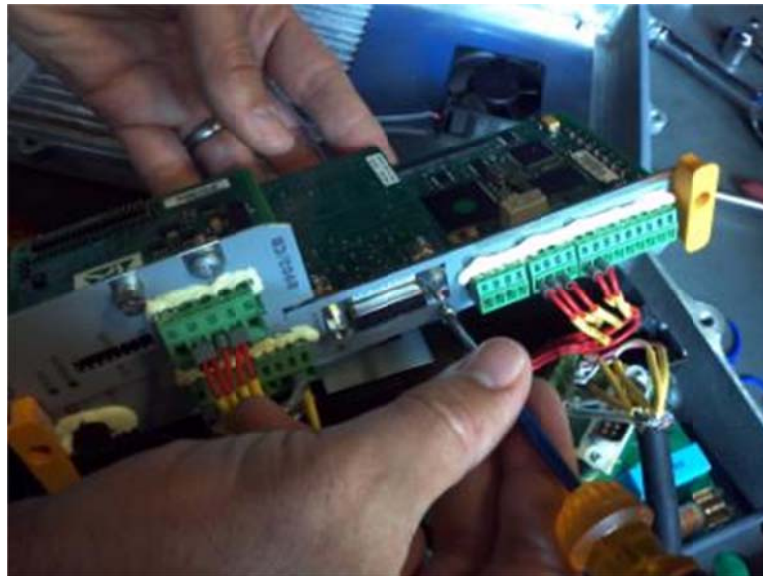




7. Insert the pin-out into the resolver card. Bend the wires from the screw terminals (there is little clearance for the ferrules to protrude without being bent) and install the DB14 from the adapter into the resolver card



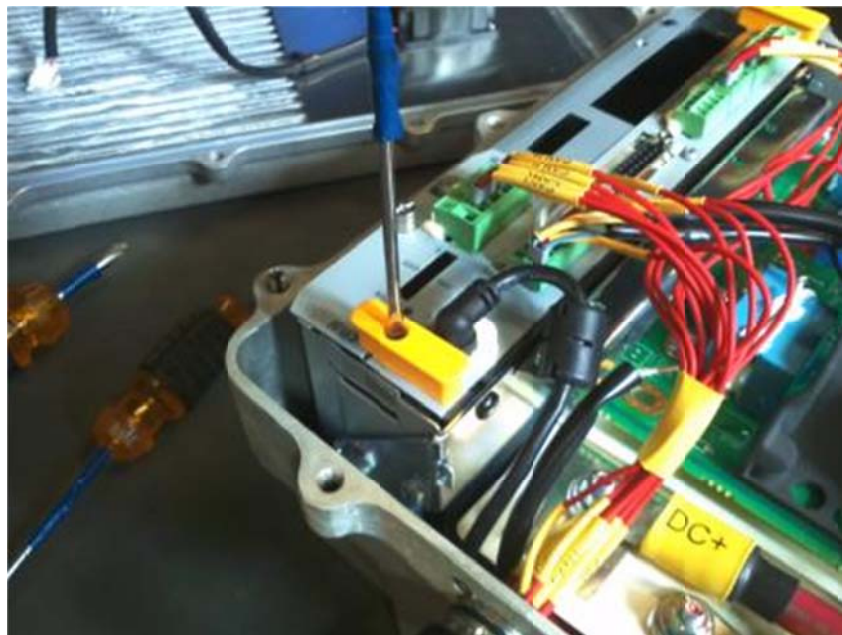
8. Reinstall resolver card into the 8903CB main card, making sure that the contacts line up properly. DO NOT over tighten the screws. They should be finger tight at the most.



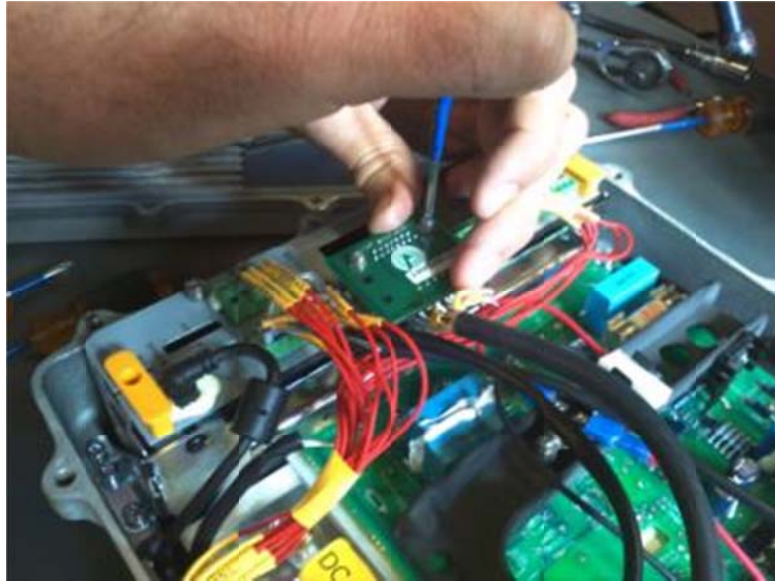
9. Slide control bay into its slots. When you slide it in, take your time because it is very tight and the wires have little flex in them.



10. Reinstall the screws from the aluminum cover and the yellow tabs



11. Screw on the resolver card DB14 connection card



12. Install the fan, close the case with the pocket side covering the PC board allowing adequate space for the fan, tighten the case bolts not very tight.